IDENTIFICATION AND CHARACTERIZATION OF INTERFERON-STIMULATED REGULATORS OF BACTERIAL INFECTION

APPROVED BY SUPERVISORY COMMITTEE

Neal Alto, Ph.D.

Lily Huang, Ph.D.

Sandra Schmid, Ph.D.

John Schoggins, Ph.D.

ACKNOWLEDGEMENTS

I would like to thank everyone who made this work possible. First, my mentor Neal Alto who was the most supportive and encouraging person, always there to share my successes and failures, and never short of new ideas. Then, my partner in crime, Michael Abrams, who I have spent countless hours discussing imaginary projects with, complaining about tough PCRs, and sharing inside knowledge of *Listeria* biology. My lab bestie, Alyssa Jimenez, who always had a good piece of advice for me, helping to keep me going when I was about to give up. And the whole everchanging Alto lab, for providing a pleasant environment and being patient enough to tolerate me for all these years.

I would like to acknowledge my dissertation committee – Lily Huang, Sandra Schmid, and John Schoggins, my work would have never been the same without your constant support and helpful suggestions.

I would also like to thank those who made my graduate school life outside of lab so wonderful, especially Melodi Tastemel, Jason Miller, and Wayne Doyle. Whether it was our everyday lunch ritual since day one or after-work bar adventures, these are the people that were always there.

Many thanks to the people who taught me the basics of science and showed what it means to be a scientist long before I even applied to graduate school, Konstantin Severinov and Dmitry Ghilarov.

And lastly, I would like to thank my parents, who have always supported me and never got tired of saying that everything will be just fine. Spasibo, Mom and Dad!

IDENTIFICATION AND CHARACTERIZATION OF INTERFERON-STIMULATED REGULATORS OF BACTERIAL INFECTION

by

SOFYA PERELMAN

DISSERTATION

Presented to the Faculty of the Graduate School of Biomedical Sciences

The University of Texas Southwestern Medical Center at Dallas

In Partial Fulfillment of the Requirements

For the Degree of

DOCTOR OF PHILOSOPHY
The University of Texas Southwestern Medical Center at Dallas

Dallas, Texas

August, 2017

IDENTIFICATION AND CHARACTERIZATION OF INTERFERON-STIMULATED REGULATORS OF BACTERIAL INFECTION

Publication No. _____

Sofya Perelman, Ph.D.

The University of Texas Southwestern Medical Center at Dallas, 2017

Supervising Professor: Neal M. Alto, Ph.D.

The type I interferon activated transcriptional response is a critical antiviral defense mechanism, yet its role in bacterial pathogenesis remains less well characterized. Using an intracellular pathogen *Listeria monocytogenes* as a model bacterial pathogen, I sought to identify the roles of individual interferon-stimulated genes in context of bacterial infection. Previously, type I interferon has been implicated in both restricting and promoting *L. monocytogenes* growth and immune stimulatory functions *in vivo*. Here, I adapted a gain-of-function flow cytometry based approach to screen a library of more than 350 human type I interferon-stimulated genes for inhibitors and enhancers of *Lm* infection. I identify 6 genes, including UNC93B1, MYD88, AQP9, and TRIM14 that potently inhibit *L. monocytogenes*

infection. These inhibitors act through both transcription-mediated (MYD88) and non-transcriptional mechanisms (TRIM14). Further, I identify and characterize the human high affinity immunoglobulin receptor FcγRIa as an enhancer of *L. monocytogenes* internalization. My data reveal that FcγRIa promotes *L. monocytogenes* uptake in the absence of known host *L. monocytogenes* internalization receptors (E-cadherin and c-Met) as well as bacterial surface internalins (InlA and InlB). Additionally, FcγRIa-mediated uptake occurs independently of *L. monocytogenes* opsonization or canonical FcγRIa signaling. Importantly, I established the contribution of FcγRIa to *L. monocytogenes* infection in phagocytic cells, thus potentially linking the interferon response to a novel bacterial uptake pathway. Finally, I demonstrate that *L. monocytogenes* virulence factor actin assembly-inducing protein (ActA) is required for the FcγRIa-mediated internalization, potentially acting as a bacterial ligand of FcγRIa. Together, these studies provide an experimental and conceptual basis for deciphering the role of type I interferon in bacterial defense and virulence at single-gene resolution.

TABLE OF CONTENTS

PRIOR PUBLICATIONS

Perelman S.S., Abrams M.E., Eitson J.L., Chen D., Jimenez A., Mettlen M., Schoggins J.W. and Alto N.M. (2016), Cell-Based Screen Identifies Human Interferon-Stimulated Regulators of *Listeria monocytogenes* Infection. PLOS Pathogens 12(12)

Abrams M.E., **Perelman S.S.**, Thompson B., McDonald J., Schoggins J.W. and Alto N.M. (2017) Interferon-mediated Regulation of Cholesterol Metabolism Limits Intracellular Bacterial Infection (manuscript in preparation).

LIST OF FIGURES

LIST OF TABLES

LIST OF APPENDICES

LIST OF ABBREVIATIONS

a.a., amino acid

BHI, brain heart infusion

CDNs, cyclic dinucleotides

CFU, colony-forming unit

CLR, C-type lectin receptor

FBS, fetal bovine serum

GFP, green fluorescent protein

IFN, interferon

ISG, interferon-stimulated gene

ITAM, immunoreceptor tyrosine-based activation motif

kDa, kilodalton

LB, Luria-Bertani

Lm, Listeria monocytogenes

LRR, leucine-rich repeat

MOI, multiplicity of infection

NLR, NOD-like receptor

n.s., not significant

OD600, optical density of a sample measured at a wavelength of 600 nm

PAMP, pathogen-associated molecular pattern

PBS, phosphate-buffered saline

PFA, paraformaldehyde

PRR, pattern recognition receptor

RFP, red fluorescent protein

RLR, RIG-I like receptor

s.d., standard deviation

TLR, Toll-like receptor

UTR, untranslated region

WT, wild type

CHAPTER ONE

Introduction and Literature review

Innate immune response

Two branches of immune response in vertebrates

The immune system recognizes foreign organisms and establishes an appropriate protective response. In vertebrates, it is subdivided into two major branches: innate immunity and adaptive immunity. The first line of defense is presented by the evolutionarily older branch –innate immunity that responds quickly by providing anatomical barriers (e.g., skin) with protective physiological conditions (low pH), pathogen clearance by professional phagocytic cells (macrophages) and activation of inflammatory pathways. Innate immunity detects pathogens by germline-encoded receptors, which are activated by common and conserved pathogenic features (see below). In contrast to innate immunity, the adaptive immune response relies on genetic rearrangement in somatic cells to generate a great variety of receptors, which recognize highly specific antigen molecules. These cells require clonal expansion and therefore take longer to become protective upon primary exposure to the pathogen. Adaptive immunity, however, establishes an immunological memory, allowing a more rapid response to repeated pathogen insults due to the population of antigen-specific lymphocytes expanded at the time of primary exposure (1).

Activation of the innate immune response

Until the late 1980s the field of immunology was dominated by studies of the adaptive immunity and the role of T and B cells. However, it was unclear why, in addition to

purified proteins, an adjuvant component (usually of bacterial origin) was required to generate protective immunity. Based on this observation, in 1989 Janeway predicted the existence of surface receptors, that recognize highly conserved microbial structures. These receptors were proposed to recognize immune stimuli and provide costimulatory signals to activate adaptive immune responses (2). This hypothesis was later confirmed by identification of Toll-like receptors as one of the first among numerous pattern recognition receptors (PRRs), changing the view on the overall importance of innate immunity (3). PRRs detect molecular patterns associated with invading bacteria, fungi, or viruses. These pathogen-associated molecular patterns (PAMPs) are often present in a broad class of microorganisms. Importantly, they are essential for microbial survival and therefore are highly conserved (4, 5). Mammalian PRRs have been extensively characterized and currently include transmembrane Toll-like receptors (TLRs) and C-type lectin receptors (CLRs), as well as cytoplasmic Nod-like receptors (NLRs), retinoic acid-inducible gene (RIG)-I-like receptors (RLRs), and numerous cytoplasmic nucleic acid sensors. Recognition of PAMPs by PRRs induces transcriptional activation of proinflammatory cytokines, interferons, and secreted antimicrobial proteins. Importantly, PAMP detection also results in nontranscriptional immune responses, such as phagocytosis, autophagy, and cell death (6).

The most well-characterized PRRs are members of the TLR family. In humans, TLRs are represented by 10 integral membrane proteins, located on either cell surface or endosomal membranes. They are comprised of an extracellular or luminal domain with 19-25 tandem leucine-rich repeat (LRR) motifs as well as a cytoplasmic signaling Toll/interleukin-1 (IL-1) receptor homology (TIR) domain. TLRs recognize their ligands directly or indirectly through

interaction with PAMP-binding molecules, such as MD2, involved in TLR4-mediated lipopolysaccharide (LPS) sensing. TLR1, TLR2, TLR4, and TLR6 primarily recognize PAMPs of lipid nature (lipopeptides, lipoproteins, etc.). TLR3, TLR7, TLR8, TLR9 sense nucleic acids, whereas TLR5 responds to bacterial flagellin. TLRs are found on various immune cells, including macrophages and dendritic cells, B and specific types of T cells, as well as on nonimmune cells (e.g., epithelial cells) (7). In humans, myeloid differentiation factor 88 (MyD88), MyD88-adaptor-like (MAL, TIRAP), TRIF-related adaptor molecule (TRAM), TIR-domain-containing adaptor protein inducing IFNβ (TRIF), and sterile α- and armadillo-motif containing protein (SARM) serve as TLR signaling adaptors. These proteins are key elements of TLR signal transduction and similarly to TLRs contain TIR domains. PAMP binding induces TLR oligomerization and adaptor recruitment to the dimerized TIR domains, ultimately leading to proinflammatory cytokine and interferon (IFN) expression via nuclear factor-κB (NF-κB) and IFN-regulatory factor (IRF) activation (7, 8).

Another large group of PRRs is represented by C-type lectins or CLRs that are primarily expressed on myeloid cells and recognize carbohydrate ligands via carbohydrate recognition domains (CRDs). These receptors initiate signaling via immunoreceptor tyrosine-based activation motif (ITAM) domains, either encoded within their cytoplasmic domains (Dectin-1, DNGR-1), or by associating with ITAM-containing adaptor molecules (such as Fc receptor γ-chain or DAP12), for example, in case of Dectin-2. CLRs have been mainly characterized in the context of fungal infections, however, their involvement in antibacterial, antiviral and antiparasitic immunity is currently also being recognized (9).

Cytoplasmic Nod-like receptors (NLRs) are found in both immune and non-immune cells. Their N-terminal protein-protein interaction domain is required for downstream signaling following PAMP recognition via the C-terminal LRR domain. Additionally, the central region of the receptor contains a nucleotide-binding oligomerization (NOD) domain allowing NLR self-oligomerization upon ligand sensing (10). NLRs are involved in recognition of a wide variety of ligands of microbial nature (peptidoglycan, flagellin, RNA, etc.), as well as multiple danger-associated molecules (cholesterol crystals, uric acid, UV radiation, etc.). Additionally, some NLRs respond to host signaling molecules, including IFNγ, among others (11, 12).

RIG-I-like receptors (RLRs) are represented by three highly related proteins: RIG-I, MDA5 and LGP2. These proteins are grouped by their shared characteristic domains responsible for binding viral RNA - a central ATPase containing DExD/H-box RNA helicase domain and the C-terminal domain. RIG-I and MDA5 also contain N-terminal tandem caspase activation and recruitment domains (CARDs) that mediate downstream signaling. In contrast to RIG-I and MDA5, LGP2 lacks the N-terminal CARDs and is proposed to act as a regulator of RLRs (13). Activated RIG-I and MDA5 interact with a mitochondrial antiviral signaling protein (MAVS) to induce type I IFN secretion (14, 15).

DNA has long been proposed to elicit an innate immune response, however, only recently has the mechanism of intracellular DNA detection been uncovered. Among multiple DNA sensors reported to date the cyclic guanosine monophosphate-adenosine monophosphate (cGAMP) synthase (cGAS) is considered to serve as the central DNA

sensing protein (16, 17). Upon interaction with dsDNA, the nucleotidyltransferase (NTase) catalytic pocket of cGAS undergoes a conformational change, allowing GTP and ATP binding, followed by 2'3'-cGAMP synthesis (18, 19). cGAMP binds and activates the ER-localized protein, Stimulator of Interferon Genes (STING) (20). In addition to 2'3'-cGAMP produced by cGAS, STING also senses other cyclic dinucleotides (CDNs), such as c-di-AMP, c-di-GMP, and 3'3'-cGAMP secreted by invading bacteria. However, affinities of interaction with bacterial CDNs are significantly lower than with endogenously produced 2'3'-cGAMP (20-22). Upon activation, STING translocates from the ER to the ER-Golgi intermediate and Golgi apparatus, activating TBK1 kinase, which in turn phosphorylates and activates IRF3 (23, 24). STING also activates the NF-κB pathway through IkB kinase (IKK) activation. Both activated IRF3 and NF-κB translocate to the nucleus, resulting in IFN and proinflammatory cytokine production (25).

Interferons

As noted above, activation of multiple PRRs by microbial pathogens results in production of interferons (IFNs), a family of secreted cytokines. Interferons are mostly characterized in terms of their antiviral properties. Members of the IFN family also inhibit cell growth, regulate apoptosis and exhibit immunomodulatory activities (26). These effects are mediated by the expression of hundreds of IFN stimulated genes (ISGs), that are transcriptionally activated in response to IFN signaling (reviewed below) (27). However, while ISGs have been identified, individual functions for most of them remain to be determined.

Introduction to interferons

The first member of the IFN family was described by Issacs and Lindenmann is 1957, as a soluble factor secreted by various types of cells in response to heat-inactivated influenza virus and capable of "interfering" with live influenza virus infection (28). It was first studied as a crude protein extract and only purified to homogeneity in 1978, which allowed its further characterization (29, 30). The IFN family includes a diverse group of cytokines, subdivided into three classes: type I, type II, and type III IFNs. These proteins are primarily characterized in context of antiviral properties, but have also been shown to regulate bacterial infections as well as overall immune cell function, via control of cell proliferation, survival and differentiation. In humans, the type I IFNs are represented by 13 homologous IFNα proteins, 1 IFNβ and less well-characterized IFNε, IFNκ, and IFNω, and are grouped by structural homology and the use of a common type I IFN receptor. Type II IFN family includes only one protein, IFNγ, which is not structurally related to any member of the type I IFN family and signals through a distinct receptor. Lastly, IFNλ1, IFNλ2 and IFNλ3 (IL-29, IL-28A, IL-28B, respectively) and IFNλ4 have recently been characterized and grouped as type III IFNs (31).

Interferon-stimulated signaling

Receptors for all types of IFN consist of two subunits: IFNAR1 and IFNAR2 make up a type I IFN receptor, IFNGR1 and IFNGR2 provide signaling for the type II IFN, whereas IFNλR1 (IL-28R) and IL-10R2 mediate type III IFN sensing. Each IFN receptor subunit interacts with a member of the Janus activated kinase (JAK) family - IFNAR1 and

IL-10R2 interact with tyrosine kinase 2 (TYK2), IFNAR2, IFNGR1 and IFNλR1 associate with JAK1, whereas IFNGR2 associates with JAK2. (Fig. 1). IFN binding to the extracellular portion of the corresponding receptor subunits leads to their dimerization, rapid autophosphorylation and activation of associated JAKs, subsequent phosphorylation of STATs (signal transducer and activator of transcription) and activation of the JAK-STAT signaling pathway. STAT1, STAT2, STAT3, and STAT5 are activated in response to type I IFN receptor stimulation by any of the type I IFNs. Phosphorylated and homo- or heterodimerized STAT proteins translocate to the nucleus. Activated STAT1 and STAT2 associate with IRF9 to form the ISG (Interferon Stimulated Gene) factor 3 (ISGF3) complex. ISGF3 initiates transcription of certain ISGs by interacting with the IFN-stimulated response elements (ISREs) of their promoters. Various other complexes are formed by activated STATs and initiate transcription by binding so called IFNγ-activated site (GAS) elements, found in the promoters of multiple ISGs. Every ISG has an ISRE, a GAS-element or both features present in their promoter. Similar signaling is initiated in response to type III IFN. Binding of IFNγ to the type II receptor results in the phosphorylation and homodimerization of STAT1. STAT1-STAT1 complex initiates transcription at the GAS-element containing promoters. Since STAT2 is not activated in response to IFN II, ISGF3 complex is not formed and transcription cannot be initiated from the ISRE-promoters. Through these signaling events IFNs induce expression of hundreds of ISGs, which in turn exert multiple effects, including IFN-activated antiviral activities (31-34).

During microbial infections, type II IFN is a strong activator of macrophages, inducing a robust antimicrobial profile, as well as a regulator of type 1 T helper (Th1) cells.

Therefore, immunologists primarily focused on type II rather than type I IFN. Recently, however, type I IFNs have become the subject of an increasing number of studies. This renewed interest emerged for several reasons, including the characterization of previously identified IFNα/β-producing cells (IPCs), identification of multiple microbial products as novel activators of IFN secretion, and the finding that type I IFN not only regulates viral pathogens but also exerts complex effects on bacterial infections, which were previously studied primarily in context of IFN II (35).

Interferon I and bacterial infection

As noted above, IFN I was originally discovered as a potent antiviral compound, and has been later shown to have a protective role against most types of viruses, including single- and double-stranded RNA as well double-stranded DNA viruses (36). Although less studied, the type I IFN response is also induced by many bacterial pathogens including *Legionella pneumophila*, *Helicobacter pylori*, *Francisella tularensis*, *Yersinia pseudotuberculosis*, *Mycobacterium tuberculosis*, and *Listeria monocytogenes* (37). Unlike the protective effects of type I IFN in acute viral infections, its role in bacterial infection is more complex and depends on the nature of the pathogen.

Immunomodulatory effects of IFN I are beneficial for the host during infection of several bacterial pathogens, including *Streptococcus pyogenes*, *S. pneumoniae*, *Legionella pneumophilia,* and group B streptococcus. Complex processes activated by IFN allow for different downstream effects depending on the pathogen lifecycle. For example, in case of *S. pneumoniae* infection, IFN I inhibits bacterial transmigration from the lung to the blood,

thereby protecting the host and reducing bacteremia following intranasal infection. Recently, this observation was explained by the IFN I mediated protection of alveolar epithelial type II cells (AECII) from inflammation-induced cell death (38, 39). Further, type I IFN together with type II IFN contributes to bacterial clearance during *L. pneumophilia* infection by remodeling of *Legionella*-containing vacuoles. Additionally, IFNs activate expression of the IFN-responsive gene 1 (IRG1) that localizes to mitochondria and mediates production of a bactericidal itaconic acid, targeting *L. pneumophilia* inside the vacuole (40, 41). Lastly, when challenged with extracellular group B streptococci (GBS) in the absence of IFNα/β signaling most mice succumb to unrestrained bacteremia, whereas wild type mice survive the infection (42).

Some pathogens, such as *M. tuberculosis*, were found to benefit from type I IFN effects. During infection, type I IFN reduced production of proinflammatory cytokines IL-1α and IL-1β by inflammatory monocyte-macrophage and dendritic cell populations in the lungs. IL-1 has been shown to control bacterial infection, as well as prevent infection-induced mortality (43, 44). The mechanism behind type I IFN mediated reduction in IL-1 secretion is unclear. However, it is proposed to be indirectly controlled by IL-10, which is upregulated by IFN (44). Interestingly, IFN I was also found to have a protective effect on *M. tuberculosis* lung infection in the absence of type II IFN signaling, which normally plays a dominating protective role (45).

F. tularensis is another example of a bacterial pathogen that benefits from type I mediated responses in mice. Type I IFN was found to be detrimental for the survival of the

host during intradermal *F. tularensis* subspecies *novicida* infection, which is used as a mouse model of tularemia disease. Increased resistance to infection in IFN receptor deficient mice (IFNAR1$^{-/-}$) was linked to an increase in IL-17 secretion by IL-17A^{+} γδ T cells, which demonstrated an increased expansion in the absence of IFN. Additionally, consistent with the contribution of IL-17A to neutrophil expansion, increased IL-17A in IFNAR1$^{-/-}$ mice correlated with an increase in splenic neutrophil numbers during infection (46).

Another bacterium, *L. monocytogenes* (herein referred to as *Lm*) exhibits a more complex relationship with the mammalian IFN response system (reviewed below).

Type I IFN mediated regulation of Lm infection

Early work demonstrated that recombinant murine IFNβ had both prophylactic and therapeutic effects, increasing the tolerance of mice to intravenous systemic *Lm* infection (47). Similarly, *Ifnar1* is required for resistance of mice to *Lm* invasion through the intestinal tract, further demonstrating a protective effect of IFN for a natural route of infection (48). However, more recent studies indicate that mice lacking a functional type I IFN receptor (*Ifnar1*-/-) or IRF3 (*Irf3-/-*) display greater resistance to intravenous *Lm* infection, suggesting that IFN exacerbates systemic *Lm* infection. IFN I was proposed to increase apoptosis of lymphocytes, potentially through increased sensitivity to listeriolysin, as well as suppress the innate immune defense by CD11b+ macrophages (49-51). The type I IFN response has also been found to suppress adaptive immunity against *Lm*, since *Sting*-deficient mice exhibit greater numbers of cytotoxic lymphocytes and show protection from *Lm* reinfection after

immunization (52). Interestingly, a recent study reported that deficiency in the type I IFN receptor did not alter the susceptibility of mice to a food-borne *Lm* infection (53).

These various effects of type I IFN on *Lm* infection likely reflect the different routes of infection as well as the pleiotropic roles of IFN in distinct tissue environments or cellular populations encountered by the pathogen. Nevertheless, type I IFN appears to play a significant role in shaping the host-pathogen interaction *in vivo*. However, it remains unclear how individual genes stimulated by type I IFN (type I ISGs) are contributing to the overall effect of IFN I on *Lm* infection. Additionally, none of the studies listed above specifically address the role of IFN I in human listeriosis or cultured human cells.

Listeria monocytogenes

Lm as a causative agent of listeriosis

Lm is a Gram-positive bacterium present in various environments, including soil, water, animals, humans as well as food products. It is an opportunistic intracellular pathogen that causes food-borne disease called listeriosis in humans, known to also infect ruminants (cattle, sheep, and goats), and other animals (54, 55). *Lm* belongs to the *Listeria* genus, which includes 17 diverse species of rod-shaped anaerobic non-spore-forming bacteria (56). Another species, *L. innocua* is highly related to *Lm* but does not encode any virulence-associated genes found in *Lm,* and is therefore nonpathogenic (57). The only other known pathogen among the *Listeria* genus, *L. ivanovii* encodes a virulence gene cluster and is primarily infectious in ruminants and is not commonly pathogenic in humans (58).

Lm was first described in 1926, as the causative agent of mononuclear leukocytosis in rabbits and guinea pigs but was only recognized as a human food-borne pathogen in the 1980s (59, 60). In healthy adults listeriosis is characterized by gastroenteritis and does not normally require hospitalization. However, in immunocompromised individuals, pregnant women, elderly and children disease is often severe and life-threatening, causing meningitis, encephalitis, septicemia, and mother-fetus infections. This variety of clinical manifestation is due to the ability of *Lm* to breach highly controlled barriers within the human body: intestinal, fetoplacental, and the blood-brain barriers (55). The incidence of listeriosis is relatively low (0.2 laboratory-confirmed cases per 100,000 population), however high mortality rates (up to 30%) make it the third leading cause of death from food-borne infection in the United States (61, 62).

Lm is successfully inactivated by pasteurization, therefore the most common source of infection in humans is contaminated raw food that undergoes minimal thermal processing, such as vegetables and fruit, unpasteurized milk, soft cheeses, as well as ready-to-eat meat products and seafood (63, 64). *Lm* is resistant to many of the conditions used to control contamination, including low temperatures, low pH, and high salt (65-67).

Regulation of virulence genes in Lm

In *Lm,* the switch from the environmental saprophyte to pathogen during infection is controlled primarily by positive regulatory factor A (PrfA) that activates transcription of *Lm* virulence genes, responsible for the invasion, survival and proliferation within the host. As expected, in animal models PrfA deficiency results in severe attenuation of *Lm* infectivity

(68-70). Gene expression studies identified a "core" group of PrfA-upregulated genes, including 12 genes. Among these genes, 10 encode well-characterized *Lm* specific virulence factors (*prfA*, *inlA*, *inlB*, *hly*, *mpl*, *plcA*, *plcB*, *actA*, *hpt*), and 2 (*lmo2219* and *lmo0788*) encode proteins of unknown function and are shared with a non-pathogenic *L. innocua* species (71).

PrfA belongs to the cAMP receptor protein (Crp) / fumarate nitrate reductase regulator (Fnr) family. Its N-terminal region is similar to a cyclic nucleotide binding domain, whereas the C-terminal possesses a DNA-binding helix-turn-helix (HTH) motif (72). PrfA forms a symmetrical homodimer with the 14bp palindromic nucleotide sequences (so called "PrfA boxes") found in promoters of *Lm* virulence gene. PrfA preferentially binds symmetrical PrfA boxes (TTAACANNTGTTAA) rather than boxes with one or two mismatches (73, 74).

Expression of a PrfA-dependent genes is not only regulated by the affinity of PrfA to the corresponding promoters, but also by the concentration of an active PrfA protein within the cell. To ensure coordinated and timely activation of virulence genes, PrfA is regulated on both transcriptional and posttranscriptional levels. Transcription of *prfA* occurs from three promoter regions: two are located directly upstream of the *prfA* gene (P*prf*A$_{P1}$ and P*prf*A$_{P2}$) and control expression of a monocistronic *prfA* transcript, while the third one (P*plc*A) is shared with the upstream *plcA* gene and regulates production of both mono- (*plcA*) and bicistronic (*plcA* and *prfA*) transcripts (75, 76). Transcripts from the P*prf*A$_{P1}$ are produced in the actively growing *Lm* cells in broth culture in a vegetative sigma factor σ^A-dependent

manner. However, at temperatures below 30°C PrfA translation from these transcripts is inhibited, due to the thermoswitch located in its 5' UTR. At higher temperatures, for example following ingestion by warm-blooded animals, the RNA hairpin is destabilized, allowing access to the ribosome binding site on the *prfA* transcript, and providing rapid production of PrfA protein from a previously generated pool of RNA (77). Transcription of *prfA* from the second monocistronic P*prf*A$_{P2}$ promoter is negatively regulated by PrfA, and is transcribed in stress sigma factor σ^B-dependent manners, ensuring sufficient PrfA production under a variety of conditions, including low pH, high osmolarity, which *Lm* often encounters during infection (78, 79). Additionally, PrfA synthesis is negatively regulated by *trans*-acting SreA and SreA, two S-adenosylmethionine (SAM) riboswitches. These small RNAs are produced under rich broth conditions and act as non-coding RNAs by associating with the 5' UTR of the prfA mRNA (80). Lastly, the third P*plc*A promoter is regulated by PrfA itself, providing a positive feedback loop and sustained production of the protein (79).

Recently, bacterial and host-generated glutathione has been shown to contribute to *Lm* virulence, serving as a PrfA cofactor. While glutathione is not required for PrfA-DNA interaction, it has been proposed to play a role in the subsequent transcriptional activation (81). Structural studies suggest that in the glutathione-bound state the C-terminal HTH fold of PrfA is stabilized in an "active" confirmation, similarly to that observed in the constitutively active PrfA G145S (79, 82).

Intracellular lifecycle of Lm

In its intracellular lifecycle, *Lm* undergoes a series of well-defined stages (Fig. 2). It invades and multiplies in a range of cell types, including both non-professional and professional phagocytes. Invasion of non-professional phagocytes occurs through a "zipper-like" mechanism. Bacterial surface ligands internalin A (InlA) and internalin B (InlB) interact with and activate their respective host plasma membrane receptors, E-cadherin and c-Met, resulting in the envelopment of *Lm* by the host cell membrane (83). These two major virulence factors belong to the internalin protein family, characterized by the N-terminal leucine-rich repeats (LRRs) that participate in protein-protein interactions. InlA is covalently anchored to the cell wall by a LPXTG motif, whereas InlB is loosely attached to the lipoteichoic acid of the cell wall by GW motif-containing repeats (84).

Bacterial InlA interacts with the host E-cadherin protein that is responsible for the formation of cellular adherence junctions (Ca^{2+}-dependent intracellular adhesion sites) between polarized epithelial cells (85). Binding of InlA leads to clustering of E-cadherinand tyrosine phosphorylation and ubiquitination of its cytoplasmic tail by Src and the E3 ubiquitin ligase Hakai, respectively, followed by clathrin recruitment to the site of invasion through its adaptor Dab2. Clathrin does not participate in the invasion process as a classic endocytic coat protein but rather acts as a site of actin recruitment and reorganization (86-88). E-cadherin is responsible for *Lm* uptake by polarized epithelial cells, thus allowing bacterial to cross intestinal and fetoplacental barriers (89).

InlB activates the receptor tyrosine kinase c-Met, also known as hepatocyte growth factor receptor (HGFR), promoting invasion of multiple cell types (90). As in the case of the

InlA/E-cadherin-dependent *Lm* internalization, upon internalin binding the host receptor undergoes posttranslational modifications and interacts with multiple downstream effectors. Activated c-Met is ubiquitinated by Clb ubiquitin ligase, leading to clathrin recruitment and rearrangement of the actin cytoskeleton at the site of bacterial attachment (87, 91, 92). PI 3-kinase is also recruited to the site of *Lm* entry, mediating local production of $PI(3,4,5)P_3$, ultimately resulting in additional actin cytoskeleton rearrangements (93).

During intestinal invasion, InlA and InlB have also been shown to act cooperatively to promote invasion of intestinal villus tips. According to the proposed model, InlA determines the specificity of *Lm* to multicellular junctions at the villus tips, whereas InlB increases endocytosis and invasion by activation of c-Met at the site of attachment (94).

Upon engulfment by the host cell, *Lm* is found in a primary phagosome and escapes into the cytoplasm by secreting pore-forming listeriolysin O (LLO, encoded by the *hly* gene) and two phospholipases - PlcA and PlcB (95). LLO belongs to the cholesterol-dependent cytolysin (CDC) family and is activated by the acidic pH in the phagosome. It is inserted into the membrane of the phagosome, causing Ca^{2+}-leakage, thereby preventing phagosomal maturation and fusion with the lysosomal compartments (96-98). PlcA and PlcB, which possess phosphatidylinositol-specific and broad-range phospholipase C activities, respectively, additionally contribute to the disruption of the phagosome (99).

Following escape from the phagosome, *Lm* replicates in the cytoplasm with an average doubling time of 60 minutes, close to that in rich broth medium (100, 101). In the cytoplasm *Lm* utilizes multiple hexose phosphates as energy sources, including glucose-1-

phosphate and glucose-6-phosphate. Their uptake is PrfA-dependent and is mediated by a hexose phosphate transporter (Hpt), which exhibits high similarity to the mammalian glucose-6-phosphate translocase (G6PT). Deficiency in *hpt* severely impairs intracellular growth and reduces virulence in a mouse model (102). Another protein that is required for intracellular growth but is dispensable for the extracellular replication - lipoate ligase-like protein LplA1 - is responsible for the addition of the thiol-containing cofactor lipoyl to its metabolic enzyme complexes, including pyruvate dehydrogenase (PDH). Since *Lm* is a lipoate auxotroph, it relies on LplA1 to scavenge lipoyl moieties from the host-derived lipoyl-modified proteins in the cytoplasm (103). Finally, biosynthesis of aromatic amino acids is also required for optimal intracellular growth and virulence of *Lm* and is mediated by the proteins encoded by *aroA*, *aroB*, and *aroE* genes (104).

Lm then spreads to adjacent cells via polarized actin polymerization, mediated by its actin nucleating protein ActA. Since the initial discovery of ActA involvement in actin assembly and cell-to-cell spread, the mechanism of actin-based motility has been characterized in detail. ActA is a surface protein, distributed in a polarized manner on the *Lm* surface, allowing for directional movement and bacterial spreading. The N-terminal domain interacts with the Arp2/3 actin nucleation complex, mimicking the function of WASP/WAVE proteins, while its central region recruits actin filaments and profilin via its interaction with the Enabled/vasodilator-stimulated phosphoprotein (Ena/VASP) (105-107). Polarized polymerization of actin on *Lm* surface creates so-called actin comet tails that propel the bacterial outward, resulting in host plasma membrane remodeling, formation of protrusions, and subsequent *Lm* internalization by neighboring cells (108). This process is

made possible by the secreted internalin InlC that displaces N-WASP from the Tuba scaffolding protein, thereby relieving cortical tension of the host cell plasma membrane, loosening membrane junctions and allowing protrusions to form (109). Recently, multiple other functions have been attributed to the ActA protein, including cell entry, maturation of the phagosome and autophagy avoidance, as well as a role in bacterial biofilm formation (110-113).

Host tropism of Lm infection

Lm infection exhibits host species specificity, which is primarily determined by the ability of bacterial invasin InlA to interact with its host receptor, E-cadherin. For example, InlA successfully interacts with E-cadherin from human, guinea pig, rabbit, and gerbil but fails to bind corresponding receptors from mouse and rat (114). This explains the observation that mice do not serve as natural hosts of *Lm* and are highly resistant to oral *Lm* infection in the lab. Pro16 of E-cadherin was identified as a residue critical for InlA interaction, and its replacement with glutamic acid in the murine E-cadherin was shown to prevent InlA recognition by the receptor (114). Similar species specificity is observed in the interaction of InlB with its host receptor c-Met: InlB recognizes c-Met of human, mouse, gerbil, and rat but not that of rabbit or guinea pig (115).

Two mouse strains have been developed to allow for oral infection in mice – ectopically expressing human E-cadherin exclusively in enterocytes in the context of the mouse E-cadherin, and a “knock-in” strain, with the E16P mutation introduced, allowing for the InlA interaction and efficient InlA-mediated colonization of the gut (116, 117).

Additionally, a so-called "murinized" *Lm* strain expressing a mutated mInlA has been generated. mInlA interacts with the murine E-cadherin with an affinity similar to that of a wild type InlA-human E-cadherin interaction (118). However, unlike InlA, mInlA may also interact with N-cadherin, expressed in villous M cells, thereby altering bacterial tissue tropism (119).

Induction of type I IFN during Lm infection

Lm is known to induce a robust type I IFN response, with macrophages serving as a primary source of IFN production (120). As shown by *in vitro* studies, *Lm* activates IFNβ secretion upon escape from the vacuole, rather than primary cell entry. Additionally, escape rather than the pore-forming listeriolysin O was required for the observed activation (121). IFN induction by *Lm* is independent of TLRs and NOD2 and is believed to exclusively rely on cytoplasmic nucleic acid sensors (122, 123).

Recent studies revealed that *Lm* stimulates a type I IFN response by secreting cyclic diadenosine monophosphate (c-di-AMP) through a multidrug efflux pump MdrT and directly stimulating STING in a cGAS-independent manner (Fig. 3). Activation of STING results in IRF3 phosphorylation and transcription of IFN genes (124, 125). Notably, STING-deficient mice fail to produce IFNβ in response to *Lm* infection (126). In mouse peritoneal macrophages, IFNβ induction is also dependent on a cytoplasmic PRR protein LRRFIP1, potentially via its ability to sense dsDNA and RNA (127). Interestingly, IFN production in these cells could also be triggered by TLR2-mediated detection of peptidoglycans on the *Lm*

surface. Deacetylation of peptidoglycan by bacterial PgdA allows *Lm* to partially avoid detection (128).

In humans, about 18% of the population express an H232 STING variant that is unresponsive to the bacterial CDNs (129, 130). In this case, *Lm* DNA instead of c-di-AMP serves as the major stimulator of IFN production in macrophages and is sensed in a manner dependent on IFI16, cGAS and STING (20, 131, 132). In non-immune cells that lack a functional STING signaling pathway, IFN secretion is induced by RIG-I-mediated detection of bacterial RNA, released into the cytoplasm upon infection via the SecA2 protein secretion system (133).

Aims of this study

Since IFN induces a robust transcriptional response, its regulatory role in bacterial infection likely depends on the cellular expression of ISGs. However, the functions of most ISGs in the antibacterial immunity have not yet been elucidated. The main aim of this study was to identify regulators of bacterial infection among type I ISGs and characterize them at the single-gene level. *Lm* was chosen as a model bacterial pathogen for the study. In addition to being an important human foodborne pathogen, *Lm* was particularly interesting since it exhibits a complex relationship with type I IFN (as reviewed above).

Recently, overexpression screens have been designed to study individual ISG functions, as they overcome the technical challenges of studying complex transcriptional responses at single-gene resolution (134-137). These approaches have proven to be highly successful for identifying genes potently suppressing invasion, replication, or egress of a wide variety of viruses; thus, similar screening methodologies could also be adapted for bacterial pathogens. Therefore, I adapted a flow cytometry based gain-of-function screening approach (134, 135) to evaluate the effects of human type I ISGs on *Lm* infection. I was aiming to uncover antibacterial genes among the type I IFN mediated response. Importantly, I also expected to identify genes that increase *Lm* infection as *Lm* might have evolved mechanisms allowing it to evade and potentially hijack elements of this immune mechanism.

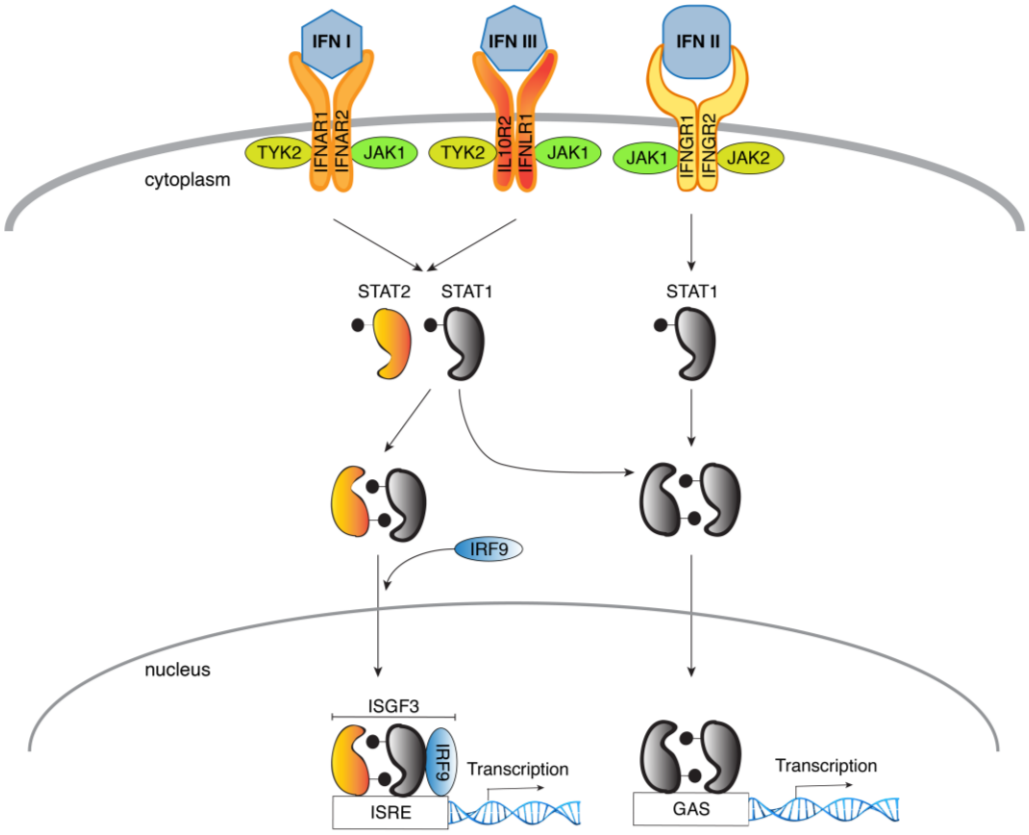

Figure 1: Interferon signaling

Type I interferon (IFN) receptor recognizes all type I IFNs and is comprised of IFNAR1 and IFNAR2. It is associated with tyrosine kinase 2 (TYK2) and Janus activated kinase 1 (JAK1). Type III IFNs bind type III IFN receptor, which consists of IL10R2 and IFNLR1. Similar to type I IFN receptor, type III IFNR is associated with TYK2 and JAK1. Type II IFN receptor is composed of IFNGR1 and IFNGR2, associated with JAK1 and JAK2, respectively. Interferon binding and JAK kinase activation lead to STAT1 phosphorylation (in case of type II IFN) and STAT1 and STAT2 phosphorylation (in case of type I and type III IFNs). Dimerized STAT1 as well as STAT1-STAT2-IRF9 complex (termed ISGF3) translocate to

the nucleus and bind IFNγ-activated site (GAS) elements and IFN-stimulated response elements (ISREs), respectively, stimulating transcription of corresponding genes.

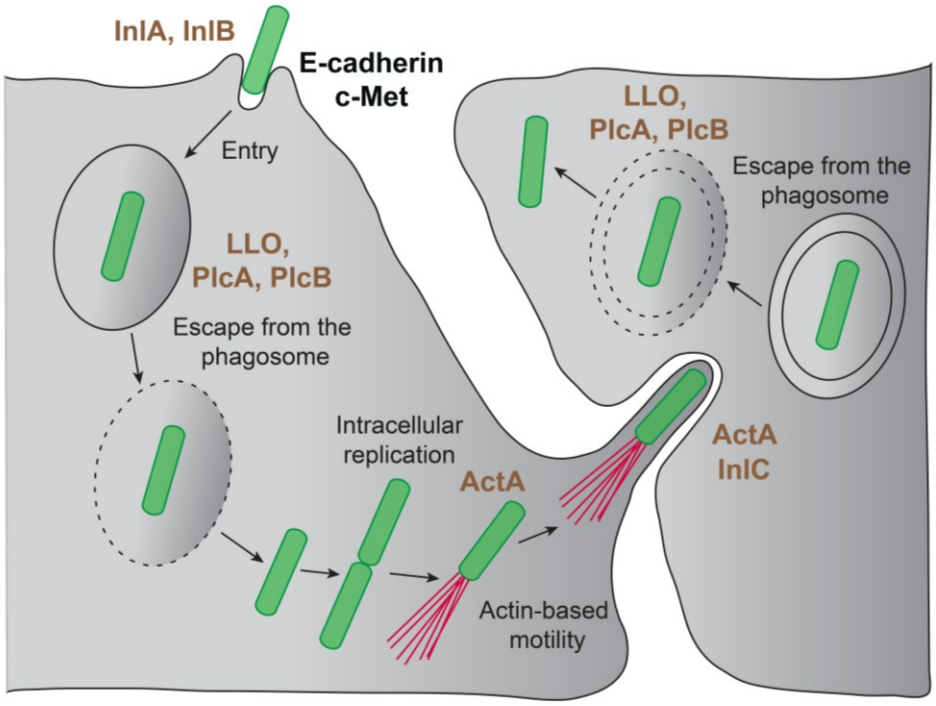

Figure 2: Intracellular lifecycle of *Lm*

(adapted from Tilney, Portnoy, 1989 with modifications (138))

Extracellular *Lm* gains access to the cytoplasm of nonphagocytic cells via interaction of internalin A (InlA) and internalin B (InlB) with host cell surface receptors E-cadherin and c-Met, respectively. Internalized bacteria disrupt the membrane of the primary vacuole by secreting listeriolysin O (LLO) and phospholipases PlcA and PlcB. *Lm* rapidly replicates in the cytoplasm and induces actin polymerization and actin-based motility via polarized expression of ActA protein. Actin polymerization and internalin C (InlC) expression allow protrusion formation and bacterial spread to neighboring cells. In the newly infected cell Lm escapes the secondary double membranes vacuole and repeats the infection cycle.

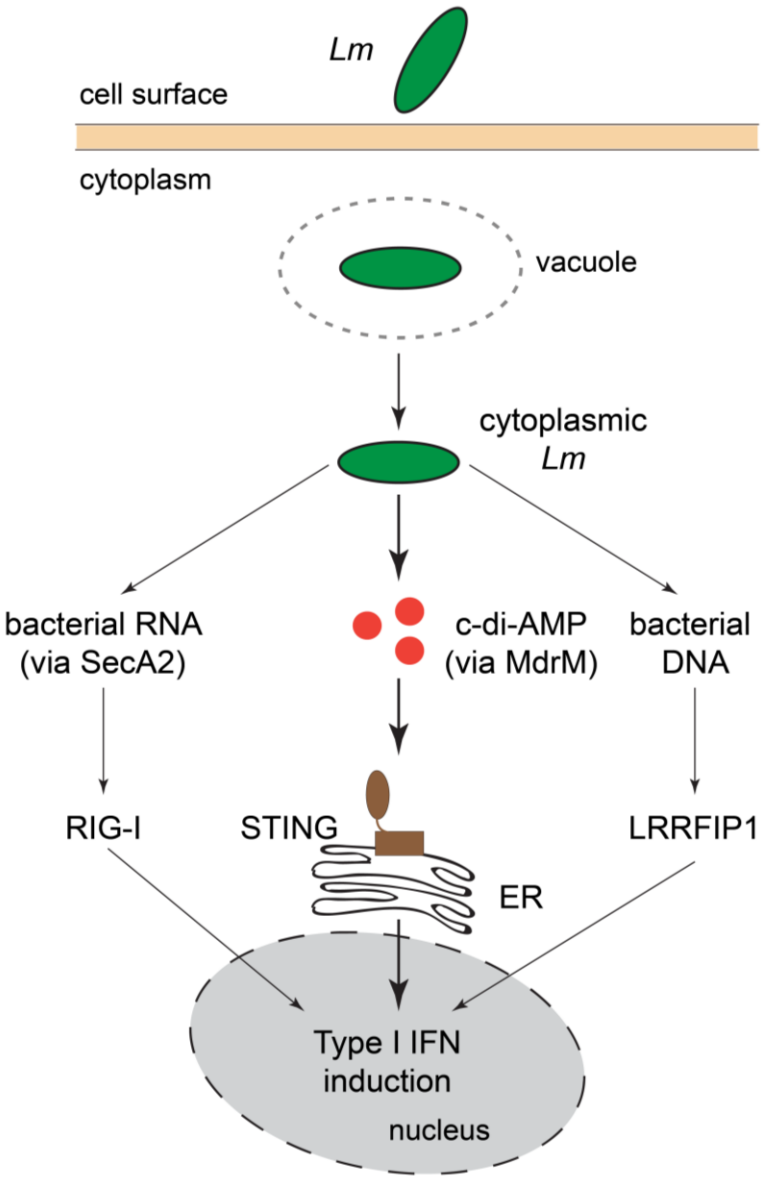

Figure 3: Induction of type I IFN during *Lm* infection

Initially upon invasion *Lm* is contained in a primary vacuole and avoids detection by the host cell. However, following disruption of the vacuole, *Lm* is detected by multiple pathways, primarily through c-di-AMP mediated STING activation, leading to type I IFN induction.

Bacterial DNA is also recognized by LRRFIP1 protein in the cytoplasm. Additionally, bacterial RNA is secreted via SecA2 and is recognized in a RIG-I-dependent manner.

CHAPTER TWO

Flow cytometry based screening

Evaluation of the flow cytometry based approach as a method to assess Lm infection

I sought to employ a gain-of-function screening approach to identify ISGs that regulate *Lm* infection of host cells. First, I optimized the screening conditions by determining the suitability of the host cell type previously used for ISG screens (134, 135) and by defining the optimal conditions of *Lm* infection. Since *Lm* is known to potently induce IFN expression (139), human *STAT1*-deficient fibroblasts were chosen as the primary host cell type for infection (140). These cells lack functional *STAT1*, have defective IFN responses, and therefore limit the spurious activation of ISGs during bacterial infection. To screen hundreds of ISGs in a single experiment, I optimized *Lm* infection of *STAT1*-deficient fibroblasts for compatibility with multicolor flow cytometry with auto-sampling functionality (134). GFP-expressing *Listeria monocytogenes* 10403s (GFP-*Lm*) was added to fibroblasts at a multiplicity of infection (MOI) of 5 bacteria per cell in the absence of antibiotics. GFP-*Lm* was incubated for 90 minutes with host cells prior to adding gentamicin-containing media to eliminate non-internalized extracellular bacteria. Approximately 10% of host cells were infected by GFP-*Lm* at this time point. Cells were then incubated for 1, 2, 4 and 6 hours, providing a temporal evaluation of infection. As shown in Fig. 4A, an increase in the percentage of GFP-positive host cells was observed over time indicating that GFP-*Lm* readily infects *STAT1*-deficient fibroblasts.

Lm infection progresses through a series of distinct stages including entry, vacuole escape, cytoplasmic replication, and cell-to-cell spread (Fig. 4A). Since ISGs could potentially affect any stage of the *Lm* lifecycle, I assessed the ability of flow cytometry to identify blocks in each of these distinct stages. *STAT1*-deficient fibroblasts were infected with mutant *Lm* strains that lack key virulence factors that are critical for cellular entry (*Lm ΔinlAΔinlB*), phagosomal escape *(Lm ΔhlyΔplcAΔplcB)*, and cell-to-cell spread *(Lm ΔactA*). As expected, *Lm ΔinlAΔinlB,* lacking the major *Lm* invasion proteins InlA and InlB, exhibited a severe infection defect observed as early as 1 hour following initial infection (Fig. 4B). In contrast, *Lm ΔhlyΔplcAΔplcB* mutant lacking listeriolysin O (LLO) and phospholipases required for phagosomal rupture and escape, invaded cells similar to wild type *Lm*, yet the percentage of infected cells and their bacterial burden (intensity of the GFP signal) did not increase over the time course of infection (Fig. 4C). This observation is consistent with the *Lm ΔhlyΔplcAΔplcB* phenotype in which the pathogen trapped in the phagosome survives but is unable to replicate (99, 100, 141, 142). Finally, *Lm ΔactA* lacking the ActA protein required for intracellular actin-based motility invaded cells initially but failed to spread from cell to cell. Importantly, the GFP fluorescence intensity of infected *STAT1*-deficient fibroblasts increased over the course of infection due to bacterial replication and accumulation in initially invaded cells (Fig. 4D). Thus, flow cytometry is a well-suited method to measure *Lm* infection of *STAT1*-deficient fibroblasts as it is capable of detecting specific infection defects that may arise due to ISG expression.

Gain-of-function screen identifies both inhibitors and enhancer of Lm infection among type I interferon stimulated genes

I next asked whether ISGs that control viral infection also regulate bacteria. Briefly, *STAT1*-deficient fibroblasts were transduced with bicistronic lentiviral vectors driving constitutive expression of an ISG and a red fluorescent protein TagRFP (Fig. 5A). Cells expressing ISGs in a one-gene one-well format were then challenged with a GFP-*Lm* and resulting infection was analyzed by flow cytometry (Fig. 5B). Infection rates were quantified as a percentage of GFP-positive host cells (a measure of infection) among the RFP-positive cell population (a measure of ISG expression). Firefly luciferase (Fluc) was used as a negative control. A panel of ISGs that enhance (*MCOLN2, LY6E*) or inhibit (*IFI6, RTP4, TREX1, IRF2, IRF7, P2RY6,* and *IFITM3*) yellow fever virus (YFV) had no effect on *Lm* infection (Fig. 5C). In addition, in the absence of IFN signaling the cytosolic DNA and RNA sensors *MB21D1* (cGAS) and *DDX58* (RIG-I) (143, 144) as well as *OASL*, an ISG that inhibits hepatitis C virus (134, 145) did not inhibit *Lm* (Fig. 5C). Thus, effects of ISGs can be differentiated between model bacterial and viral pathogens.

Next, I expressed a library of over 350 ISGs in a one-gene to one-well format (134) and performed *Lm* infection as described above. Infectivity of *Lm* obtained from the average of two screen replicates is shown as a dot plot in Fig. 5D (also see Appendix A). The majority of ISGs had little effect on *Lm* infection with the cellular bacterial burdens falling within two standard deviations of the population mean (Z-score less than 2, Fig. 5D). I defined inhibitors of *Lm* infection as those ISGs that restricted infection with Z-score greater than 2. Six ISGs fulfilled these criteria including *PKRD2, UNC93B1, MYD88, AQP9, MAP3K14*, and *TRIM14* (Fig. 5E). In addition, two genes *FCGR1A* and *SCO2* enhanced *Lm* infection with Z-score greater than 2. Repeat trials with independent lentiviral preparations

confirmed statistically significant inhibitory effects for all six ISGs and an enhancing effect for *FCGR1A* (Fig. 5E).

Conclusions

Previously, gain-of-function ISG screens have been highly successful in discovering factors restricting viral infection of human cells (134, 135). Here, I used this technology to examine genes that regulate infection of a model bacterial pathogen.

First, I adapted the flow cytometry based screening approach established by Schoggins et al. to assess infection of GFP-expressing *Lm.* Using a series of virulence gene knockout strains, I demonstrated that flow cytometry is suitable for the detection of all the stages of *Lm* intracellular lifecycle. Preliminary screening suggested, that *Lm* infection is not affected by the known pro- and antiviral genes, suggesting that unique regulators of bacterial infection can be identified. Finally, I screened a library of human type I ISGs for their effects on *Lm* infection. Interestingly, most of the genes tested had no detectable effects on infection, potentially due to their requirement for coexpression with other ISGs or expression in other cell types. As described above, I confirmed infection inhibition by 6 genes (*PKRD2, UNC93B1, MYD88, AQP9, MAP3K14*, and *TRIM14*) as well as an increase in presence of 1 gene (*FCGR1A*). Identification of an enhancer of *Lm* infection among type I ISGs supported our hypothesis that *Lm* could evolve mechanisms to hijack elements of the interferon-mediated immunity to promote its infection and overcome inhibitory mechanisms induced by interferon signaling.

Importantly, this experimental approach can be further expanded to study effects of various other immune transcriptional programs at a single gene level on a diverse range of bacterial pathogens, including both intracellular and extracellular bacteria. Indeed, several collaborative projects have been initiated in the Alto laboratory using the technology described above. I collaborated with Michael Abrams, who generated and assayed a library of type II IFN stimulated genes for inhibitors of *Lm* infection. Further, this approach was successfully utilized by Zixu Liu to identify regulators of *Lm* and *Shigella flexneri* infection among genes stimulated by MAP3K14 (NIK).

In the next chapters, I addressed the mechanisms of *Lm* infection regulation by the strongest inhibitors identified in the ISG screen (MYD88 and TRIM14), as well as the enhancing effect observed in FcγRIa-expressing cells.

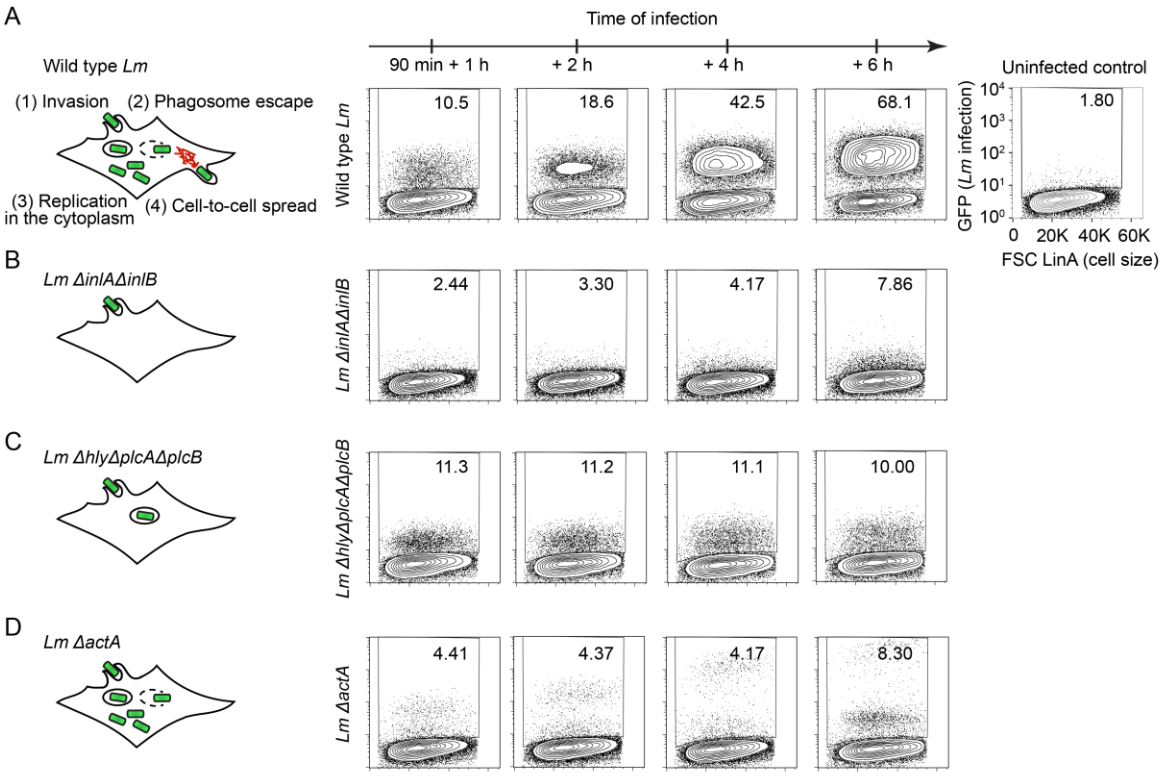

Figure 4: Fluorescence-based screening approach

(A-D) Diagram illustrating cellular lifecycle of wild type *Lm* (A), *Lm ΔinlAΔinlB* (B), *Lm ΔhlyΔplcAΔplcB* (C), *Lm ΔactA* (D). Representative flow cytometry plots of *STAT1*-deficient fibroblasts infected with GFP-expressing wild type *Lm* (A), *Lm ΔinlAΔinlB* (B), *Lm Δhly ΔplcA ΔplcB* (C), and *Lm ΔactA* (D) strains for 1, 2, 4, and 6 h following 1.5 h initial infection. Values in the upper right corner of each plot indicate the percentage of GFP-positive cells in singlet cell population. The uninfected control is presented on the right.

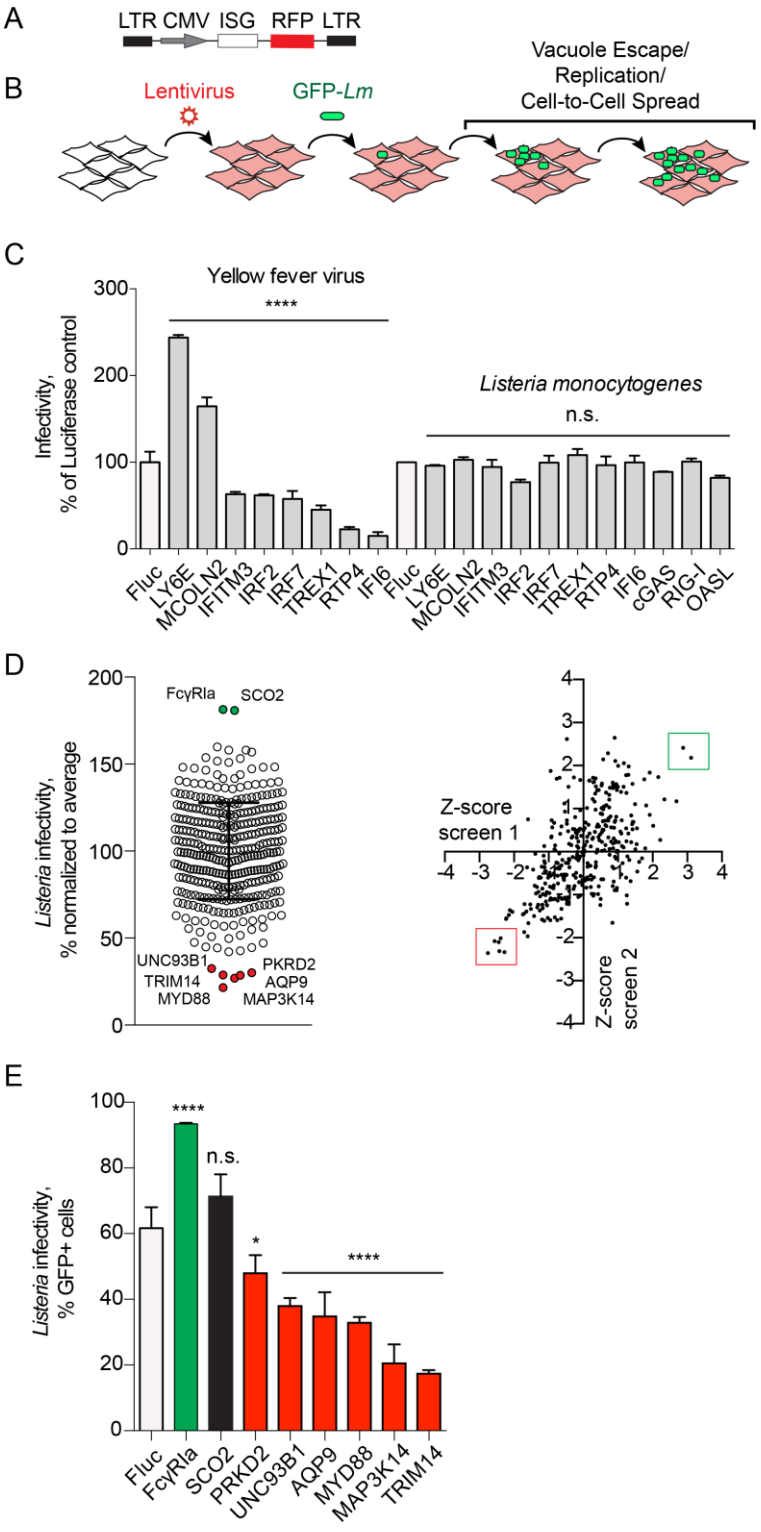
A
LTR CMV ISG RFP LTR
B
Lentivirus
GFP-Lm
Vacuole Escape/
Replication/
Cell-to-Cell Spread
C
Yellow fever virus
****
Listeria monocytogenes
n.s.
Infectivity,
% of Luciferase control
300
200
100
0
Fluc
LY6E
MCOLN2
IFITM3
IRF2
IRF7
TREX1
RTP4
IFI6
Fluc
LY6E
MCOLN2
IFITM3
IRF2
IRF7
TREX1
RTP4
IFI6
cGAS
RIG-I
OASL
D
Listeria infectivity,
% normalized to average
200
150
100
50
0
FcγRIa
SCO2
UNC93B1
TRIM14
MYD88
PKRD2
AQP9
MAP3K14
Z-score
screen 1
Z-score
screen 2
4
3
2
1
-1
-2
-3
-4
E
Listeria infectivity,
% GFP+ cells
100
80
60
40
20
0
****
n.s.
*
****
Fluc
FcγRIa
SCO2
PRKD2
UNC93B1
AQP9
MYD88
MAP3K14
TRIM14

Figure 5: Flow cytometry based gain-of-function screen identifies regulators of *Lm* infection

(A) Schematic of the bicistronic lentiviral vector; CMV, immediate early promoter from human cytomegalovirus; LTR, HIV-1 long terminal repeat. (B) Diagram illustrating the gain-of-function fluorescence-based screen for regulators of *Lm* infection. (C) YFV and *Lm* infectivity in the presence of ISG inhibitors and enhancers of viral infection. Infectivity was measured by flow cytometry as a percentage of GFP-positive cells in RFP-positive population and normalized to a Fluc control for each pathogen (white bars). Error bars represent s.d., n=3 (YFV), n=2 (*Lm*). Statistical significance was determined by one-way analysis of variance (ANOVA) for each pathogen prior to normalization (****, P<0.0001; n.s., not significant). (D) (*Left*) Dot plot of *Lm* infectivity in the presence of expressed ISGs. *Lm* infectivity was measured by flow cytometry in two replicate screens and presented as an average. Error bars represent s.d., n=2. (*Right*) Scatter plot of Z-scores of screen replicates 1 and 2. Genes selected for further confirmation are labeled (*left*) and boxed (*right*). (E) Infectivity of *Lm* in *STAT1*-deficient fibroblasts transduced with lentivirus expressing Fluc (white bar) and selected ISGs from the large-scale screen in (D). *Lm* infectivity was measured similarly to Fig. 5C. Error bars represent s.d., n=3 (*, P<0.05; ****, P<0.0001; n.s., not significant).

CHAPTER THREE

Inhibitors of *Lm* infection

Toll-like receptor signaling components identified as inhibitors of Lm infection in vitro

The identification of *UNC93B1* and *MYD88* as cell-intrinsic inhibitors of *Lm* provided positive validation of the ISG screen. These genes are key components of the immune response to pathogens and function to properly target Toll-like Receptors (TLR) to subcellular compartments and to propagate NF-κB signal transduction, respectively (146, 147). Consistent with the initial ISG screen, a dose-response to infection revealed that *MYD88* and *UNC93B1* reduced *Lm* infectivity (defined as the MOI of *Lm* required to achieve 50% cellular infection during the course of 8 hours) by 9.7-fold and 5.7-fold compared to firefly luciferase control (Fig. 6A).

To determine if the anti-*Lm* activity of MYD88 results from increased NF-κB transcriptional response as predicted, I isolated mRNA from *STAT1*-deficient fibroblasts ectopically expressing MYD88. RNA-seq revealed 123 genes that were upregulated over 2-fold (Appendix B) and included NF-κB signature genes involved in inflammation (e.g. *IL6, IL8, IL1B, CXCL1-3, CXCL5, CCL2*), signal transduction (e.g. *NFKB1/2, RELB, IRAK2, C1QTNF1*), cell adhesion (e.g. *ICAM-1, LAMB3, MMPs*), and complement activation (C3) (Appendix C). To then establish the role of NF-κB activation in the observed antibacterial activity of MYD88, I tested the function of a naturally occurring single nucleotide polymorphism of *MYD88* (rs1319438) that confers a S34Y substitution. While this mutation does not affect the interaction of MYD88 with IRAK1, IRAK4, and Mal, it disrupts MYD88 signaling and NF-κB activation by preventing oligomeric Myddosome complex formation

required for downstream signaling (Fig. 6B) (148, 149). The cellular expression level of MYD88 S34Y was comparable to wild type MYD88 (Fig. 6C), however the mutated protein failed to activate NF-κB (Fig. 6D). More importantly, MYD88 S34Y did not inhibit *Lm* infection (Fig. 6E). These findings indicate that MYD88-dependent suppression of *Lm* infection results from strong NF-κB transcriptional activation and currently unknown effector mechanisms.

The ISG screen also revealed *AQP9, PKRD2*, *MAP3K14*, and *TRIM14* as potent inhibitors of *Lm* infection, suggesting that these proteins may harbor novel antibacterial activities. Aquaporin 9, encoded by *AQP9*, is a transmembrane channel involved in water and small solute transport (150), whereas PRKD2 and MAP3K14 are kinases implicated in membrane trafficking and immune signaling, respectively (151, 152). It is currently unclear how expression of these genes blocks *Lm* infection. Among the newly identified anti-listerial ISGs, TRIM14 exhibited the greatest inhibitory activity (Fig. 5E). Interestingly, this protein has recently been linked to antiviral defense through several independent mechanisms (153-155) but has not been previously implicated in antibacterial immunity.

Antiviral protein TRIM14 inhibits Lm infection in the absence of a transcriptional response

TRIM14 is a member of the tripartite motif-containing (TRIM) gene superfamily that includes proteins involved in innate immunity, transcriptional regulation, cell proliferation, and apoptosis (156). While several family members exhibit anti-viral functions (157), their role in bacterial pathogenesis remains poorly understood. Previously, I found that expression of IFN-inducible TRIM5, TRIM21, TRIM25, TRIM34, and TRIM38 had no effect on *Lm* infection (Fig. 7A), suggesting that TRIM14 is a unique anti-bacterial effector among the

IFN-stimulated TRIMs. As shown in Fig. 7B, the domain architecture of TRIM14 is distinct from other family members as it is does not encode the RING E3-ligase domain typically found within the N-terminal tripartite motif, and is therefore likely to function through an alternative mechanism (156). I next asked if TRIM14-mediated antibacterial activity could be attributed to one of its structural domains. Based on the available crystal structures of truncated TRIM proteins (158, 159), I generated TRIM14 constructs consisting of either the B-box with coiled-coil (residues 1-255) or the PRY/SPRY domain (residues 158-442). Notably, separate domains of TRIM14 had no effect on *Lm* infection (Fig. 7C), indicating that the full-length TRIM14 is required for the anti-bacterial activity.

TRIM14 was recently reported to play an important role in IFN and NF-κB activation during viral infection (153, 154). It associates with the mitochondria wherefrom it links MAVS and NEMO to NF-κB and IRF3-activated transcription (154). It has also been shown to positively regulate type I IFN signaling by inhibiting cGAS degradation (153). However, my studies were performed in *STAT1*-deficient fibroblasts that cannot be activated by IFN, suggesting that the anti-*Lm* activity of TRIM14 is not associated with this ascribed function. Furthermore, a critical lysine in TRIM14, K365, was shown to be required for IFN activation by TRIM14 in mitochondria (154). However, I found that K365 was not necessary for the antibacterial function of TRIM14 (Fig. 7C). Finally, ectopic expression of TRIM14 in *STAT1*-deficient fibroblasts induced the expression of 43 genes by over 2-fold and only 5 genes had greater than 5-fold increase compared to over 100-fold increase in TRIM14 (Appendix D). Ingenuity Pathway Analysis failed to identify possible upstream transcriptional regulators (Fig, 7D), and the observed transcriptional response did not exhibit

an NF-κB or IRF3 signature as would be predicted if TRIM14 regulated MAVS and NEMO as previously reported.

To then determine if TRIM14 functioned through a transcription-independent mechanism during infection, I compared host mRNA produced during *Lm* infection (6 hours) in cells expressing TRIM14 or luciferase as a control. *Lm* infection altered expression of hundreds of genes in luciferase-expressing cells (Appendix E). As expected, TNFα, NF-κB and IL1A were among the strongest predicted upstream regulators (Fig. 7E and Appendix F). Interestingly, expression of TRIM14 did not alter the host transcriptional response to *Lm* infection, further suggesting that TRIM14 has a direct anti-bacterial function in host cells. Taken together, these results indicate that the gain-of-function ISG screening technique can resolve direct mechanisms of inhibition of bacteria, similar to what has been demonstrated for viruses (134).

Conclusions

In the current chapter, I performed initial characterization of the ISGs identified as the strongest inhibitors of *Lm* infection in the large-scale screen, as described earlier. By using both RNA sequencing and a naturally occurring disease-related mutation, I confirmed that the TLR adaptor protein MYD88 relied on the NF-κB activation for the observed reduction in bacterial infection. Future studies will address the roles of MYD88 and individual MYD88-upregulated genes in context of *Lm* infection and overall interferon signaling.

In contrast to MYD88, another inhibitor TRIM14 was not found to activate a robust transcriptional profile in *STAT1*-deficient fibroblasts, potentially acting as a direct antibacterial protein. Interestingly, this mechanism is distinct from the TRIM14-mediated

antiviral immunity, that has been proposed to rely on activation of both NF-κB and type I IFN (153, 154). More in-depth studies will be required to characterize the mechanism of TRIM14-mediated inhibition of *Lm* infection and potentially its regulation of other intracellular bacteria.

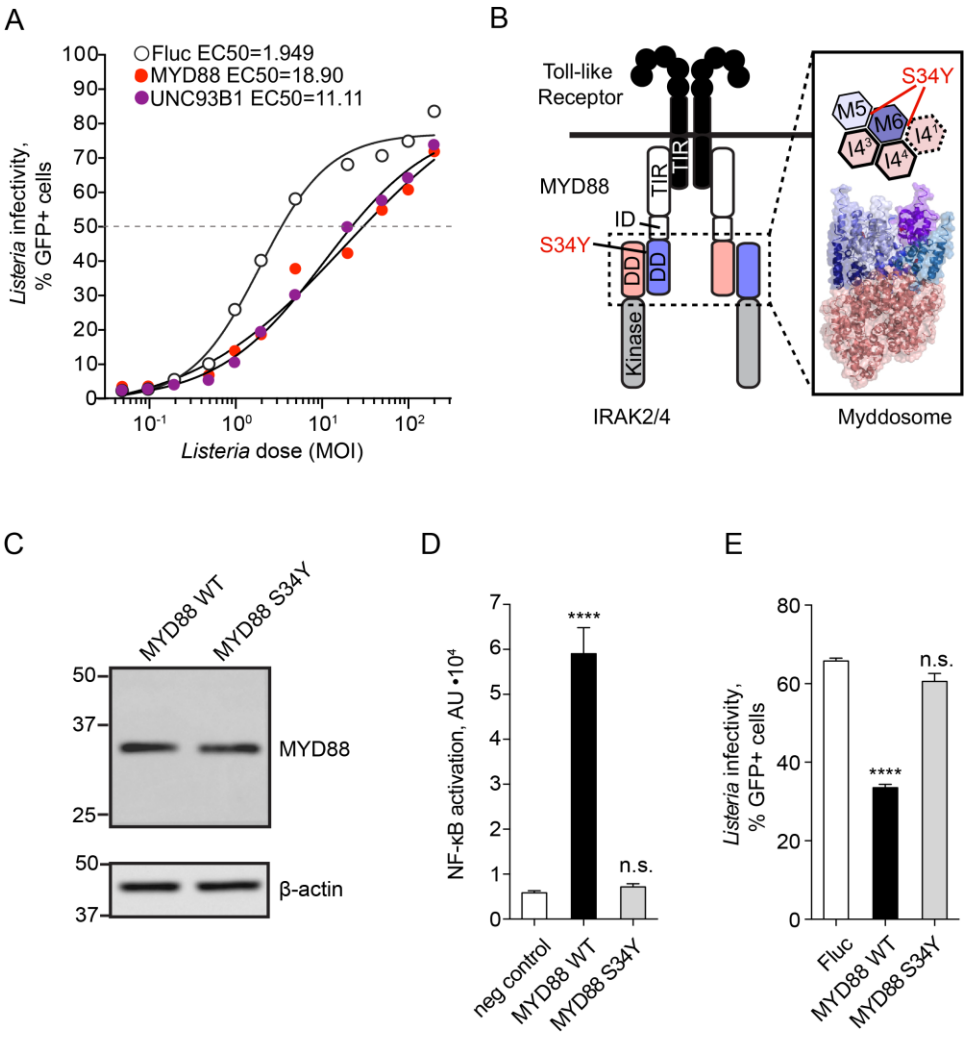

Figure 6: MYD88 induces an anti-bacterial transcriptional response

(A) Infectivity of *Lm* in *STAT1*-deficient fibroblasts transduced with lentivirus expressing Fluc (empty circles), *MYD88* (red) and *UNC93B1* (purple) was tested over a range of MOI. Dose-response curves were fitted to a four-parameter sigmoidal model and EC50 values calculated using GraphPad Prism software: $EC50_{Fluc}$=1.949, $EC50_{MYD88}$=18.90, $EC50_{UNC93B1}$=11.11. (B) Diagram illustrating Toll-like receptor (TLR) signaling complex (left) and fragment of planar arrangement of the Myddosome complex (PDB 3MOP) and

localization of the MYD88 Ser34 between MYD88 M5 and M6 as well as MYD88 M6 and IRAK I4[1] is shown. (C) Western blot analysis of MYD88 expression in *STAT1*-deficient fibroblasts transduced with lentivirus expressing wild type and S34Y mutant MYD88. Equal amounts of each lysate (30μg total protein as measured by BCA assay) were loaded per lane. Actin is shown below as a loading control. (D) NF-κB-luciferase activity in untransduced *STAT1*-deficient fibroblasts (negative control, white bar), transduced with lentivirus expressing wild type (WT, black bar), or S34Y mutant MYD88 (S34Y, grey bar) and transfected with the reporter plasmid pNF-κB-luciferase. Error bars represent s.d., n=3. Statistical significance was determined by one-way analysis of variance (ANOVA) (****, $P< 0.0001$; n.s., not significant). (E) Infectivity of *Lm* in *STAT1*-deficient fibroblasts transduced with lentivirus expressing Fluc (white bar), wild type MYD88 (WT, black bar), or MYD88 S34Y mutant (S34Y, grey bar). *Lm* infectivity was measured by flow cytometry and statistical significance determined by one-way ANOVA, error bars represent s.d., n=3 (****, $P< 0.0001$, n.s., not significant).

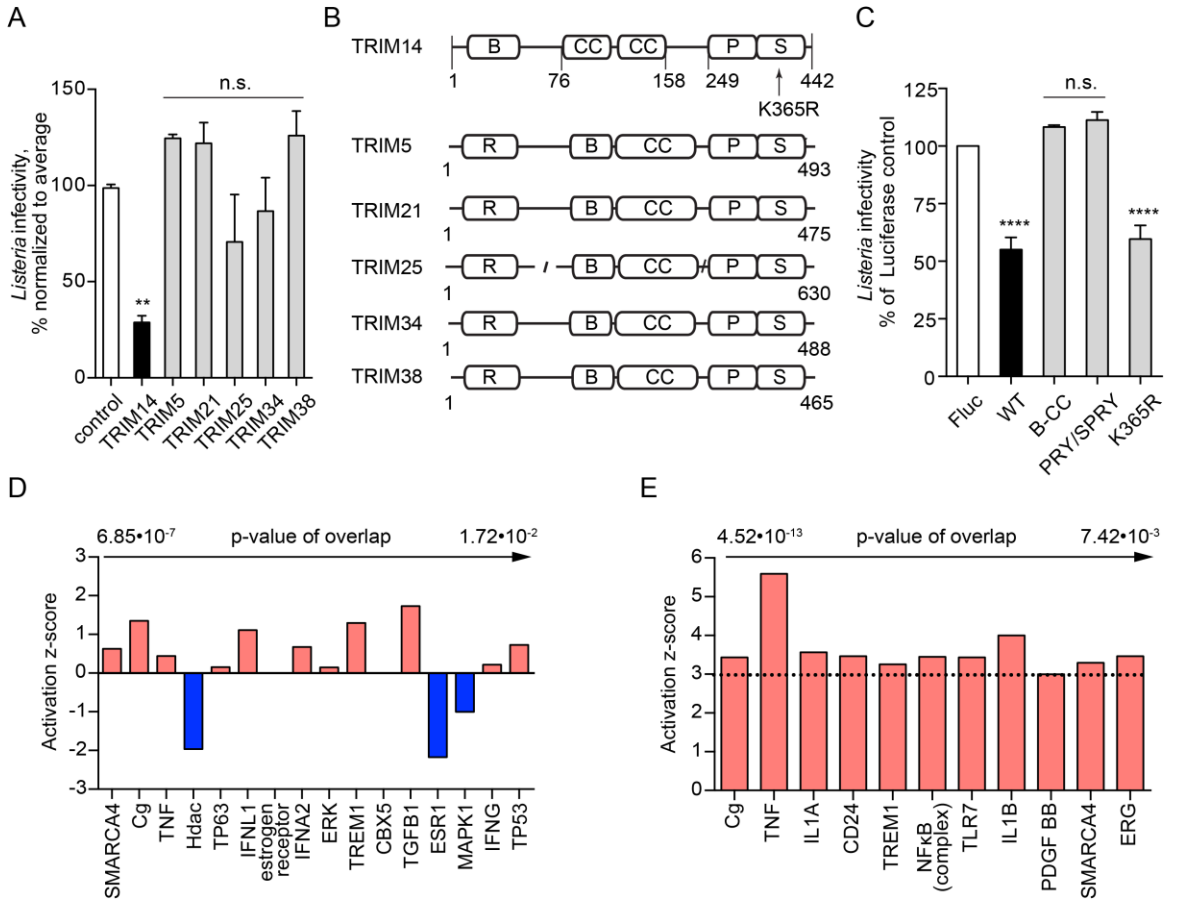

Figure 7: TRIM14 inhibits *Lm* infection in the absence of transcriptional response

(A) Infectivity of wild type *Lm* in *STAT1*-deficient fibroblasts transduced with lentivirus expressing control gene (white bar), *TRIM14* (black bar), *TRIM5*, *TRIM21*, *TRIM25*, *TRIM34*, and *TRIM38* (grey bars) in a large-scale screen. *Lm* infectivity was measured as in Fig. 5C, error bars represent s.d., n=2 (**, P<0.01; n.s., not significant). (B) Domain architecture of IFN I regulated TRIM proteins. R, RING-type zinc finger domain; B, B box-type zinc finger domain; CC, coiled-coil domain; P S, PRY/SPRY domain. (C) Infectivity of wild type *Lm* in *STAT1*-deficient fibroblasts transduced with lentivirus expressing Fluc (white bar), wild type TRIM14 (WT, black bar), only B-box and coiled-coil domains of

TRIM14 (B-CC, grey bar), only PRY/SPRY domain of TRIM14 (PRY/SPRY, grey bar), and TRIM14 K365R mutant (K365R, grey bar). *Lm* infectivity was measured as in Fig. 5C, error bars represent s.d., n=3 (****, P<0.0001; n.s., not significant). (D) Upstream regulators identified by Ingenuity Pathway Analysis for TRIM14-regulated genes, only top regulators by p-value of overlap are shown. (E) Upstream regulators identified by Ingenuity Pathway Analysis for genes, regulated by *Lm* infection in *STAT1*-deficient fibroblasts, sorted by p-value of overlap with a cutoff of z-score≥3

CHAPTER FOUR

FcγRIa as an enhancer of *Lm* infection

FcγRIa increases Lm internalization independently of the canonical host receptors

In addition to anti-bacterial ISGs, I identified a high affinity immunoglobulin receptor FcγRIa (CD64) as an enhancer of *Lm* infection. A dose-response experiment indicated that FcγRIa potentiated *Lm* infectivity by over 100-fold (Fig. 8A). Consistent with the flow cytometry measurements, a greater number of individual bacteria were found in the cytoplasm of FcγRIa-expressing cells (Fig. 8B) and FcγRIa increased the total number of cell surface protrusions emanating from infected cells (Fig. 8C).

Because FcγRIa is a cell surface expressed protein, I hypothesized that it may enhance *Lm* infection by promoting primary internalization into host cells or secondary cell-to-cell spread. To distinguish between these possibilities, I visualized *Lm* infection foci, which are formed from *Lm* invasion of a single host cell followed by rapid cell-to-cell transmission. Cell monolayers were infected with very low doses of *Lm* (at MOI 0.015, 0.05, 0.1) and the formation of foci was evaluated 30 h post infection (see Materials and Methods). Cellular expression of FcγRIa increased the total number of infection foci compared to control (Fig. 9A). However, the diameter and surface area of individual foci were not altered in presence of FcγRIa (Fig. 9B). Thus, FcγRIa enhances efficiency of primary *Lm* invasion, yet has little effect on secondary cell-to-cell spread.

I next asked if FcγRIa potentiated *Lm* entry by coordinating interactions with the host *Lm* internalization receptors E-cadherin or c-Met (160). In order to do this, I introduced frameshift mutations into *CDH1* (encoding E-cadherin) and *MET* (encoding c-Met) by

CRISPR/Cas9 resulting in non-coding genetic disruption of these loci (Appendix G). As expected, the invasive capacity of *Lm* was significantly attenuated in *CDH1/MET*-deficient cells (Appendix G), which could be restored by ectopic expression of either *CDH1* or *MET* (Fig. 9C). Remarkably, ectopic expression of FcγRIa in *CDH1/MET*-deficient cells increased *Lm* infection to levels comparable with *MET* complementation (Figs 9C and 9E). In addition, mutant *Lm ΔinlAΔinlB* lacking the invasins InlA and InlB that directly bind host surface proteins E-cadherin and c-Met, respectively, readily infected *CDH1/MET*-deficient cells expressing FcγRIa (Figs 9D, 9F, 9G). Therefore, FcγRIa supports bacterial uptake independently of "classic" host *Lm* internalization receptors E-cadherin and c-Met as well as bacterial invasins InlA and InlB.

Reconstitution of Fcγ receptor function in non-phagocytic cells

Fcγ receptors bind the Fc (antigen non-specific) region of IgG antibodies produced as a part of adaptive response to infection in mammals. The human Fcγ receptor family includes activating receptors FcγRIa, FcγRIIa, FcγRIIc, FcγRIIIa and FcγRIIIb, as well as an inhibitory receptor FcγRIIb. Crosslinking of activating Fcγ receptors by IgG typically results in the phagocytosis of opsonized particles and cellular activation, facilitating destruction of the pathogens and induction of inflammation, respectively (161). In humans, FcγRIa is constitutively expressed on monocytes and macrophages, and its expression is upregulated by type I and II interferons and other signaling molecules, such as IL-10 (162). It consists of three extracellular immunoglobulin (Ig)-like domains, a single transmembrane domain, and a short cytoplasmic tail that does not contain any known signaling motifs. During receptor engagement with IgGs, FcγRIa recruits the accessory immunoreceptor tyrosine-based

activation motif (ITAM)-containing γ-chain (FcεRIg). Clustering of the FcγRIa with γ-chain triggers intracellular signaling cascades involving Syk and Src family kinases necessary for FcγRIa-mediated particle phagocytosis (163, 164). Additionally, FcγRIa has been shown to interact with FcγRIIa, using its ITAM-motif to signal in the absence of the γ-chain (165).

To compare the mechanism of *Lm* invasion to the classic IgG-coated particle uptake though FcγRIa alone in the absence of possible crosstalk with other Fcγ receptors (161, 165), I developed a model of Fc-receptor functions in a non-phagocytic cell type (163, 166-168). I first reconstituted IgG-coated particle internalization via FcγRIa. U-2 OS cells were transduced with a lentivirus expressing FcγRIa, or Fluc as a negative control. Latex beads were coated with human IgG and labeled with anti-human secondary antibody conjugated to Alexa Fluor 488 (green). The IgG opsonized particles were incubated with U-2 OS cells for 1.5 h at 37°C and then shifted to 4°C to inhibit further uptake. Cell-surface bound beads were differentiated from internalized beads by incubating samples with anti-human secondary antibody conjugated to DyLight 405 (blue) without cell permeabilization (Fig. 10A). Under these conditions, internalized beads are protected from the secondary antibody and are visualized as green beads by fluorescence microscopy. In contrast, surface-bound beads are labeled with both green and blue secondary antibodies.

As expected, luciferase-expressing U-2 OS cells showed no interaction with IgG-coated beads. In contrast, FcγRIa recruited IgG-beads to the cell surface, but revealed low levels of bead internalization (Figs 10B and 10C). This may be anticipated since U-2 OS cells do not express endogenous γ-chain (FcεR1g). Indeed, co-expression of FcγRIa with the γ-chain (FcεR1g) fully reconstituted FcγRIa-mediated internalization of IgG-coated beads

(Fig. 10C). I also cloned and tested another Fcγ receptor – FcγRIIa – a low-affinity immunoglobulin receptor that possesses its own internal ITAM motif and therefore, does not require interaction with the γ-chain for particle internalization. FcγRIIa mediated similar high levels of IgG-coated bead phagocytosis (Figs 10B and 10C). Thus, I have established a robust and simplified cellular system to study the function of individual human Fcγ receptors in context of both particle opsonization and pathogenic *Lm* infection.

FcγRIa mediates Lm internalization independent of γ-chain and pathogen opsonization

As shown in Fig. 8A, *Lm* readily invaded U-2 OS cells expressing FcγRIa. Surprisingly, this phenotype did not require co-expression of the ITAM-containing γ-chain, suggesting that *Lm* internalization by FcγRIa occurs through a distinct mechanism compared to IgG-coated particle uptake. It has been previously reported that FcγRIa interacts with the γ-chain exclusively through the transmembrane domain (169). I therefore asked if this region of FcγRIa was necessary for *Lm* internalization. I targeted the extracellular Ig-like domains of FcγRIa to the cell surface via a GPI-anchor signal of LFA-3 (FcγRIa-GPI) (170). This chimeric protein was expressed on the cell surface similar to the wild type FcγRIa (Fig. 11A). Notably, as shown in Fig. 11B, FcγRIa-GPI induced the same level of *Lm* infection as the wild type protein (3.03 fold), further confirming that FcγRIa does not interact with the γ-chain during *Lm* internalization. Additionally, FcγRIa does not require interaction with any other signaling protein through the transmembrane domain.

The ability of *Lm* to be internalized by FcγRIa in the absence of the signaling γ-chain suggested that the recognition of *Lm* might also occur independently of IgG opsonization. Several lines of evidence support this conclusion. First, *Lm* infection was not enhanced by

expression of other members of the Fc receptor family (Fig. 11C), including FcγRIIa that, as shown in Fig. 10C, was able to internalize IgG-coated beads. Second, FcγRIa potentiated *Lm* invasion in serum-free (and therefore, IgG-free) conditions (Fig. 11D). Third, reducing the FcγRIa affinity for all types of IgG up to 100-fold by introducing an H174E mutation in the D2 Ig-like domain (171) did not affect its ability to enhance *Lm* infection (Fig. 11E). Finally, FcγRIa had no effect on the infection rate of other intracellular bacteria *Shigella flexneri* or *Salmonella* Typhimurium (Fig. 11F). Therefore, internalization through FcγRIa is independent of non-specific pathogen opsonization with serum IgG. Together, these data indicate that *Lm* invades cells independently of the well-established route of phagocytosis, which involves IgG opsonization and ITAM-mediated intracellular signaling through the FcγRIa-γ-chain complex.

FcγRIa contributes to the Lm internalization in human phagocytic cells in vitro

To determine the contribution of FcγRIa to *Lm* infection in a naturally phagocytic human cell type that expresses endogenous FcγRIa, I disrupted cell surface expression of *FCGR1A* in THP-1 human monocytes using a lentiviral CRISPR/Cas9 system (172) (Figs 12A and 12B). *Lm* infected 54.45 ± 2.19% wild-type THP-1 cells compared to 44.48 ± 2.98% of *FCGR1A*-deficient cells (Fig. 12C) representing a statistically significant decrease in infection ($p=0.0095$, $n=3$). These data suggest that *Lm* is internalized through multiple pathways with 18.13 ± 8.1% ($n=3$) of the total host cell infection mediated by FcγRIa (Fig. 12D). To then determine if the observed decrease in *Lm* infection was due to the newly defined mechanism of FcγRIa-*Lm* interaction described above rather than a general defect in IgG-coated pathogen internalization, I performed experiments in serum-free conditions. A

significant reduction in *Lm* infection was observed in *FCGR1A*-deficient THP-1 (44.52 ± 1% infected wild type cells compared to 38.44 ± 0.69% of *FCGR1A*-deficient cells; p=0.0010, n=3) (Fig. 12C) with a 13.63 ± 2.52 % (n=3) relative contribution of FcγRIa under these conditions (Fig. 12D). Thus, endogenous FcγRIa contributes to *Lm* invasion of phagocytic monocytes independently of IgG opsonization similar to what was observed in the reconstituted cellular system.

FcγRIa-Lm interaction exhibits a narrow host species tropism

Having established that human FcγRIa enhances *Lm* infection, I next asked whether mammalian FcγRIa orthologs exhibit similar functions. Species-specific FcγRIa coding sequences were commercially synthesized, and included (1) mouse (naturally resistant to oral *Lm* infection), (2) sheep and rabbit (known to be susceptible to *Lm*), and (3) panda (uncharacterized susceptibility to *Lm* infection). All FcγRIa orthologs were expressed on the cell surface of U-2 OS cells as determine by IgG-coated latex bead binding assays (Fig. 13A). I then co-expressed these receptors with the γ-chain and tested whether they were fully functional in human cells by measuring the rates of IgG-opsonized particle internalization. All tested FcγRIa induced similar levels of IgG-bead phagocytosis (Fig. 13B), suggesting that they were indeed functioning as internalization receptors for opsonized particles. Next, I assessed the ability of non-primate FcγRIa to potentiate internalization of *Lm*. FcγRIa of mouse, sheep and panda failed to enhance *Lm* infection (Fig. 13C). Moreover, murine FcγRIa did not affect *Lm* infection even when co-expressed with the γ-chain in murine cells (Fig. 13D). Unexpectedly, rabbit FcγRIa was found to potentiate *Lm* internalization in the absence of the γ-chain (Fig. 13D). Rabbit is a natural host for *Lm* and exhibits severe listeriosis upon

infection (59). Analysis of the multiple sequence alignment of FcγRIa from these species did not pinpoint a single residue or a motif that was common between human and rabbit yet divergent from other FcγRIa proteins tested, suggesting a more complex interaction between host and pathogen molecules (Appendix H). Nevertheless, these data indicate that FcγRIa-*Lm* interaction is not only pathogen-specific (Fig. 11F), but also demonstrates host protein tropism.

Conclusions

In this chapter, I focused on dissecting the mechanism of FcγRIa-mediated potentiation of *Lm* infection. First, using CRISPR/Cas9-mediated gene editing and modified plaque assay I demonstrated that in an overexpression system FcγRIa acts as a *Lm* internalization factor rather than an adhesion molecule and mediates *Lm* uptake in the absence of the classic *Lm* invasion receptors (Fig. 9). Further, I successfully reconstituted phagocytosis of the IgG-opsonized particles by the canonical FcγRIa-mediated pathway in non-phagocytic cells (Fig. 10). Notably, *Lm* uptake by FcγRIa followed a distinct non-canonical pathway that I characterized as independent of both ITAM-initiated signaling and IgG opsonization (Fig. 11). Importantly, endogenous FcγRIa expressed on phagocytic cells was found to contribute to *Lm* uptake, confirming the phenotype observed in an overexpression system (Fig. 12). Lastly, FcγRIa-*Lm* interaction exhibits a narrow host tropism, with only human and rabbit FcγRIa potentiating infection among other species tested, both susceptible and resistant to natural *Lm* infection (Fig. 13)

Taken together, these data provide important initial insights into a novel mechanism of *Lm* internalization through an immunoglobulin receptor FcγRIa. Identification of FcγRIa as a *Lm* uptake factor seems especially significant, since FcγRIa-expressing cells, such as macrophages and activated neutrophils, represent one of the major targets of *Lm* during infection. Several aspects of FcγRIa-*Lm* interaction and internalization, however, remain to be uncovered. These include identifying the FcγRIa-binding bacterial ligand, dissecting the intracellular signaling pathways behind the ITAM-independent internalization, as well as the role of FcγRIa in *Lm* pathogenesis *in vivo*. Since murine FcγRIa was found to have no enhancing effect on *Lm* infection, the latter would require use of a humanized mouse model with all murine Fc gamma receptors replaced with their human homologues. One of the FcγR-humanized mouse model was generated by the laboratory of Dr. J. Ravetch and shown to fully recapitulate the functions of Fcγ receptors *in vivo* (173).

To begin to address the outstanding questions regarding FcγRIa-mediated *Lm* uptake, I next performed a series of genetic experiments aiming to identify *Lm* surface protein responsible for the interaction with FcγRIa and subsequent internalization.

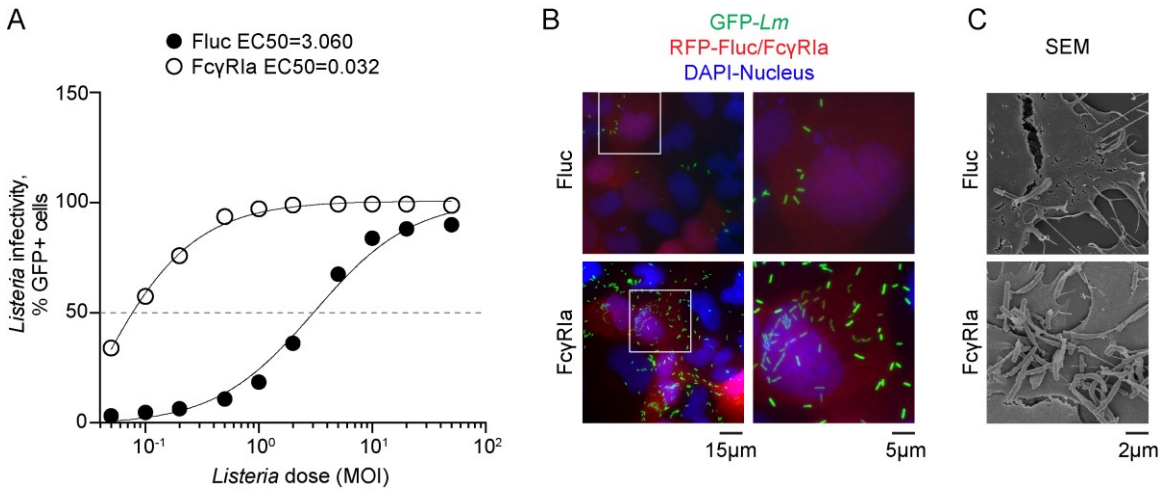

Figure 8: FcγRIa induces a robust *Lm* infection

(A) U-2 OS cells transduced with lentivirus expressing Fluc or FcγRIa were infected with increasing MOI of wild type GFP-expressing *Lm* for 12 h after initial infection. Infectivity was measured by flow cytometry. Dose-response curves were fitted to a sigmoidal model using GraphPad Prism software. (B)(C) Fluorescence microscopy (B) and scanning electron microscopy (C) of U-2 OS cells transduced with lentivirus co-expressing TagRFP and Fluc (*upper*) or FcγRIa (*lower*) and infected with GFP-expressing wild type *Lm* for 5.5 h (B) and 7.5 h (C), following 1.5 h of initial infection.

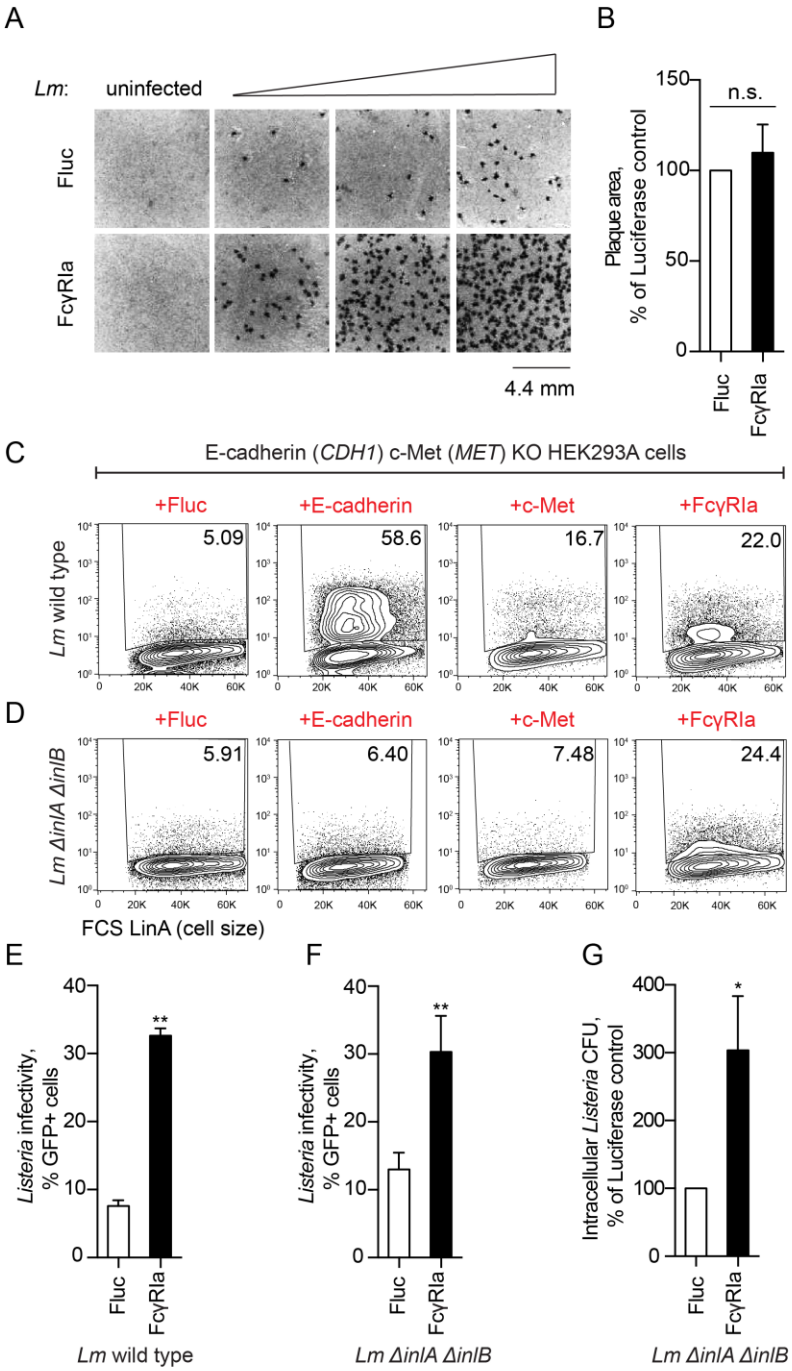

Figure 9: FcγRIa increases *Lm* invasion independently of known *Lm* internalization receptors

(A) Confluent monolayers of HEK293A cells transduced with lentivirus expressing Fluc (*upper*) or FcγRIa (*lower*) were infected with wild type *Lm* and stained for bacteria with (3-(4, 5-dimethylthiazolyl-2)-2,5-diphenyltetrazolium bromide (tetrazolium MTT) 30 h after initial infection. Non-infected controls shown on the left, samples infected with increasing amounts of *Lm* shown left to right. A representative field of each sample is shown. (B) Area of individual plaques obtained in (A) was quantified by using ImageJ software, and presented normalized to Fluc control. Error bars represent s.d., n=3 independent experiments. Statistical significance was determined by t-test (n.s., not significant). (C-D) Representative flow cytometry plots showing wild type *Lm* (C) or *Lm ΔinlAΔinlB* (D) infection of *CDH1/MET*-deficient HEK293A (clone P4E4) transduced with lentivirus co-expressing TagRFP and Fluc, c-Met, E-cadherin or FcγRIa as indicated. Values in the upper right corner of each plot indicate the percentage of GFP-positive cells in the total RFP-positive cell population. (E-G) Infectivity of wild type *Lm* (WT) (E) and *Lm ΔinlAΔinlB* (F, G) in *CDH1/MET*-deficient HEK293A cells transduced with lentivirus expressing Fluc (white bars) or FcγRIa (black bars). *Lm* infectivity was measured by flow cytometry (E, F) or as a CFU number of surviving *Lm* in a gentamicin protection assay and normalized to Fluc control (G). Error bars represent s.d., n=3. Statistical significance was determined by t-test (*, $P<0.05$; **, $P<0.01$).

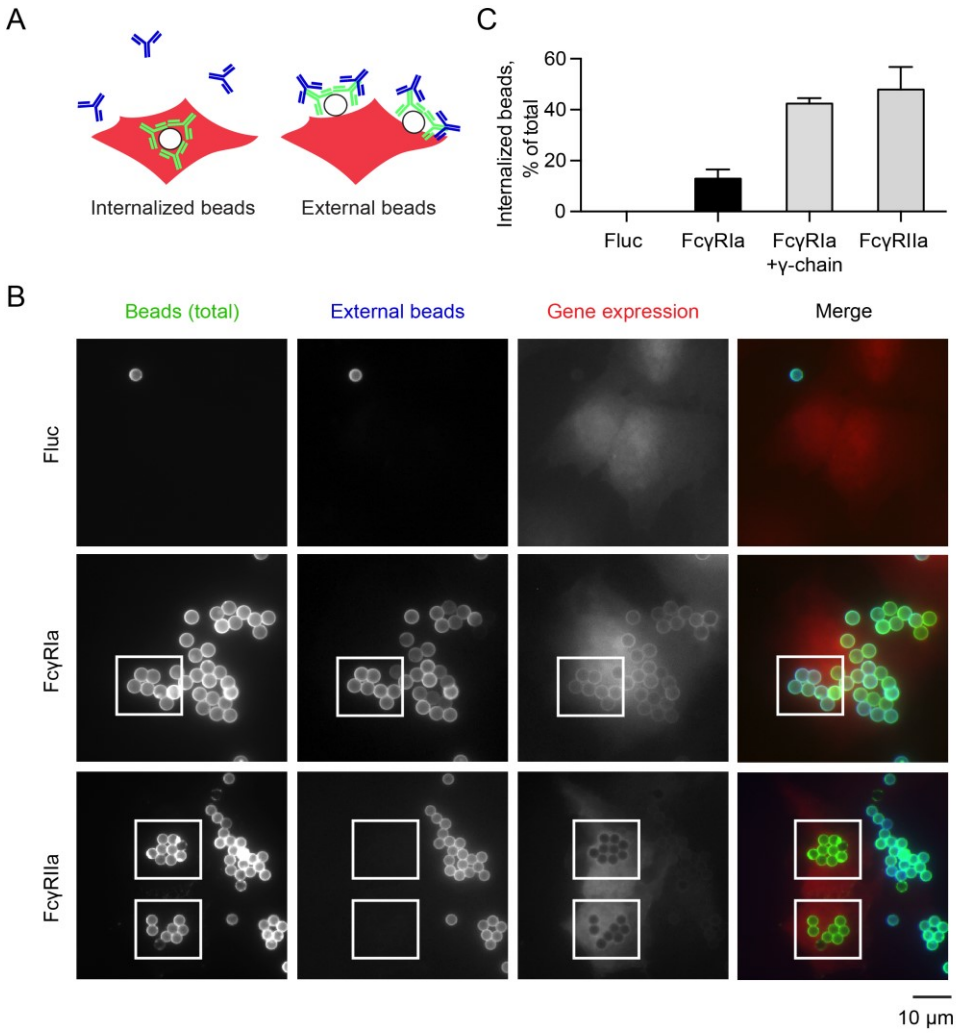

Figure 10: Developing a cellular model of FcγRIa function

(A) Diagram illustrating the phagocytic assay used to reconstitute FcγR function using Alexa Fluor 488 IgG (green) and DyLight 405 (blue) IgG-labeled polystyrene beads. (B) Representative fluorescence microscopy images of U-2 OS cells transduced with lentivirus co-expressing TagRFP and Fluc, FcγRIa, or FcγRIIa, incubated with Alexa Fluor 488 IgG-opsonized beads (green) for 1.5 h, followed by secondary DyLight 405 IgG labeling (blue) of

external beads. (C) Quantification of phagocytosed IgG-coated beads. Error bars represent s.d., 160 cells were counted for each of three independent experiments.

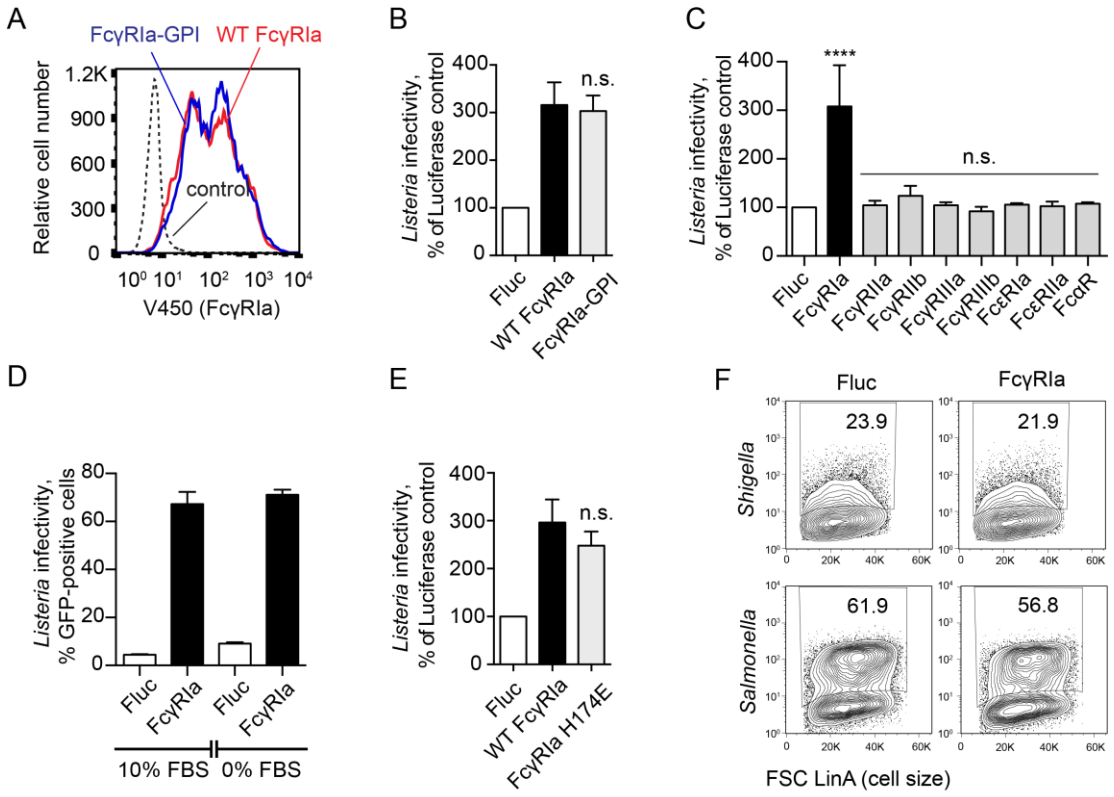

Figure 11: FcγRIa increases *Lm* infection independently of the γ-chain and opsonization by IgG

(A) Flow cytometric analysis of surface expression of wild type FcγRIa and FcγRIa-GPI in lentiviral transduced HEK293A cells. (B) Infectivity of *Lm ΔinlAΔinlB* in HEK293A cells transduced with lentivirus expressing Fluc (white bar), wild type FcγRIa (black bar), or FcγRIa-GPI (grey bar). *Lm* infectivity was measured as in Fig 2C, error bars represent s.d., n=3 (n.s., not significant, as compared to wild type FcγRIa). (C) Infectivity of wild type *Lm* in *CDH1/MET*-deficient HEK293A cells (clone P4E4) transduced with lentivirus expressing the indicated Fc-receptors. *Lm* infectivity was measured as in Fig 2C, error bars represent s.d., n=3 (****, P<0.0001, n.s., not significant). (D) Infectivity of wild type *Lm* in U-2 OS

cells stably expressing Fluc (white bars) or FcγRIa (black bars) in DMEM media, containing 10% FBS (*left*) or FBS-free media (*right*). *Lm* infectivity was measured after 2 h initial invasion time and 3 h infection, by flow cytometry and represented as a percentage of GFP-positive cells, n=3, s.d. (E) Infectivity of wild type *Lm* in HEK293A cells transduced with lentivirus expressing Fluc (white bar), wild type FcγRIa (black bar), or H174E mutant FcγRIa (grey bar). *Lm* infectivity was measured as in Fig 2C, error bars represent s.d., n=3 (n.s., not significant, as compared to wild type FcγRIa). (F) Representative flow cytometry plots of *Shigella flexneri* (*top*) and *Salmonella* Typhimurium (*bottom*) infections in *STAT1*-deficient fibroblasts transduced with lentivirus co-expressing TagRFP and Fluc (*left*) or FcγRIa (*right*).

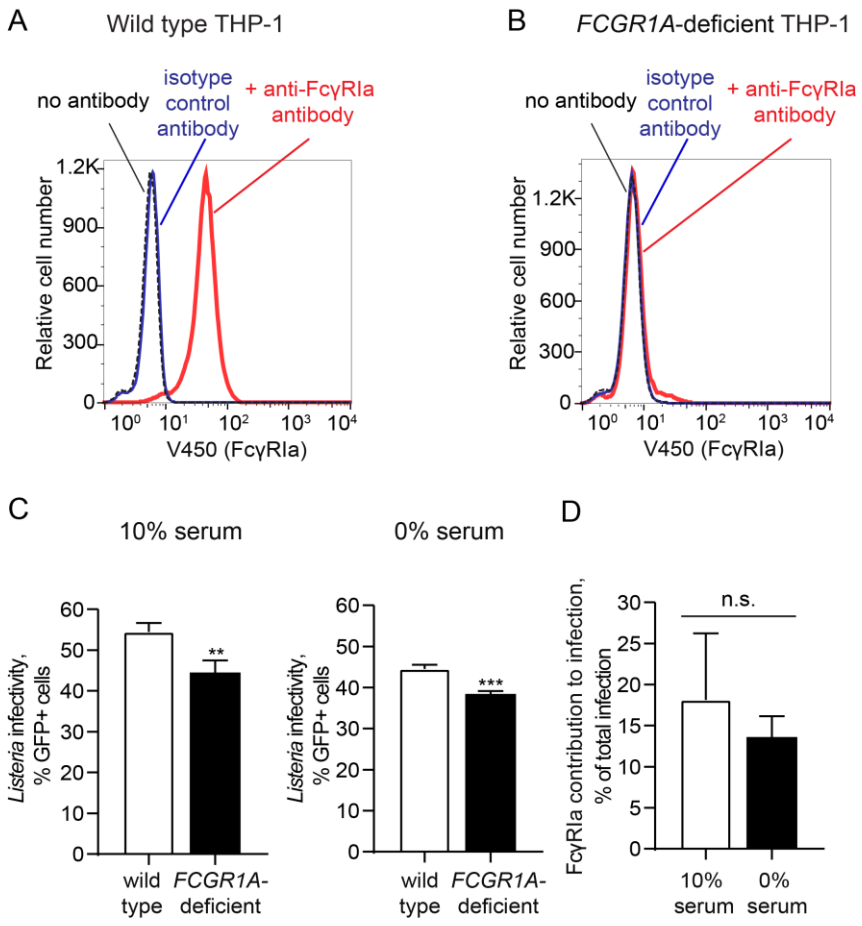

Figure 12: FcγRIa contributes to the *Lm* internalization in human phagocytic cells *in vitro*

(A-B) Surface expression of FcγRIa in wild type (A) and *FCGR1A*-deficient (B) THP-1 cells was analyzed by flow cytometry. (C) Infectivity of wild type *Lm* in wild type (white bars) and *FCGR1A*-deficient (black bars) THP-1 cells in 10% FBS/RPMI medium (*left*) or serum-free RPMI (*right*). Cells were infected (MOI=5) for an initial 90 min period, when gentamicin was added and infection was allowed to proceed for an additional 6 h prior to collection. *Lm* infectivity was measured as percentage of GFP-positive cells, n=3, error bars represent s.d., significance was determined by t-test for each condition (**, P<0.01; ***,

P<0.001). (D) Relative contribution of FcγRIa to *Lm* infection in THP-1 cells in 10% FBS/RPMI and serum-free RPMI medium, calculated as described in Materials and Methods, n=3, error bars represent s.d. (n.s., not significant).

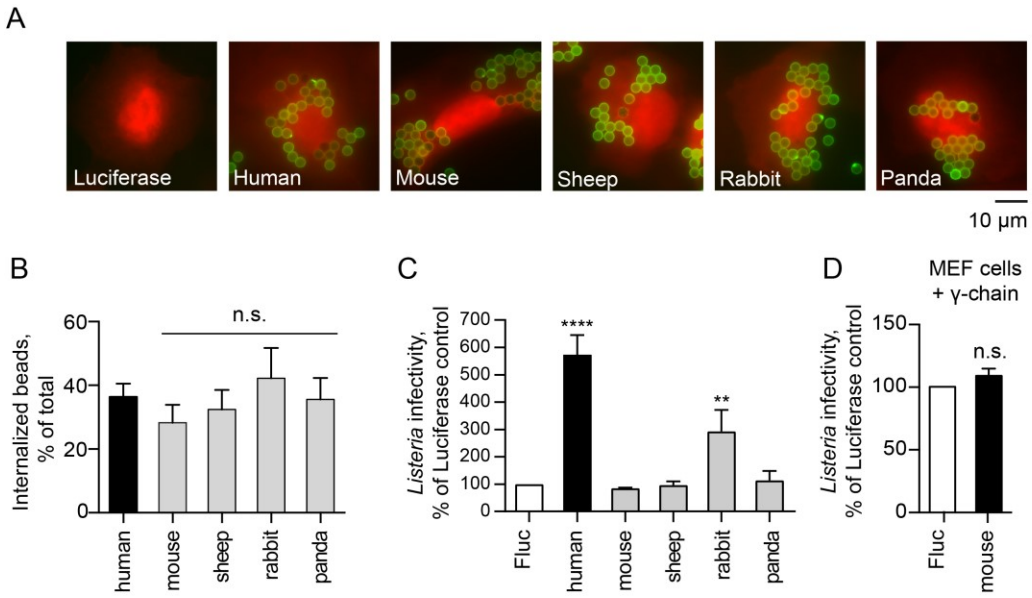

Figure 13: FcγRIa-mediated *Lm* invasion exhibits host species tropism

(A) Representative fluorescence microscopy images of U-2 OS cells transduced with lentivirus co-expressing TagRFP and Fluc or FcγRIa from indicated species incubated with Alexa Fluor 488 IgG-opsonized beads (green) for 1.5 h. (B) Quantification of phagocytosed human IgG-coated beads in U-2 OS cells transduced with lentivirus expressing γ-chain and FcγRIa of indicated species. Error bars represent s.d., 40 cells were counted for each of the four independent experiments (n.s., not significant). (C) Infectivity of *Lm ΔinlAΔinlB* in HEK293A cells transduced with lentivirus expressing Fluc (white bar), human FcγRIa (black bar) or FcγRIa from indicated species (grey bars). *Lm* infectivity was measured as in Fig 2C, n=3, error bars represent s.d. (****, P<0.0001). (D) Infectivity of wild type *Lm* in MEFs transduced with lentivirus expressing human γ-chain and Fluc or murine FcγRIa. *Lm*

infectivity was measured as in Fig 2C, error bars represent s.d., n=3, statistical significance was determined by t-test prior to normalization (n.s., not significant).

CHAPTER FIVE

The search for bacterial ligand of FcγRIa

Introduction

I have previously demonstrated that FcγRIa does not promote uptake of other intracellular bacteria, such as *Shigella flexneri* and *Salmonella* Typhimurium and internalizes *Lm* independently of immunoglobulin opsonization (see Chapter Four). The most obvious explanation for these findings is that *Lm* directly engages FcγRIa at the surface of immune cells. However, the identity of the bacterial surface protein (or proteins) involved in the interaction and internalization remained unclear. Notably, a similar IgG-independent interaction has been reported between FcγRIa and *Escherichia coli* K1. *E. coli* K1 invades macrophages by interacting with FcγRIa via its Outer membrane protein A (OmpA) (174). It therefore appears that targeting IgG-independent functions of FcγRIa may be a general pathogenic strategy to evade immune clearance during systemic infection. Here, I applied a genetic approach to identify the bacterial surface protein, required for the FcγRIa-mediated *Lm* internalization.

FcγRIa-mediated Lm internalization is blocked by human Fc protein

Having established the role of FcγRIa in immunoglobulin-independent *Lm* internalization, I sought to confirm that FcγRIa-mediated uptake of *Lm* was due to a direct interaction of bacteria with the receptor. To prevent *Lm* from interacting with the Fc receptor, I treated control and FcγRIa-expressing cells with excess amounts of recombinant Fc protein (referred to as Fc block). As shown in Fig. 14A, Fc block treatment did not affect *Lm* uptake by untransduced or firefly luciferase expressing cells. However, it eliminated *Lm*

internalization by FcγRIa (Fig. 14A). These data confirm that the direct bacteria-receptor interaction is indeed required for the increased *Lm* uptake in FcγRIa-expressing cells.

FcγRIa-Lm interaction is PrfA-dependent

I hypothesized that because interaction with FcγRIa could be beneficial for *L. monocytogenes* survival and dissemination during infection, the bacterial Fcγ receptor ligand would be conserved among pathogenic species of *Listeria*. In the *Listeria* genus, *L. monocytogenes* and *L. ivanovii* are the only pathogenic strains, primarily known to cause listeriosis in humans and ruminants, respectively. Another sequenced and fully characterized species, *L. innocua* is closely related to *Lm* but lacks a 10-kb virulence locus and therefore, is non-pathogenic (57). To determine, if the bacterial FcγRIa-interacting protein was shared between pathogenic and nonpathogenic *Listeria* species, I assessed internalization rates of these bacteria in FcγRIa-expressing cells compared to control cells expressing firefly luciferase. As expected, cellular invasion by *Lm* was increased 12.72-fold in presence of FcγRIa. Similarly, internalization of *L. ivanovii* was 3.79-fold higher in FcγRIa-expressing cells as compared to control cells. However, FcγRIa failed to confer invasiveness to a non-pathogenic *L. innocua* (Fig. 14B). Confirming my initial hypothesis, these findings indicate, that the FcγRIa-interacting bacterial protein is only expressed by pathogenic *Listeria* species and may also serve as a virulence factor.

In *L. monocytogenes*, transition from a saprotrophic free-living bacterium to an intracellular pathogen is mediated by the transcriptional activator positive regulatory factor A (PrfA) that activates expression of the key virulence proteins. Consistent with its role in virulence, PrfA is present in both *Lm* and *L. ivanovii* but is absent from *L. innocua* (57, 58). I

next asked whether the FcγRIa-mediated *Lm* uptake was PrfA-dependent. As predicted, *prfA*-deficient *Lm* strain exhibited decreased internalization in control luciferase-expressing cells, likely due to the absence of PrfA-mediated expression of the invasion receptors InlA and InlB (175). Notably, invasion of the *prfA*-deficient *Lm* was not increased in presence of FcγRIa, suggesting that the ligand involved in internalization was not expressed due to the *prfA* deficiency (Fig. 14C). These results indicate that FcγRIa-*Listeria* interaction and internalization require a PrfA-dependent protein (or proteins) expressed on the surface of both *L. monocytogenes* and *L. ivanovii.*

ActA is required for the FcγRIa-mediated uptake of Lm

PrfA has been previously shown to positively regulate a core set of 12 genes preceded by a PrfA box and expressed in a σ^A dependent manner. Additionally, it regulates a group of σ^B-dependent genes, most of which are not preceded by a PrfA box. The core group includes major virulence factors – invasion factors internalin A and internalin B, listeriolysin O, phospholipases A and B, together responsible for vacuolar escape of *Listeria*, metalloprotease Mpl, involved in phospholipase maturation, secreted protein internalin C, implicated in protrusion formation during bacterial cell-to-cell spread, hexose phosphate transporter Hpt, responsible for the uptake of phosphorylated carbohydrates by bacteria within host cytoplasm, and an actin-assembly inducing protein ActA. Finally, products of two other PrfA-upregulated genes *lmo2218* and *lmo0788* have not been characterized (71, 95, 99, 102, 105, 109, 176-178).

I predicted that FcγRIa-interacting protein would be associated with the bacterial surface, rather than secreted. Among candidate genes from the core group of PrfA-dependent

proteins, only three were associated with bacterial surface via a single anchoring domain (InlA, InlB, ActA). Therefore, I first tested if FcγRIa expression increased invasion levels of *Lm* lacking either of these genes. As shown in Fig. 14D, consistent with my prior observation, *Lm ΔinlAΔinlB* exhibited increased internalization in presence of FcγRIa, indicating that InlA and InlB were dispensable for FcγRIa-mediated *Lm* invasion (Fig. 14D). I next tested if FcγRIa-mediated uptake was dependent on another membrane-associated PrfA-dependent protein - ActA. Interestingly, internalization of *Lm ΔactA* was not increased by FcγRIa (Fig. 14D), suggesting that ActA might be the involved in the FcγRIa-mediated *Lm* uptake. This finding is consistent with the fact that FcγRIa increased internalization of *L. ivanovii* that expresses iActA – an actin-assembly inducing protein with regions of close homology to the *Lm* ActA (179).

Next, to verify the requirement for ActA in FcγRIa-*Lm* interaction, I complemented *Lm ΔactA* with a single copy of *actA* with its proximal promoter (180). Expression of *actA* rescued actin-mediated motility in a previously cell-to-cell spread deficient *Lm ΔactA* as observed by intracellular actin comet tail formation (Fig. 14E). Importantly, *actA* integration also restored FcγRIa-mediated internalization to the level of the wild type *Lm* (Fig. 14F), confirming the requirement for ActA in *Lm* uptake via FcγRIa.

Actin nucleation ability of ActA is dispensable for invasion via FcγRIa

In *Lm*, ActA is a 90 kDa protein with a 29-amino acid N-terminal signaling peptide and a 26-amino acid long C-terminal hydrophobic membrane anchoring sequence, which also serves as a mitochondrial targeting peptide when expressed in eukaryotic cells (181). N-terminal region of ActA is subdivided into an acidic stretch, actin-monomer binding, and

cofilin homology regions (182). Cofilin homology region (135-165 a.a.), shared with the Wiscott-Aldrich Syndrome protein (WASP) family proteins, is critical for the actin-based motility (182). Within the cofilin region, arginine residues ^{146}KKRRK^{150} are essential for the recruitment of actin-nucleation complex Arp2/3, allowing ActA to serve as an actin nucleation-promoting factor (183-185). ActA also contains four proline-rich repeats in its central domain (264-390 a.a.), which is not required for actin comet tail formation. However, through interaction with the Vasodilator-stimulated phosphoprotein (VASP) and subsequent profilin (actin monomer-binding protein) recruitment, this region is responsible for ensuring efficient motility, increasing both the percentage of moving bacteria and the overall rate of actin-based motility (186, 187).

To distinguish between the ActA functions in actin-based motility and FcγRIa-mediated internalization, I tested *Lm* strains expressing *actA* mutants with abrogated actin nucleating activity. As expected, *Lm* harboring a minimal (Δ146-150) as well as a full deletion (Δ135-165) of the cofilin homology region did not form actin comet tails and lacked the ability for cell-to-cell spread in HEK293A cells (Fig. 15A). However, these strains were still internalized through FcγRIa, with an increase in invasion of 8.49 and 9.23-fold as compared to luciferase-expressing cells (Fig. 15B). Further, to determine if the N-terminal region of ActA is involved in FcγRIa-mediated uptake, I infected FcγRIa-expressing cells with *Lm* expressing ActA Δ31-165. Interestingly, invasion of this mutant strain was increased by FcγRIa only 3.61-fold, as compared to 9.846-fold observed with wild type *Lm* (Fig. 15D). Since deletion of the cofilin homology domain (135-165) did not affect internalization, we concluded that the 31-135 region is important for the FcγRIa-mediated

uptake and potentially FcγRIa-*Lm* interaction. Therefore, using mutant *Lm* strains I determined that the function of ActA in FcγRIa-mediated invasion is independent of its role in actin nucleation and cell-to-cell spread. Additionally, I demonstrated that the N-terminal region of ActA (amino acids 31-135) but not the cofilin homology domain is involved in FcγRIa-mediated internalization.

Conclusions

In this chapter, I demonstrated that in addition to *Lm*, FcγRIa expression increases internalization of another pathogenic strain of *Listeria – L. ivanovii,* but does not confer invasiveness to a closely related non-pathogenic bacteria *L. innocua*. Further, narrowing down the search for the bacterial surface ligand of FcγRIa to the virulence regulator PrfA-dependent proteins, I found that the actin assembly inducing protein ActA is necessary for *Lm* uptake by FcγRIa. Assessing invasion levels of various ActA deletion mutants allowed me to distinguish between ActA functions in actin nucleation and FcγRIa-mediated invasion and demonstrate that the 31-135 a.a. region of ActA is involved in the internalization, potentially through the interaction with FcγRIa.

While I found that ActA is required for the FcγRIa-mediated *Lm* internalization, it remains to be determined if ActA is also sufficient for the uptake. It is unclear if ActA interacts with FcγRIa directly or if other bacterial or host surface proteins are involved in the productive *Lm*-FcγRIa interaction. Further biochemical assays with recombinant extracellular domains of FcγRIa and ActA as well as evaluation of ActA-coated bead uptake will allow me to demonstrate a direct interaction or point to the requirement for other interacting

proteins. Protein crosslinking of *Lm* with FcγRIa-expressing cells will be utilized to determine the identity of any other proteins involved.

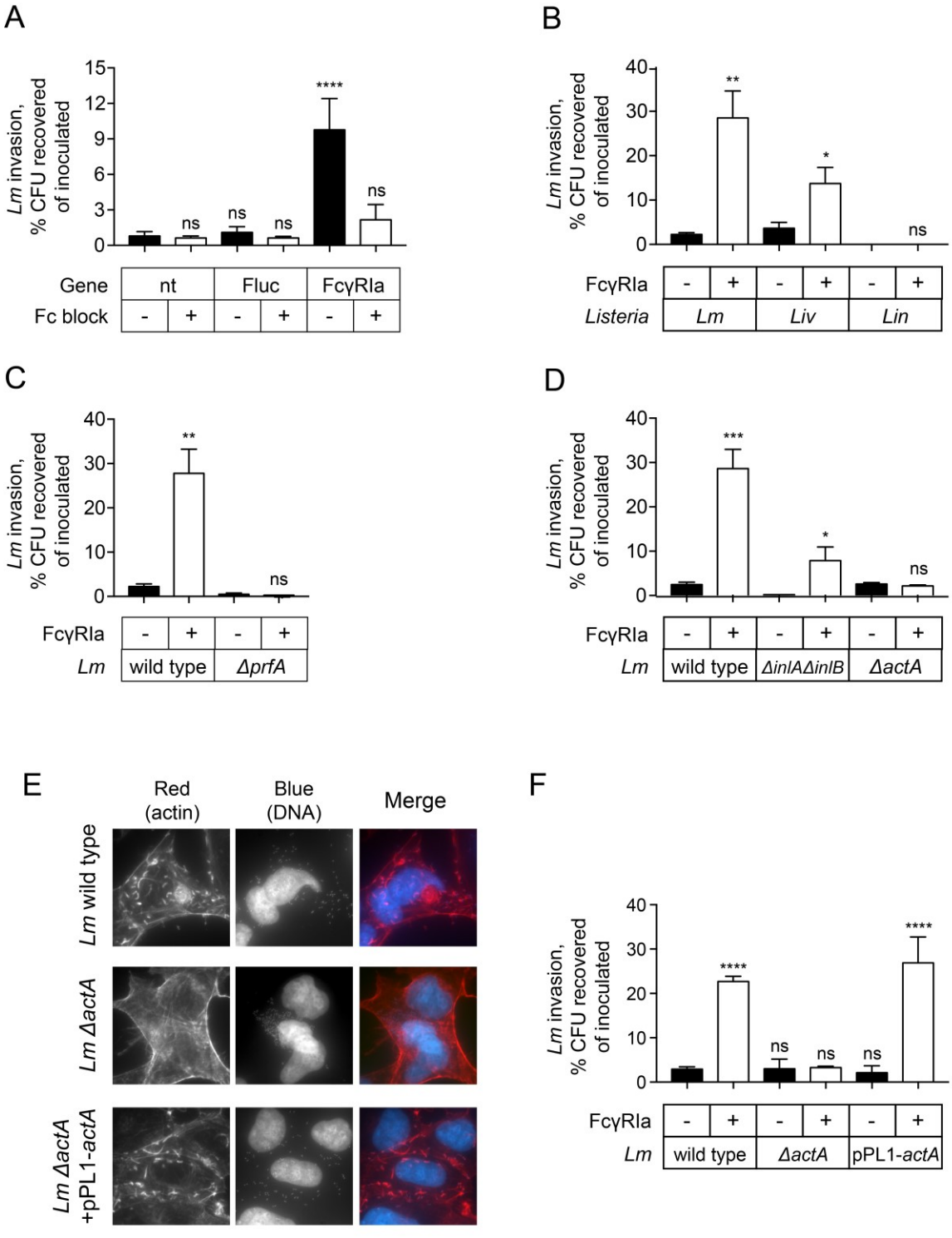
A
Lm invasion, % CFU recovered of inoculated
15
12
9
6
3
0
****
ns
ns
ns
ns
Gene
nt
Fluc
FcγRIa
Fc block
- + - + - +
B
Lm invasion, % CFU recovered of inoculated
40
30
20
10
0
**
*
ns
FcγRIa
- + - + - +
Listeria
Lm
Liv
Lin
C
Lm invasion, % CFU recovered of inoculated
40
30
20
10
0
**
ns
FcγRIa
- + - +
Lm
wild type
ΔprfA
D
Lm invasion, % CFU recovered of inoculated
40
30
20
10
0
***
*
ns
FcγRIa
- + - + - +
Lm
wild type
ΔinlAΔinlB
ΔactA
E
Red (actin)
Blue (DNA)
Merge
Lm wild type
Lm ΔactA
Lm ΔactA +pPL1-actA
F
Lm invasion, % CFU recovered of inoculated
40
30
20
10
0
****
ns
ns
ns
****
FcγRIa
- + - + - +
Lm
wild type
ΔactA
pPL1-actA

Figure 14: FcγRIa-mediated *Lm* internalization requires ActA protein expression

(A) Invasion of wild type *Lm* in HEK293A cells untransduced or transduced with lentivirus expressing Fluc or FcγRIa, untreated (black bars) or treated with 5μg/ml Fc block (white bars). Cells were infected for 1.5 h in gentamicin-free media, followed by incubation for 1 h with 50 μg/ml gentamicin. Invasion was measured as a number of *Listeria* colony forming units (CFU) surviving in a gentamicin protection assay, divided by the total CFU used for infection. Error bars represent s.d., n=3. MOI=10. Statistical significance was determined by t-test (****, P<0.0001, n.s., not significant). (B) Invasion of wild type *Lm, L.ivanovii,* and *L. innocua* in HEK293A cells transduced with lentivirus expressing Fluc (black bars) or FcγRIa (white bars). Invasion was measured as in Fig. 14A. Error bars represent s.d., n=3. MOI=10. Statistical significance was determined by t-test (*, P<0.05; **, P<0.01; n.s., not significant). (C) Invasion of wild type *Lm* and *Lm ΔprfA* in HEK293A cells transduced with lentivirus expressing Fluc (black bars) or FcγRIa (white bars). Invasion was measured as in Fig. 14A. Error bars represent s.d., n=3. MOI=10. Statistical significance was determined by t-test (**, P<0.01; n.s., not significant). (D) Invasion of wild type *Lm, Lm ΔinlAΔinlB,* and *Lm ΔactA* in HEK293A cells transduced with lentivirus expressing Fluc (black bars) or FcγRIa (white bars). Invasion was measured as in Fig. 14A. Error bars represent s.d., n=3. MOI=10. Statistical significance was determined by t-test (*, P<0.05; **, P<0.01; n.s., not significant). (E) Fluorescence microscopy of HEK293A cells infected with wild type *Lm, Lm ΔactA,* and *Lm ΔactA* harboring pPL1-*actA* plasmid for 4.5 h following 1.5 h of initial infection. Cells were stained with Alexa Fluor 594 phallioidin (actin, red) and DAPI (DNA, blue). (F) Invasion of wild type *Lm, Lm ΔactA,* and *Lm ΔactA* harboring pPL1-*actA* in HEK293A cells

transduced with lentivirus expressing Fluc (black bars) or FcγRIa (white bars). Invasion was measured as in Fig. 14A. Error bars represent s.d., n=3. MOI=10. Statistical significance was determined by t-test (****, P<0.0001, n.s., not significant).

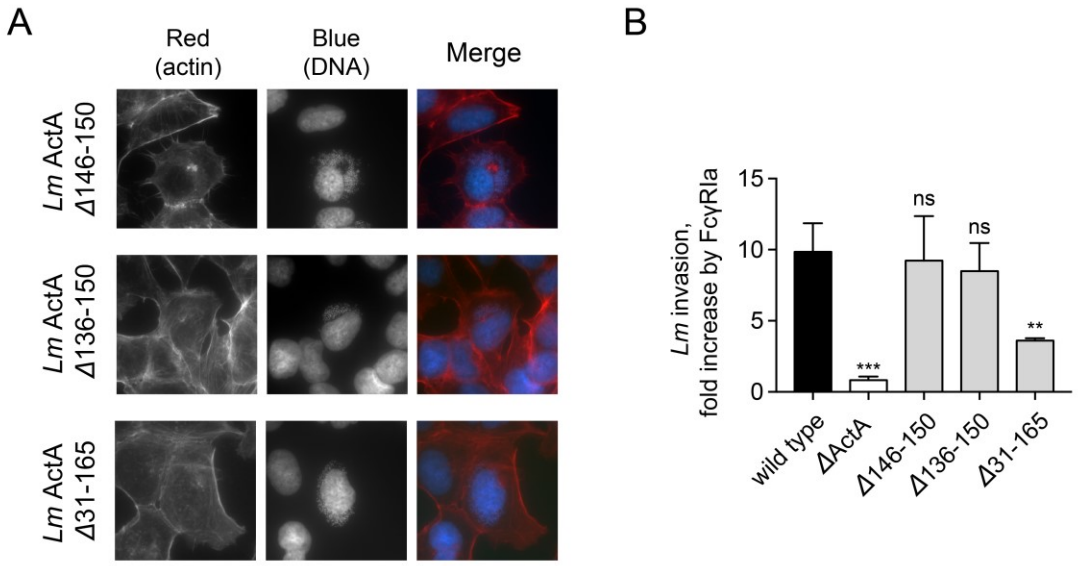

Figure 15: FcγRIa-mediated *Lm* internalization is independent of the ActA-induced actin polymerization

(A) Fluorescence microscopy of HEK293A cells infected with *Lm* ActA Δ146-150*, Lm* ActA Δ136-165, *Lm* ActA Δ31-165 for 4.5 h following 1.5 h of initial infection. Cells were stained as in Fig. 14E. (B) Fold increase in invasion of wild type *Lm, Lm* ActA Δ146-150*, Lm* ActA Δ136-165, *Lm* ActA Δ31-165 in HEK293A cells transduced with lentivirus FcγRIa as compared to HEK293A cells expressing Fluc. Invasion was measured as in Fig. 14A. Error bars represent s.d., n=3. MOI=10. Statistical significance was determined by t-test (**, P<0.01, ***, P<0.001, n.s., not significant).

CHAPTER SIX

Discussion and future directions

The host type I interferon response is stimulated by numerous bacterial pathogens. However, the roles of individual ISGs in restricting bacterial infection are not well characterized. In the current dissertation, to address this gap in the knowledge of IFN biology, I adapted a gain-of-function screening approach to identify cellular regulators of *Lm* infection among approximately 350 type I ISGs. The screen revealed strong cell-autonomous inhibitors of *Lm* infection, such as TRIM14, AQP9, MYD88, UNC93B1 and MAP3K14. Interestingly, it also identified the human immunoglobulin receptor FcγRIa as an enhancer of *Lm* internalization, suggesting an intriguing possibility that bacterial pathogens have evolved virulence factors to directly hijack the IFN response system.

I identified type I IFN-stimulated inhibitors of *Lm* infection that function through the upregulation of complex gene expression profiles (e.g. MYD88) and/or through direct anti-microbial mechanisms (e.g. TRIM14). These ISGs may contribute to the regulation of *Lm* in a wide variety of tissue environments. For example, upregulation and activation of MYD88 in TLR-expressing lymphocytes would result in the expression of NF-κB-regulated genes with broad antibacterial activity. My data indeed suggest that a MYD88-induced transcription program suppresses *Lm* infection through NF-κB activation (Figs 6C-6E). Notably, *Lm* has been previously reported to counteract host defense systems, including interfering with NF-κB activation, thus dampening the overall inflammatory response to infection (188). My findings now indicate that inhibition of NF-κB by *Lm* may protect the pathogen from previously unknown cell-autonomous immune mechanisms. Further studies

are needed to confirm this speculation. Another strong inhibitory ISG, TRIM14 is widely expressed throughout the body, including organs targeted by *Lm*, such as intestine and liver (154, 189). However, this is not the first study to implicate TRIM14 in anti-microbial defense. Recent studies characterized TRIM14 as an antiviral protein that activates both NF-κB and type I IFN through bridging MAVS and NEMO proteins as well as inhibiting cGAS degradation (153, 154). Interestingly my data support an alternative mechanism for the function of TRIM14. Here, I found that TRIM14 inhibited *Lm* infection in cells with defective IFN responses and that ectopic expression of TRIM14 did not alter the host transcriptional profile induced by *Lm* (Fig. 7). Further studies are needed to reveal the precise inhibitory mechanisms of TRIM14 as well as other antilisterial ISGs including PRKD2, AQP9, and MAP3K14 identified here.

Perhaps the most surprising discovery of this work is that the immunoglobulin receptor FcγRIa mediates *Lm* uptake, contributing to *Lm* invasion of phagocytic cells. This finding is particularly insightful since these cells are not only an important target of *Lm* infection, but also aid the transmission of *Lm* to peripheral tissues during infection (190). Currently, the precise molecular mechanisms of *Lm* internalization in phagocytic cells have not been characterized in detail and are believed to be mediated by C3bi and C1q complement receptors and phagocyte scavenger receptors (191, 192). However, my studies now suggest that *Lm* hijacks an alternative pathway to invade phagocytic cells through an immunoglobulin-independent interaction with FcγRIa. While studies presented here have elucidated many key aspects of the internalization process (see below), several questions remain unanswered: (1) what is the nature of the IgG-independent interaction between *Lm*

and FcγRIa resulting in *Lm* uptake by the host cells, (2) what is the cellular mechanism of FcγRIa-mediated *Lm* internalization and, finally, (3) what are the consequences of this interaction for both pathogen and host in terms of pathogen proliferation and disease outcomes.

In this study, I provide compelling evidence that *Lm* internalization by FcγRIa occurs independently of IgG opsonization (Fig. 11). It, however, requires ActA protein expression on *Lm* surface (Fig. 14). Recently, ActA has been implicated in several processes beyond its canonical role in actin-based motility and cell-to-cell spread during infection. It has been shown to contribute to *Lm* adhesion and invasion of various cell types, maturation of *Lm*-containing phagosomes, escape from autophagy, as well as bacterial aggregation and host colonization (110-113, 193-195). *Lm* might be directly engaging FcγRIa at the surface of immune cells, potentially through the ActA-FcγRIa interaction. While ActA is required, it is currently unclear if its presence is sufficient for the FcγRIa-mediated uptake or if other bacterial and host surface proteins are involved in the interaction. Both biochemical studies on ActA as a candidate bacterial ligand as well as unbiased genetic screens will help determine if ActA indeed serves as FcγRIa ligand and which other factors are implicated in *Lm* invasion of FcγRIa-expressing cells.

While work presented in this study clearly indicates that FcγRIa facilitates entry of *Lm* into host cells, the intracellular signaling mechanisms required for this process remain unknown. Since FcγRIa itself does not contain any known signaling motifs, the FcγRIa-mediated phagocytosis of IgG-coated particles requires receptor interaction with the ITAM-domain containing γ-chain, which in turn mediates downstream signaling, triggering

cytoskeleton rearrangement and particle internalization (163, 196). Interaction of FcγRIa with the γ-chain occurs exclusively through the transmembrane domain of the receptor (169). However, I found that GPI-anchored FcγRIa preserved its ability to internalize *Lm* in the absence of the transmembrane domain (Fig. 11B), indicating that both transmembrane and intracellular domains of FcγRIa were dispensable for this process. Thus, my data reveal the existence of an alternative non-canonical mechanism of FcγRIa internalization. It is currently unclear if FcγRIa-mediated uptake of *Lm* resembles the extensively characterized mechanism of *Lm* uptake by non-phagocytic cells through E-cadherin and c-Met receptors. *Lm*-induced clustering of these receptors leads to the recruitment of clathrin-mediated endocytosis machinery, actin cytoskeleton organization, and modulation of the phosphoinositide metabolism at the site of bacterial adhesion, resulting in the engulfment of the pathogen by a zipper-like mechanism (83). It will be of interest to define the involvement of actin, clathrin, and intracellular signaling pathways in the FcγRIa-mediated *Lm* entry.

It is intriguing to speculate on the potential role of FcγRIa in *Lm* pathogenesis. I found that a small but reproducible percentage of THP-1 infection (~18%) was dependent on cell surface expression of endogenous FcγRIa (Fig 12). Therefore, my data reveal the existence of at least two distinct pathways for *Lm* invasion including a canonical phagocytic pathway and a novel FcγRIa-mediated pathway described here. I hypothesize that *Lm* may have evolved surface molecules to engage the FcγRIa internalization pathway and bypass cell-mediated killing induced by other phagocytic routes of internalization. Consistent with this idea, *Lm* did not specifically engage the major phagocytic Fcγ receptor FcγRIIa involved in pathogen clearance in neutrophils and monocytes (Fig. 11C). In addition, previous studies

have demonstrated fundamental differences in intracellular signaling pathways, receptor trafficking, antigen presentation, and kinetics of oxidative burst triggered by high-affinity IgG receptors (FcγRIa) compared to low affinity receptors (FcγRIIa) (197). Thus, the ability of *Lm* to exploit the high affinity IgG receptor rather than being phagocytosed through the canonical opsonization pathway by FcγRIIa, may provide an opportunity for internalized *Lm* to produce phagosome rupture factors and escape into the cytoplasm. While this scenario has not yet been substantiated *in vivo*, the challenge for future studies will be to examine *Lm* internalization by FcγRIa in primary human cells revealing the role of FcγRIa in *Lm* pathogenesis.

In conclusion, flow cytometry based screening approach presented herein not only uncovered type I IFN stimulated suppressors of *Lm* infection but also revealed a novel *Lm* uptake pathway, which may play an important role in human *Lm* infection and disease pathogenesis. This work also opens new experimental avenues to examine the role of IFNs, and potentially other immune modulatory transcriptional programs, in the pathogenesis of a wide range of bacterial species, including both intracellular bacteria that replicate in either vacuoles or cytoplasmic environment, and extracellular bacteria that may be affected by secreted ISGs.

CHAPTER SEVEN

Materials and methods

Bacterial strains

Bacterial strains used in the study are listed in Table 1 (see below).

Cell culture

STAT1-deficient fibroblasts (an SV40 large T antigen immortalized skin fibroblast line, kindly provided by Jean-Laurent Casanova, Rockefeller University) were grown in RPMI Medium 1640 (Gibco, Thermo Fisher Scientific), supplemented with 10% Fetal Bovine Serum (FBS) (Gibco, Thermo Fisher Scientific) and non-essential amino acids (NEAA) (Gibco, Thermo Fisher Scientific). HEK293A (Jack Dixon, UC San Diego), HEK293T (Paul Bieniasz, Aaron Diamond AIDS Research Center), U-2 OS (ATCC), and MEF (Charles Rice, Rockefeller University) cells were maintained in Dulbecco's Modified Eagle Medium (DMEM) (Gibco, Thermo Fisher Scientific), supplemented with 10% FBS and NEAA. THP-1 cells (ATCC) were cultured in RPMI Medium 1640, ATCC modification (Gibco, Thermo Fisher Scientific), supplemented with 10% FBS and NEAA.

DNA constructs

All plasmid backbones used in the study are listed in Table 2 (see below).

cDNA for human *FCGR1B*, *FCGR2B*, *FCGR3A*, *FCGR3B*, *FCER1A*, *FCER2A*, *FCER1G, FCAR1* were obtained from the Ultimate ORF Clones (96-well plate) collection (Life Technologies) as Gateway-compatible pENTR clones. cDNA for human *FCGR2A* was a gift from Dr. Eric Hansen (UTSW). These genes were amplified by PCR with primers

encoding attB sites. Polymerase chain reaction (PCR) products were purified with the QIAquick PCR Purification Kit (Qiagen) and then recombined into a pDONR221 vector using BP Clonase II Enzyme mix (Life Technologies). BP reactions were transformed into chemically competent DH5a *Escherichia coli*, and colonies verified by sequencing. Resulting pENTR clones were further recombined into a pTRIP.CMV.IVSb.ires.TagRFP Destination vector (134) using LR Clonase II Enzyme mix (Life Technologies). LR reactions were transformed into DH5α cells and verified by sequencing.

pLenti CMV Puro DEST (w118-1) for generation of stable cell lines was a gift from Eric Campeau (Addgene plasmid #17452) (198). *FLUC, FCGR1A, and FCER1G* (referred to as γ-chain) were introduced using LR Clonase II Enzyme mix (Life Technologies) as described above.

Point mutations and truncations were generated by PCR of the corresponding pENTR clones using a QuikChange II XL Site-Directed Mutagenesis Kit (Agilent) and primers designed according to manufacturer's instructions. Glycosylphosphatidylinositol (GPI) anchored FcγRIa (previously described in (170) was generated by overlap extension PCR, using *FCGR1A* and *LFA3*, obtained from the Ultimate ORF Clones (96 well plate) collection (Life Technologies), as templates.

Sheep (NM_001139452.1), rabbit (XM_008264510.1), and panda (XM_011217915.1) *FCGR1A* cDNA were codon optimized for expression in human cells using Codon Optimization Tool (Integrated DNA Technologies) and synthesized as gBlocks Gene Fragments (Integrated DNA Technologies) with addition of attB sites. Mouse

(NM_010186) *FCGR1A* cDNA was synthesized as a pENTR clone (GeneCopoeia, Inc). Genes were recombined into pDONR221 and subsequently into expression vector pTRIP.CMV.IVSb.ires.TagRFP Destination vectors as described above.

pX335-U6-Chimeric_BB-CBh-hSpCas9n(D10A) was a gift from Feng Zhang (Addgene plasmid # 42335) (199). LentiCRISPR v2 was a gift from Feng Zhang (Addgene plasmid # 52961) (172).

pPL1-*actA* was generated as previously described (180). Briefly, *actA* gene with its proximal promoter were cloned into pPL1 using BamHI and NotI restriction sites. To generate pPL2-pactA::GFP, sGFP was PCR amplified from the genomic DNA of *Listeria* strain LM124 and then cloned downstream of the *actA* proximal promoter (200bp upstream) in the pPL2 vector.

Bacterial conjugation

Conjugation was used to introduce pPL1 or pPL2 integration vectors into *L. monocytogenes*. Briefly, pPL1 or pPL2 derived plasmid constructs were first chemically transformed into *E. coli* strain SM10 (200) by using standard procedures. Transformed SM10 (donor) were grown at 30°C with shaking to mid-log phase (optical density at 600 nm OD600, ~ 0.6) in LB medium supplemented with 25 μg/ml of chloramphenicol. Recipient phage-cured *L. monocytogenes* were grown at 30°C with shaking to mid-log phase in antibiotic-free BHI medium. Donor culture (250 μl) was harvested by centrifugation and washed twice with antibiotic-free BHI before combining with the recipient culture (150 μl).

The mixture was plated on BHI plates and incubated at 30°C for at least 12 h. Following incubation, bacteria were streaked out into 150 µl sterile water, and 20 µl of resulting suspension plated on BHI plates supplemented with 7.5µg/ml of chloramphenicol and 50µg/ml of streptomycin. The plate was then incubated at 37°C for 36 h. Individual colonies were picked and screened by PCR for integration with primers PL14 and PL61 (180).

Bacterial infection

Listeria monocytogenes was inoculated from a frozen stock and grown for 13 h at 30°C in brain–heart infusion media (BHI) (Difco, BD Biosciences) without shaking. 1 ml of bacteria was then washed in phosphate buffer saline (PBS) and resuspended in 1ml of PBS. A 1:10 dilution of the bacterial suspension was used to read the optical density at 600 nm (OD_{600}). Bacteria were then added to each well of cells to achieve multiplicity of infection (MOI) of 10, unless otherwise stated, and incubated for 90 min at 37°C, 5% CO_2 (unless otherwise noted). Culture media was then removed and replaced with media supplemented with 25 µg/ml gentamicin (Quality Biological) and cells incubated at 37°C, 5% CO_2 for the indicated time. *STAT1*-deficient fibroblasts were infected with *Lm* for 6 h, HEK293A – for 4 h, MEF – 3.5 h, THP-1 – 6 h, unless otherwise stated in figure legend, U-2 OS – see specific figure legends.

To assess invasion levels, cells were initially infected for 1.5 h in gentamicin-free media, followed by 1h in gentamicin-containing media. For the Fc block experiment, prior to infection cells were pretreated with 200µl of 0.0125 µg/ml Fc block (BD Biosciences 564219) in 10%FBS / DMEM for 15 min, washed once with 10%FBS / DMEM and infected for 2 h in gentamicin-free media, followed by 1h in gentamicin-containing media.

L. innocua and *L. ivanovii* infections were performed following a similar protocol with MOI of 10, invasion was measured as described in "Measuring intracellular bacterial burden" (see below).

For *Lm* infection of THP-1 cells, $8x10^4$ cells were seeded per well in 96-well tissue culture plates in 10% FBS/RPMI or serum-free RPMI. 24 h later later *Lm* infection was performed as described above (MOI=5). Following 1.5 h initial invasion time, gentamicin-containing media was added to the wells (final concentration 30 μg/ml) and infection was allowed to proceed for 6 h. Contribution of FcγRIa to *Lm* infection in each independent experiment was calculated using the following equation: [(percent infected wild type cells) – (percent infected *FCGR1A*-deficient cells) / [(percent infected wild type cells)] x 100%.

To visualize bacterial infection by epifluorescence microscopy, cells were washed once in PBS, fixed in 3.7% formaldehyde in PBS for 10 min at room temperature. Cells were then washed three times in PBS and incubated for 2 min in 4',6-diamidino-2-phenylindole (DAPI) solution.

Shigella flexneri strain M90T was inoculated from a frozen stock and grown overnight at 30°C in BHI medium (Difco, BD Biosciences). Bacteria were then back-diluted 1:50 and incubated at 37 °C until reaching $OD_{600} \approx 0.5–0.6$. Bacteria were then washed in 1×PBS and incubated at 37 °C for 15 min in 0.003% Congo red. Bacteria were added to each well to achieve MOI=10 and centrifuged at 1000 x *g* for 10 min at room temperature to facilitate bacterial adherence. The plates were then incubated for 90 min at 37°C, 5% CO_2. The media was removed and replaced with media supplemented with 50 μg/ml gentamicin

(Quality Biological) and cells incubated at 37 °C, 5% CO_2 for 4.5 h. Cells were washed once with PBS before collecting for flow cytometry analysis.

Salmonella Typhimurium strain SL1344 was inoculated from a frozen stock and grown at 37 °C in BHI (Difco, BD Biosciences) in a glass flask with high aeration overnight, then subcultured (1:30) and grown for 3 h at 37°C. 1 ml of bacterial suspension was then washed in PBS and resuspended in 1ml of PBS. 1:10 dilution of the bacterial suspension was used to read the optical density at 600 nm (OD600). Bacteria were added to each well to achieve MOI=100 and incubated for 1 h at 37°C, 5% CO_2, washed three times with PBS and incubated at 37 °C, 5% CO_2 in medium supplemented with 100 μg/ml gentamicin (Quality Biological) and cells incubated at 37°C, 5% CO_2 for 8 h. Cells were washed again with PBS before collecting for flow cytometry analysis.

Generation of lentiviral pseudoparticles

Lentiviral pseudoparticles were generated as previously described (Schoggins et al., 2011). Briefly, $4x10^5$ HEK293T cells in 6-well plates were co-transfected with plasmids expressing the pTRIP.CMV.IVSb.ISG.ires.TagRFP proviral DNA, HIV-1 gag–pol and VSV-G in a ratio of 1/0.8/0.2, respectively. For each transfection, 6μl XtremeGENE 9 DNA Transfection Reagent (Roche) was combined with 2.0 μg total DNA in 100 μl Opti-MEM (Gibco) and incubated for 30 min at room temperature before adding to the cells. Transfections were carried out for 6 h, followed by a medium change to DMEM containing 3% FBS. Supernatants were collected at 48 h and 72 h, pooled, cleared by centrifugation and stored at -80°C.

Lentiviral transduction

Lentiviral transduction was performed as previously described (134). Briefly, cells were seeded in 24-well tissue culture plates at a density of $7x10^4$ cells per well and transduced the following day with lentiviral pseudoparticles via spinoculation at 1,000 x *g* for 45 min in medium containing 3% FBS, 20mM HEPES and 4 µg/ml polybrene. 6 h after spinoculation, pseudoparticle-containing media was removed and replaced with full cell culture medium, containing 10% FBS and NEAA. For subsequent bacterial infection, cells were split 1:2 48h after transduction. For generation of stable expressing cell lines using pLenti CMV Puro DEST (w118-1), cells were transduced with the lentivirus and selected for puromycin resistance for 7 days 48h after transduction.

Yellow Fever Virus infection

YFV-17D-Venus infection was performed as previously described (134).

Flow cytometry analysis

For flow cytometry analysis, cells were detached from the tissue culture plate by incubating in 150µl of Accumax Cell Dissociation Solution (Innovative Cell Technologies, Inc.) for 5 min at 37°C, transferred to V-bottom 96-well plates, pelleted by centrifugation at 800 x *g* for 5 min, resuspended in 1% paraformaldehyde (PFA) and incubated at 4°C for at least 30 min. Fixed cells were then pelleted at 800 x *g* for 5 min and resuspended in 150µl of 1×PBS containing 3% FBS. Plates were stored at 4°C if flow cytometry was not carried out immediately. Samples were analyzed using a Stratedigm S1000 flow cytometer equipped with 405nm, 488nm and 561nm lasers. Data was analyzed using FlowJo Software (Treestar).

Immunoblotting

Cells were washed once with PBS and lysed using RIPA Lysis and Extraction Buffer (Pierce, Thermo Fisher Scientific) supplemented with Protease Inhibitor Cocktail (Sigma). Total protein concentration was determined using the BCA Protein Assay Kit (Pierce, Thermo Fisher Scientific). Proteins were separated on SDS-PAGE and transferred to 0.45 μm nitrocellulose membranes (Biorad). Membranes were then blocked with 5% (w/v) skim milk (Difco, BD) in Tris-buffered saline with 0.1% Tween 20 (TBST) for 1 h at room temperature and immunoblotted with primary antibodies in TBST containing 5% nonfat milk at 4°C overnight, followed by incubation with appropriate secondary antibodies coupled to horseradish peroxidase (HRP) for 1 h at room temperature. Proteins were detected using ECL Western Blotting Substrate (Pierce, Thermo Fisher Scientific). The following antibodies were used in this study: anti- MYD88 (AF2928, R&D Systems), anti-E-cadherin (BD 610181, BD Biosciences), anti-c-Met (CST 4560, Cell Signaling Technology), anti-actin (a-2066, Sigma Aldrich), goat anti-rabbit (31460, Thermo Fisher Scientific), donkey anti-goat (sc-2020, Santa Cruz Biotech), goat anti-mouse (115-035-146, Jackson ImmunoResearch).

RNA sequencing

RNA was isolated from *STAT1*-deficient fibroblasts, ectopically expressing the gene of interest, using an RNeasy Mini Kit (Qiagen) per the manufacturer's instructions. For each condition, two independent replicates were prepared. Further procedures were performed at the UTSW Next Generation Sequencing Core (McDermott Center). The quality of the total RNA samples was first confirmed on a 2100 Bioanalyzer (Agilent) using the total RNA 600 Nano Kit (Agilent) and amount of RNA quantified using the Qubit RNA Assay kit (Life Technologies). 4μg of total RNA with an RNA Integrity Number (RIN score) above 8, were

further processed as described in TruSeq Stranded mRNA Sample Preparation Guide (Illumina). Samples were fragmented at a lower temperature than recommended (80°C for 4 min instead of 94°C for 8 min) to obtain 400-800bp libraries. Additionally, 12 PCR cycles were performed, instead of 15 cycles recommended by the protocol. Resulting libraries were analyzed on 2100 Bioanalyzer (Agilent) using DNA High Sensitivity Kit (Agilent) and quantified using Qubit. Sequencing was performed on Illumina Hiseq2500 with 100 bp paired end reads. Further procedures were performed at the UTSW Bioinformatics Core (McDermott Center). Sequencing reads were trimmed to remove adaptor sequences and low quality bases using fastq-mcf (v1.1.2-806, https://expressionanalysis.github.io/ea-utils/). Filtered reads were then mapped to human genome (hg19) using Tophat (v2.0.10) (201), guided by igenome annotations (https://ccb.jhu.edu/software/tophat/igenomes.shtml). Duplicate reads were marked but not removed. Expression abundance estimate and differential expression test were performed using Cufflinks/Cuffdiff (v2.1.1) software (201). Differential expression was considered as statistically significant when q-value was lower than 0.05, fold change was greater than 2, and FPKM value of at least one sample was greater than 0.01. The upstream regulator analyses were generated through the use of QIAGEN's Ingenuity Pathway Analysis (IPA, QIAGEN Redwood City, www.qiagen.com/ingenuity).

NF-κB reporter activation assay

STAT1-deficient fibroblasts were seeded into 48-well plates at a density of $2.5x10^4$ per well and transduced the following day with lentivirus expressing the gene of interest. 24 h later cells were transfected with 200 ng of the reporter plasmid pNF-kB–luciferase and 150

ng normalization vector pLacZ (to correct for transfection efficiency using a beta-galactosidase assay). 24 h after transfection, cells were lysed and luciferase was measured according to manufacturer protocol (Luciferase Assay System, Promega). LacZ expression was measured in a β-Galactosidase Activity Assay with ortho-Nitrophenyl-β-galactoside (ONPG), and used to normalize luciferase values for each sample.

Gentamicin survival assay

Following *Listeria* infection, mammalian cells were washed three times with 1×PBS and then lysed by incubating in 0.5% Triton X-100 for 5 min at room temperature, followed by vigorous pipetting to complete the lysis. Intracellular bacterial burden was determined by plating serial dilutions of suspension on BHI-agar plates, incubating at 37°C, and counting bacterial colony forming units (CFU) the next day. Additionally, serial dilutions of bacterial culture used for infection were plated to obtain the inoculated CFU. Finally, the following equation was used: [CFU recovered per well/CFU inoculated per well] x 100% = invasion and normalized to control values, if needed.

Scanning electron microscopy

Cells were plated at $1.4x10^5$ cells/well in a 12-well plate and transduced the next day with lentiviruses as described above. Two days after transduction cells were split 1:2 on circular glass coverslips in 12-well plates, and the next day infected with *Lm*, according to the standard protocol. After infection samples were fixed in 2.5% glutaraldehyde in 0.1 M cacodylate buffer for a minimum of 2 h. Further procedures were performed at the UTSW Electron Microscopy Facility. Fixed cells were rinsed in the fixation buffer and fixed with Osmium tetroxide as secondary fixative. After several water rinses they were dehydrated in

serial concentrations (50%, 70%, 85%, 95%, 100%), and critical point dried. The samples were coated for 30s with gold palladium and viewed in the Zeiss Sigma VP FE scanning electron microscope. Images were acquired using the Secondary Electron 2 (SE2) detector.

CRISPR/Cas9-mediated gene editing

CRISPR/Cas9-mediated MET and CDH1 gene editing and clone evaluation

Guides targeting exon 3 of *CDH1* and exon 3 of *MET* were designed using the Optimized CRISPR Design Tool (http://crispr.mit.edu/), and cloned into the pX335-U6-Chimeric_BB-CBh-hSpCas9n(D10A) vector as previously described (202). For each guide pair, $4x10^5$ HEK293A cells were seeded in a 6-well plate, and the following day were transfected with 1 μg of GFP-N3, and 1 μg of the positive and negative guides, according to the FuGENE 6 (Promega) protocol. Approximately 48 h post transfection, fluorescence-activated cell sorting (FACS) was used to deposit single GFP-positive cells into 96-well plates. Approximately 2 weeks after sorting, colonies were transferred to 24-well plates in duplicate, and screened for reduced GFP-*Lm* infection. Whole cell lysates of putatively edited clones were prepared in RIPA buffer, and western blot against either E-cadherin (BD 610181) or c-Met (CST 4560) was carried out according to a standard protocol. Further, DNA from the samples with substantially lower infection than the wild type control and no detectable E-cadherin or c-Met as determined by western blot was extracted using the Quick Extract kit. PCR using Phusion High-Fidelity DNA Polymerase (NEB) was carried out genomic primers to genotype the indels for *CDH1* and *MET* by cloning into the Zero Blunt cloning vector (Life Technologies) with subsequent Sanger sequencing at the UTSW Sequencing Core.

CRISPR/Cas9-mediated generation of FCGR1A-deficient THP-1 cells

Two guides targeting exon 3 of *FCGR1A* were designed using the Optimized CRISPR Design Tool (http://crispr.mit.edu/), and cloned into lentiCRISPR v2 vector as previously described (172). Lentiviruses were generated as described above and used to transduce THP-1 cells. Lentivirally transduced cells were selected in 2 μg/ml puromycin for 7 days 48h after transduction. The absence of FcγRIa on the cell surface in the generated cell line was confirmed by antibody staining as described above.

***In vitro* phagocytosis assay**

In vitro phagocytosis assay was performed as described previously (203). U-2 OS cells, stably expressing Fluc or FcγRIa were first transduced with lentivirus coexpressing TagRFP and Fluc, FcγRIIa or FcεRIg (γ-chain), to generate desired gene combinations. 48 h after transduction, cells were plated at $7x10^4$ cells/ml in 4-well chamber slides (Falcon). The day before the assay latex beads (3.87μm in diameter) (Bangs Laboratories, PS05N/6749) were opsonized with human IgG by washing a 10% slurry of beads in 1×PBS and mixing overnight with 1.5 mg/ml human IgG (Jackson ImmunoResearch). The day of the experiment, beads were washed in 1×PBS and labeled with an Alexa Fluor 488 AffiniPure Donkey Anti-Human IgG (H+L) (green) antibody (Jackson ImmunoResearch), while rotating at room temperature for 1h. Following secondary labeling, beads were washed, resuspended in DMEM and added to cells in chamber slides. Slides were centrifuged at 300 x *g* for 1 min, and then placed 37°C for 90 min. After the incubation, slides were placed on ice and washed with ice-cold medium to inhibit further phagocytosis. Extracellular beads were then labeled with DyLight 405 AffiniPure Donkey Anti-Human IgG (H+L) (blue) antibody (Jackson

ImmunoResearch) for 10 min on ice. Cells were washed 5 times with ice-cold 1×PBS and fixed with 3.7% PFA for 20 min at room temperature. Next, cells were washed with 1×PBS and incubated with 100 mM glycine for 10 min at room temperature to quench PFA. All samples were washed twice with 1×PBS and chamber removed from the slide. When the excess liquid dried, the coverslips were mounted on the samples with ProLong Gold reagent (Molecular Probes, Life Technologies). Samples were observed with a fluorescent microscope Zeiss Observer Z1. Numbers of green and blue beads were counted for 80 Red Fluorescent Protein (TagRFP)-positive cells per sample, two technical replicates per gene. Phagocytosis efficiency was measured as a percentage of internalized beads, determined by subtracting the number of extracellular (blue) beads from the total (green) beads, divided by the number of total (green) beads.

Agarose overlay (plaque) assay

Cells were plated at $1.4x10^5$ cells/well in a 12-well plate and transduced the next day with FcγRIa or Fluc-encoding lentiviruses as described above. Two days post-transduction, cells were infected with wild type *Lm* for 1 h (MOI = 0.015, 0.05, 0.1), washed with medium, supplemented with 50 μg/ml gentamicin (Quality Biological), and then gently overlaid with 1.5ml/well of DMEM, containing with 10% FBS, 0.4% agarose, and 20 μg/ml gentamicin (Quality Biological). The overlay was allowed to solidify for 15 min at room temperature, when plates were moved back to an incubator at 37°C. Foci of *Lm* infection were visualized 30 h after initial infection by adding 200μl of 5mg/ml (3-(4, 5-dimethylthiazolyl-2)-2,5-diphenyltetrazolium bromide (tetrazolium MTT) (Sigma) solution to each well and

incubating at 37°C for 3 h. Plates were scanned and foci of infection quantified using ImageJ software.

Cell surface immunofluorescence staining for flow cytometry analysis

To detect surface expression of FcγRIa V450 Mouse anti-Human CD64 (BD 561202) and V450 Mouse IgG1, κ Isotype control (BD 560373) antibodies were used according to the manufacturer's protocol. Briefly, adherent cell ($4x10^5$ cells per well) were washed once with PBS, detached from the surface by incubating in 150µl of Accumax Cell Dissociation Solution (Innovative Cell Technologies, Inc.) for 5 min at 37°C, transferred to V-bottom 96-well plates, pelleted by centrifugation at 300 x *g* for 5 min, washed once PBS and staining buffer (2% FBS in 1×PBS). Cells were then resuspended in 50µl of staining buffer and 2.5µl of fluorescently tagged antibody was added. Cells were incubated for 30 min at room temperature, in the dark. After incubation, cells were washed twice in staining buffer, resuspended in 150µl of staining buffer and analyzed immediately by flow cytometry.

Statistical analysis

All experiments were performed in as three independent replicates, unless otherwise stated. For experiments where only two groups of samples were compared, unpaired t-test was used to determine if difference between groups was statistically significant. To determine statistical significance in experiments with three or more groups of samples, one-way analysis of variance (ANOVA) with Dunnett's procedure for multiple comparisons was used. Data analysis was performed in GraphPad Prism software.

Table 1. Bacterial strains used in this study

Strain	Description	Source
Escherichia coli DH5α	*E. coli* strain used for general cloning procedures	Thermo Fisher Scientific
E.coli ccdB Survival	Used for propagation of plasmids containing the *ccdB* gene	Thermo Fisher Scientific (A10460)
E.coli SM10 λpir	Used as a donor strain for bacterial conjugation	Provided by Sebastian Winter
E.coli Stbl3	Derived from the HB101 *E. coli* strain for cloning unstable inserts	Thermo Fisher Scientific (C737303)
Listeria monocytogenes 10403s, GFP	Wild type *L. monocytogenes* 10403s strain with constitutive GFP expression	Provided by Dan Portnoy
L. monocytogenes DP-L3078	*L. monocytogenes ΔactA*	Provided by Dan Portnoy (182)
L. monocytogenes DP-L3078, pPL2-pactA::GFP	*L. monocytogenes ΔactA* with pactA-dependent GFP expression	This study
L. monocytogenes DP-L2319	*L. monocytogenes Δhly ΔplcA ΔplcB*	Provided by Dan Portnoy (141)
L. monocytogenes DP-L2319, pPL2-pactA::GFP	*L. monocytogenes Δhly ΔplcA ΔplcB* with pactA-dependent GFP expression	This study
L. monocytogenes	*L. monocytogenes*	Provided by Manuel Amieva

LM 124	wild type, Cm^R with constitutive sGFP expression	(94)
L. monocytogenes LM 128	*L. monocytogenes* wild type, Erm^R with constitutive sGFP expression	Provided by Manuel Amieva (94)
L. monocytogenes LM 131	*L. monocytogenes ΔinlA ΔinlB,* Erm^R with constitutive sGFP expression	Provided by Manuel Amieva (94)
L. monocytogenes DP-L4317	*L. monocytogenes ΔprfA*	Provided by Dan Portnoy (204)
L. monocytogenes DP-L3992	*L. monocytogenes* expressing ActA Δ146-150	Provided by Dan Portnoy (182)
L. monocytogenes DP-L3990	*L. monocytogenes* expressing ActA Δ136-165	Provided by Dan Portnoy (182)
L. monocytogenes DP-L3984	*L. monocytogenes* expressing ActA Δ31-165	Provided by Dan Portnoy (182)
L. monocytogenes DP-L4029	Phage-cured *L. monocytogenes ΔactA*	Provided by Dan Portnoy (180)
L. monocytogenes DP-L4029 + pPL1-*actA*	DP-L4029 complemented with *L. monocytogenes* ActA	This study
L. ivanovii subsp. ivanovii Seeliger et al. (DP-393)	Wild type *L. ivanovii* strain	Provided by Dan Portnoy (ATCC 19119)
L. innocua Seeliger CLIP 11262	Genome sequencing *L. innocua* strain	ATCC BAA-680
Shigella flexneri M90T, GFP	Wild type *S. flexneri* strain	Provided by Jack Dixon

	with constitutive GFP expression	
Salmonella enterica serovar Typhimurium strain SL1344, GFP	Wild type *S.* Typhimurium strain with constitutive GFP expression	Provided by Sing Sing Way

Table 2. Plasmid backbones used in this study

Plasmid	Description	Source
pDONR221	Gateway-adapted vector used to generate attL-flanked entry clones containing the gene of interest	Thermo Fisher Scientific
pTRIP-TagRFP	Lentiviral vector Gateway destination vector pTRIP.CMV.IVSb.ISG.ires.TagRFP	Provided by John Schoggins (134)
gag-pol	Packaging vector used for producing lentiviral particles	Provided by John Schoggins (134)
VSVg	Plasmid expressing vesicular stomatitis virus G glycoprotein for producing lentiviral particles	Provided by John Schoggins (134)
pLenti CMV Puro DEST (w118-1)	Lentiviral Gateway destination vector with puromycin resistance gene (Addgene #17452)	Gift from Eric Campeau (198)
pX335-U6-	A human codon-optimized SpCas9 nickase and	Gift from

Chimeric_BB-CBh-hSpCas9n(D10A)	chimeric guide RNA expression plasmid (Addgene #42335)	Feng Zhang (199)
LentiCRISPR v2	Lentiviral vector, used to for mammalian expression of Cas9 and sgRNA (Addgene #52961)	Gift from Feng Zhang (172)
pPL1	Integrative *E. coli/Listeria* shuttle vector, contains the listeriophage U153 integrase and provides integration into the attachment site within the *Lm comK* gene for chromosomal insertion	Provided by Dan Portnoy (180)
pPL2	Integrative *E. coli/Listeria* shuttle vector, utilizes the PSA phage integrase and allows integration into the 3' end of an arginine tRNA gene	Provided by Dan Portnoy (180)
pNF-kB - luciferase	NF-κB reporter plasmid	(205)
pTK-LacZ	Transfection normalization vector	(205)

APPENDIX A:

Large-scale screen

Gene name	Percent infected replicate 1	Z-score replicate 1	Percent infected replicate 2	Z-score replicate 2
PSMB9	34.1	-0.600263141	37.8	-0.189862188
PSMB8	30.4	-0.913363711	50.1	0.73096469
IFI6	37.2	-0.337935636	44.7	0.326699231
GBP1	41.3	0.009013645	47	0.498886371
IFITM3	44.5	0.279803328	44.7	0.326699231
MX1	52.7	0.973701889	59.5	1.434686043
PLSCR1	66.8	2.166868928	63.5	1.734141939
RTP4	58	1.422197301	47.3	0.521345563
IFIH1	41.8	0.051324533	42.4	0.154512092
EIF2AK2	31.3	-0.837204113	49.3	0.671073511
CCDC75	34.7	-0.549490075	55.3	1.120257354
IFIT3	38.4	-0.236389505	51.1	0.805828664
IFI27	50.1	0.753685272	54.1	1.030420585
CHMP5	55.9	1.244491572	43.6	0.24434886
PMAIP1	51.6	0.880617936	44.5	0.311726437
MT1X	30.1	-0.938750244	32.9	-0.556695659
DEFB1	30.4	-0.913363711	45.1	0.356644821
CMAHP	34.7	-0.549490075	33.3	-0.52675007
C15orf48	31.7	-0.803355403	40.7	0.027243336
SNN	28.7	-1.05722073	27.8	-0.938501926
CCL5	48.4	0.609828253	54.4	1.052879777
CCL4	49.7	0.719836562	50	0.723478292
CXCL11	47.6	0.542130833	43.4	0.229376065
CXCL10	27.9	-1.124918151	37.4	-0.219807777
CCL19	31.4	-0.828741936	41.1	0.057188926
CCL2	45.5	0.364425103	60.6	1.517036415
CCL8	27.9	-1.124918151	42.1	0.1320529
GLRX	28.2	-1.099531618	30.5	-0.736369196
VAMP5	52.4	0.948315357	51.2	0.813315061
B2M	49.1	0.669063496	54.8	1.082825367
SAA1	52.2	0.931391001	43.7	0.251835258

IFITM1	29.7	-0.972598954	33.8	-0.489318083
CXCL9	21.1	-1.700346227	24.1	-1.215498629
RPL22	24.8	-1.387245656	39.7	-0.047620638
C4orf32	26	-1.285699525	32.2	-0.609100441
NRN1	48.8	0.643676964	48.6	0.618668729
RNASE4	57.5	1.379886413	51.6	0.84326065
GLIPR2	32.9	-0.701809272	26.3	-1.050797886
LMO2	20.9	-1.717270582	21.1	-1.44009055
MAFF	33.7	-0.634111851	36.1	-0.317130943
TMEM140	52.2	0.931391001	43.3	0.221889668
HESX1	43.8	0.220568085	42	0.124566502
GPX2	56.9	1.329113348	37.8	-0.189862188
PHF11	36.5	-0.397170879	37.8	-0.189862188
ANKRD22	45.3	0.347500748	58.4	1.352335672
COMMD3	40.2	-0.084070308	62.6	1.666764362
SOCS2	50.3	0.770609627	60.2	1.487090825
CD69	57.6	1.388348591	43.3	0.221889668
C4orf33	50.5	0.787533983	51.3	0.820801458
MS4A4A	52.1	0.922928824	50	0.723478292
SOCS1	63.8	1.913003601	51.8	0.858233445
C10orf10	37.7	-0.295624748	47.4	0.528831961
FAM125B	49.6	0.711374384	70.9	2.288135345
CRP	35.6	-0.473330477	75.3	2.617536829
CD9	38	-0.270238215	63.4	1.726655541
RNF114	55.8	1.236029394	47.6	0.543804755
BATF2	46.5	0.449046879	59.5	1.434686043
GZMB	47.4	0.525206477	60.9	1.539495607
CCDC109B	50.7	0.804458338	47.9	0.566263947
LGALS3	44.6	0.288265505	61.9	1.614359581
GCH1	43.3	0.178257197	46	0.424022397
TMEM51	36.1	-0.431019589	60.5	1.509550017
TNFAIP6	52.1	0.922928824	68.5	2.108461808
TNFSF10	48	0.575979543	69	2.145893794
TNFSF13B	32.1	-0.769506693	63	1.696709952
CD80	46	0.406735991	41	0.049702528
FBXO6	40.2	-0.084070308	53.2	0.963043009
GEM	48.7	0.635214786	50	0.723478292

EPSTI1	30.6	-0.896439356	47.9	0.566263947
UPP2	43.2	0.169795019	62.4	1.651791567
MAFB	51.9	0.906004469	75.7	2.647482419
BCL2L14	30.1	-0.938750244	65.4	1.876383489
CCDC92	41.6	0.034400178	40.7	0.027243336
APOL2	44.8	0.30518986	62	1.621845978
SLFN5	47.5	0.533668655	61.5	1.584413991
ETV7	49.1	0.669063496	48.3	0.596209537
APOL6	43.3	0.178257197	62.4	1.651791567
LRG1	35.6	-0.473330477	49	0.648614319
FAM70A	35.3	-0.49871701	36.9	-0.257239764
HSH2D	45.9	0.398273814	59.4	1.427199646
MKX	44.5	0.279803328	63.3	1.719169144
ARG2	34.9	-0.53256572	52.8	0.933097419
CCR1	41.1	-0.00791071	47.2	0.513859166
G6PC	42	0.068248888	49.4	0.678559908
MAB21L2	38.2	-0.25331386	47.3	0.521345563
CSDA	45.4	0.355962926	53.4	0.978015803
FCGR1A	75.3	2.886154023	72.6	2.4154041
FAM46C	39.3	-0.160229907	38.2	-0.159916598
IDO1	68.8	2.33611248	56.6	1.217580519
HELZ2	43.6	0.203643729	36	-0.324617341
IFI44L	45.4	0.355962926	35.5	-0.362049327
LAMP3	36.4	-0.405633057	28.2	-0.908556336
SMAD3	27.1	-1.192615572	19.3	-1.574845703
IL17RB	42.7	0.127484131	36.8	-0.264726162
PUS1	47.9	0.567517365	49.8	0.708505498
ZBP1	34.6	-0.557952253	31.6	-0.654018825
PDK1	40.9	-0.024835065	31.6	-0.654018825
PLIN2	38.7	-0.211002972	38.4	-0.144943804
TRIM14	10.9	-2.56348834	12.6	-2.076434327
ETV6	47.5	0.533668655	46.4	0.453967987
NFIL3	50.2	0.76214745	41.2	0.064675323
NUP50	35.2	-0.507179187	33	-0.549209262
TNFRSF10A	20.6	-1.742657114	20.9	-1.455063345
IRF7	39.7	-0.126381196	30.9	-0.706423607
SCARB2	41.5	0.025938	40.2	-0.010188651

PI4K2B	39	-0.185616439	45.9	0.416536
IFIT5	46.6	0.457509057	48.2	0.58872314
TYMP	47.6	0.542130833	40.6	0.019756939
IFNGR1	38.7	-0.211002972	33.8	-0.489318083
NAMPT	29.4	-0.997985487	33.1	-0.541722865
ANGPTL1	26.1	-1.277237347	32.5	-0.586641249
SERPING1	45.5	0.364425103	37.1	-0.242266969
ALDH1A1	41.3	0.009013645	41.6	0.094620913
SIRPA	33.7	-0.634111851	48.2	0.58872314
C22orf28	39.4	-0.151767729	47	0.498886371
PRAME	39.5	-0.143305551	37.7	-0.197348585
OASL	33.1	-0.684884917	35.1	-0.391994917
GTPBP2	44.3	0.262878972	44.3	0.296753642
LAP3	41.3	0.009013645	40.6	0.019756939
PFKFB3	38.6	-0.21946515	32.3	-0.601614044
CDK17	43	0.152870664	48.7	0.626155127
GK	36	-0.439481767	46.7	0.476427179
SLC1A1	41.7	0.042862355	47.7	0.551291153
FUT4	39.5	-0.143305551	41.6	0.094620913
CYP1B1	32	-0.77796887	37	-0.249753367
HPSE	46.7	0.465971234	43.9	0.266808052
SPTLC2	44	0.23749244	31.7	-0.646532428
EIF3L	30.3	-0.921825889	44.8	0.334185629
CES1	42.4	0.102097598	53.9	1.01544779
THBD	25.5	-1.328010413	23.1	-1.290362602
PXK	28.1	-1.107993796	36.8	-0.264726162
DCP1A	51.2	0.846769226	60.1	1.479604428
BTN3A3	53.1	1.0075506	67	1.996165847
PFKFB3	48.1	0.584441721	47.1	0.506372768
GBP5	39.2	-0.168692084	40.3	-0.002702253
CSRNP1	39	-0.185616439	44.7	0.326699231
GBP2	32.6	-0.727195805	30.5	-0.736369196
SAMHD1	37.9	-0.278700393	33.1	-0.541722865
NDC80	45	0.322114216	55.9	1.165175738
AMPH	56.7	1.312188993	66.8	1.981193052
CTCFL	55.8	1.236029394	64.1	1.779060323
PADI2	49.7	0.719836562	44.8	0.334185629

DHX58	41.2	0.000551467	39.2	-0.085052624
OAS2	42.4	0.102097598	43.5	0.236862463
PARP12	49.8	0.728298739	50.7	0.775883074
SP110	32.5	-0.735657982	32.9	-0.556695659
IFI16	49	0.660601319	58.7	1.374794864
DTX3L	55.1	1.176794151	67.8	2.056057026
EXT1	50.1	0.753685272	58	1.322390083
CFB	42.5	0.110559776	45	0.349158423
STAT3	39.1	-0.177154262	39.4	-0.07007983
PLEKHA4	27.2	-1.184153394	28.9	-0.856151554
PHF15	44.4	0.27134115	56.7	1.225066917
ABTB2	52.4	0.948315357	61.3	1.569441196
EPAS1	45.4	0.355962926	63.1	1.704196349
PML	51.1	0.838307048	35.7	-0.347076533
TLR3	42.8	0.135946309	31.8	-0.639046031
ENPP1	39.5	-0.143305551	43.5	0.236862463
DDX58	53.3	1.024474955	43.3	0.221889668
MAP3K14	12.6	-2.419631321	9.45	-2.312255845
BUB1	52.3	0.939853179	38.2	-0.159916598
ANKFY1	46.1	0.415198169	48.8	0.633641524
MAP3K5	33.1	-0.684884917	35.6	-0.35456293
S100A8	31.6	-0.81181758	25.7	-1.095716271
FZD5	33.3	-0.667960562	45.9	0.416536
DYNLT1	35.6	-0.473330477	50.1	0.73096469
LY6E	50	0.745223095	56.5	1.210094122
NEURL3	44.8	0.30518986	27.2	-0.98342031
UBE2L6	39.1	-0.177154262	42.1	0.1320529
KIAA0040	39.8	-0.117919019	38.4	-0.144943804
CDKN1A	29.9	-0.955674599	19.1	-1.589818498
ISG15	33.8	-0.625649674	22.6	-1.327794589
ATF3	45.5	0.364425103	36	-0.324617341
ISG20	63.8	1.913003601	64.9	1.838951502
FLJ39739	54.3	1.109096731	50.1	0.73096469
RGS1	62.7	1.819919648	54.7	1.075338969
STARD5	46.5	0.449046879	29.6	-0.803746773
RAB27A	53	0.999088422	40.6	0.019756939
DDIT4	50.7	0.804458338	43.5	0.236862463

CD74	55.8	1.236029394	32.3	-0.601614044
HEG1	52	0.914466646	38.8	-0.114998214
PMM2	55.9	1.244491572	58.6	1.367308467
SECTM1	46.4	0.440584702	44.9	0.341672026
SCO2	78	3.114632818	69.5	2.183325781
SPSB1	52.5	0.956777534	40.6	0.019756939
STEAP4	51.7	0.889080114	47.8	0.55877755
IMPA2	62	1.760684404	62.8	1.681737157
IFI35	56.2	1.269878105	38.9	-0.107511817
CD38	45.7	0.381349459	40.1	-0.017675048
CASP7	54.9	1.159869796	60.5	1.509550017
XAF1	54.1	1.092172375	58.9	1.389767659
LGALS9	59.4	1.540667787	42.7	0.176971284
PIM3	50.2	0.76214745	39.4	-0.07007983
PNRC1	45.8	0.389811636	48.1	0.581236742
P2RY6	24.6	-1.404170011	29.8	-0.788773978
IGFBP2	56.6	1.303726815	46	0.424022397
FFAR2	51.3	0.855231403	41.4	0.079648118
HLA-G	53	0.999088422	60.5	1.509550017
AIM2	54.2	1.100634553	46	0.424022397
GMPR	40.3	-0.075608131	32.8	-0.564182057
USP18	47.7	0.55059301	52	0.87320624
PDGFRL	51.2	0.846769226	61.8	1.606873183
APOL1	58.3	1.447583834	49.6	0.693532703
TXNIP	36.4	-0.405633057	42.8	0.184457681
SERPINE1	52.3	0.939853179	60.3	1.494577222
VMP1	51.3	0.855231403	61	1.546982004
VEGFC	53.8	1.066785843	46.6	0.468940782
AGPAT9	48	0.575979543	53.5	0.985502201
IFI44	33.1	-0.684884917	63.3	1.719169144
MSR1	58.9	1.498356899	55.1	1.105284559
FKBP5	46.9	0.48289559	45.7	0.401563205
CREB3L3	56.6	1.303726815	64.2	1.78654672
TRIM38	48.2	0.592903898	54.4	1.052879777
WARS	57.9	1.413735124	48.9	0.641127921
CDK18	39.6	-0.134843374	46.8	0.483913576
TRIM21	47.1	0.499819945	52.2	0.888179035

IFIT1	22.3	-1.598800096	50.4	0.753423882
TRIM5	51.9	0.906004469	49.6	0.693532703
FAM134B	30.8	-0.879515001	25.6	-1.103202668
RIPK2	34.9	-0.53256572	26.1	-1.065770681
RNF19B	42.7	0.127484131	35.7	-0.347076533
ULK4	35.7	-0.4648683	25.1	-1.140634655
CRY1	58.1	1.430659479	49.6	0.693532703
ELF1	65	2.014549732	48.4	0.603695934
ARNTL	60.3	1.616827386	37.2	-0.234780572
GBP4	51.2	0.846769226	29.7	-0.796260375
DDX3X	35.9	-0.447943944	26.2	-1.058284284
TAP2	35.5	-0.481792655	33.2	-0.534236467
MX2	29.8	-0.964136777	25.4	-1.118175463
PNPT1	54.4	1.117558908	42.1	0.1320529
TAP1	54.9	1.159869796	41.7	0.10210731
FTSJD2	46.2	0.423660347	27.2	-0.98342031
MASTL	40.8	-0.033297243	30.8	-0.713910004
HK2	30.1	-0.938750244	25.9	-1.080743476
RNF213	32.2	-0.761044515	35.2	-0.38450852
TDRD7	23.3	-1.51417832	22.6	-1.327794589
MYOF	59.5	1.549129965	47.6	0.543804755
MTHFD2L	48.7	0.635214786	42.4	0.154512092
RARRES3	52.5	0.956777534	40.3	-0.002702253
CD274	40.2	-0.084070308	26.8	-1.013365899
STAP1	38.2	-0.25331386	29.7	-0.796260375
NAPA	29.8	-0.964136777	29.5	-0.81123317
BLVRA	36.5	-0.397170879	35.5	-0.362049327
MYD88	8.68	-2.751348682	8.87	-2.355676949
NMI	54.2	1.100634553	33.3	-0.52675007
IRF1	43.8	0.220568085	33	-0.549209262
GJA4	48.4	0.609828253	40.8	0.034729734
MCL1	41.8	0.051324533	31.4	-0.66899162
HLA-E	35.9	-0.447943944	29.6	-0.803746773
SLC25A28	15.8	-2.148841638	20.7	-1.47003614
SSBP3	31	-0.862590646	29	-0.848665157
TREX1	26.4	-1.251850815	22.1	-1.365226576
SERPINB9	51.4	0.863693581	42.9	0.191944079

EHD4	29.1	-1.02337202	19.8	-1.537413716
CYTH1	42.2	0.085173243	29.2	-0.833692362
CLEC4E	36.3	-0.414095234	24.1	-1.215498629
PPM1K	41.7	0.042862355	32	-0.624073236
CPT1A	31.1	-0.854128468	29.9	-0.781287581
LGMN	31.2	-0.845666291	33.2	-0.534236467
BCL3	51.9	0.906004469	28.4	-0.893583541
GALNT2	73	2.691523938	56	1.172662135
OPTN	62.3	1.786070937	41.4	0.079648118
SLC15A3	47.3	0.5167443	31.8	-0.639046031
TRAFD1	34.4	-0.574876608	32.2	-0.609100441
TRIM25	22	-1.624186628	35.5	-0.362049327
IL1RN	31.1	-0.854128468	33.6	-0.504290878
TIMP1	33.8	-0.625649674	33.2	-0.534236467
ARHGEF3	39.5	-0.143305551	26.3	-1.050797886
ERLIN1	37.5	-0.312549103	38.7	-0.122484611
ANXA2R	32.4	-0.74412016	36.8	-0.264726162
RASSF4	29.2	-1.014909842	32.3	-0.601614044
IRF2	28.8	-1.048758553	23.8	-1.237957821
CCNA1	27.7	-1.141842506	39.1	-0.092539022
MT1F	37.1	-0.346397813	42.4	0.154512092
MT1M	40.8	-0.033297243	40.2	-0.010188651
HLA-F	35.2	-0.507179187	25.7	-1.095716271
ALYREF	40	-0.100994664	47.5	0.536318358
C5orf27	31.6	-0.81181758	42.3	0.147025694
CEBPD	38.6	-0.21946515	46.4	0.453967987
SAMD4A	34	-0.608725318	25.7	-1.095716271
ZNF385B	28	-1.116455973	35.5	-0.362049327
MCOLN2	25.9	-1.294161703	27.9	-0.931015528
UNC93B1	13	-2.385782611	13.5	-2.009056751
TAGAP	27.9	-1.124918151	18.9	-1.604791292
HERC6	40.5	-0.058683776	45.3	0.371617616
NOD2	58	1.422197301	61.4	1.576927594
FNDC3B	28.4	-1.082607263	34.3	-0.451886096
IFI30	42.5	0.110559776	32.4	-0.594127646
ADM	27	-1.201077749	35.7	-0.347076533
LIPA	36	-0.439481767	36.8	-0.264726162

CX3CL1	25.8	-1.30262388	23.9	-1.230471423
MT1G	40.1	-0.092532486	38.9	-0.107511817
MT1H	37.5	-0.312549103	45.1	0.356644821
FNDC4	28.1	-1.107993796	34.2	-0.459372493
IL15RA	48	0.575979543	31.8	-0.639046031
SPATS2L	27.4	-1.167229039	27.2	-0.98342031
SUN2	32.4	-0.74412016	25.2	-1.133148258
NPAS2	41.3	0.009013645	40.5	0.012270541
TNFAIP3	47.4	0.525206477	53.9	1.01544779
C9orf91	45.2	0.339038571	46.5	0.461454384
NT5C3	25.1	-1.361859123	27.4	-0.968447515
BAG1	36.3	-0.414095234	24.8	-1.163093847
PPM1K	36.3	-0.414095234	38.1	-0.167402996
MICB	27.3	-1.175691216	22.8	-1.312821795
DUSP5	47.8	0.559055188	47.2	0.513859166
B4GALT5	47.1	0.499819945	25.7	-1.095716271
FAM46A	33	-0.693347094	39.8	-0.04013424
AKT3	39	-0.185616439	38.2	-0.159916598
TRIM34	40.8	-0.033297243	30	-0.773801183
ABLIM3	44.1	0.245954617	27.3	-0.975933913
C1S	28.3	-1.091069441	26.9	-1.005879502
STAT1	44.6	0.288265505	26.7	-1.020852297
TBX3	54.6	1.134483263	36.8	-0.264726162
NCOA3	57.3	1.362962058	31.2	-0.683964415
STAT2	14.8	-2.233463414	19.5	-1.559872908
PRKD2	12.3	-2.445017854	12.3	-2.098893519
CD163	21.8	-1.641110983	21.8	-1.387685768
DDX60	34.6	-0.557952253	32.5	-0.586641249
IL6ST	51.6	0.880617936	35.2	-0.38450852
IRF9	67.4	2.217641994	44	0.27429445
CLEC2B	52.7	0.973701889	29.1	-0.84117876
IL15	15	-2.216539059	19.7	-1.544900113
CCND3	25.4	-1.336472591	29.4	-0.818719568
ODC1	23.1	-1.531102675	24	-1.222985026
PTMA	24.4	-1.421094366	20.4	-1.492495332
SLC25A30	28.4	-1.082607263	24.9	-1.15560745
APOBEC3A	59	1.506819077	41.1	0.057188926

NCF1	61.2	1.692986984	38.3	-0.152430201
TCF7L2	16.1	-2.123455106	22.2	-1.357740179
MAX	29.6	-0.981061132	27.5	-0.960961118
SLC16A1	22.2	-1.607262273	14.1	-1.964138367
GCA	28.9	-1.040296375	23.7	-1.245444218
JUNB	32.3	-0.752582337	19.1	-1.589818498
MARCKS	59.6	1.557592142	34.2	-0.459372493
IFIT2	52.6	0.965239712	28.4	-0.893583541
HLA-C	17	-2.047295507	21.7	-1.395172166
GAK	24.1	-1.446480899	34.8	-0.414454109
ADAMDEC1	26.5	-1.243388637	26.5	-1.035825092
AQP9	14.3	-2.275774302	9.13	-2.336212316
JAK2	43.7	0.212105907	29.4	-0.818719568
FLJ23556	56.1	1.261415927	24.2	-1.208012231
ATP10D	51.6	0.880617936	31.1	-0.691450812
ARHGAP17	51.1	0.838307048	18.3	-1.649709677
HES4	26.7	-1.226464282	32.3	-0.601614044
AHNAK2	30.6	-0.896439356	29.2	-0.833692362
WHAMM	21	-1.708808404	15.4	-1.866815201
GBP3	27.2	-1.184153394	23.9	-1.230471423
IL1R1	56	1.25295375	26.8	-1.013365899
MB21D1	31.5	-0.820279758	20	-1.522440921
CLEC4D	47	0.491357767	23.8	-1.237957821
LEPR	22.4	-1.590337918	18.2	-1.657196074
RBCK1	33.8	-0.625649674	25.9	-1.080743476
OGFR	33.6	-0.642574029	19.6	-1.552386511
ADAR	35.6	-0.473330477	24.2	-1.208012231
IL28RA	37.9	-0.278700393	28.8	-0.863637952
RBM25	44.8	0.30518986	32.4	-0.594127646

Appendix B:

Differential gene expression between *STAT1*-deficient fibroblasts transduced with lentivirus expressing Fluc or MYD88

Gene	FPKM Fluc	FPKM MyD88	Fluc vs MyD88 log2.fold change	p_value	q_value
CCL11	0	3.16706	Inf	5.00E-05	0.00250269
IL8	2.37879	323.206	7.08608	5.00E-05	0.00250269
CXCL3	0.610676	61.0592	6.64366	5.00E-05	0.00250269
CXCL1	0.705719	64.1805	6.5069	5.00E-05	0.00250269
MYD88	12.4104	924.991	6.21982	5.00E-05	0.00250269
IL1B	0.257312	18.3904	6.15929	5.00E-05	0.00250269
CXCL2	0.470388	24.8206	5.72154	5.00E-05	0.00250269
CXCL5	0.183147	6.99708	5.25568	5.00E-05	0.00250269
C3	0.510861	19.0678	5.22206	5.00E-05	0.00250269
C15orf48	0.22687	8.02917	5.14531	9.00E-04	0.0278237
IGF2	0.338392	8.66277	4.67806	5.00E-05	0.00250269
IL6	0.525721	11.9889	4.51126	5.00E-05	0.00250269
BCL2A1	0.179148	3.88876	4.44009	0.00045	0.0161622
CTSS	0.0705021	1.399	4.31059	5.00E-05	0.00250269
CCL2	4.35278	79.8738	4.19771	5.00E-05	0.00250269
SERPINB2	0.911039	16.5751	4.18536	5.00E-05	0.00250269
TNFRSF9	0.130581	1.14681	3.13461	5.00E-05	0.00250269
MMP1	0.397125	3.37328	3.08649	5.00E-05	0.00250269
C1QTNF1	0.47403	3.71428	2.97003	5.00E-05	0.00250269
MMP3	1.27538	9.04336	2.82594	5.00E-05	0.00250269
NFKBIZ	2.02944	14.1793	2.80463	5.00E-05	0.00250269
LCP1	0.279346	1.92301	2.78324	5.00E-05	0.00250269
POU2F2	0.810941	5.5354	2.77102	5.00E-05	0.00250269
ICAM1	1.17554	7.67142	2.70617	5.00E-05	0.00250269
TNFAIP3	1.81959	11.6633	2.68029	5.00E-05	0.00250269
ZC3H12A	3.79894	22.8976	2.59153	5.00E-05	0.00250269
IL32	2.60612	14.9164	2.51693	5.00E-05	0.00250269
ESM1	1.04591	5.90853	2.49804	5.00E-05	0.00250269
AMPD3	0.388526	2.00026	2.3641	5.00E-05	0.00250269
SCG5	0.707392	3.63139	2.35994	5.00E-05	0.00250269
SOD2	41.6553	211.923	2.34696	5.00E-05	0.00250269
LIF	4.91347	24.699	2.32964	5.00E-05	0.00250269
CFB	0.528157	2.61806	2.30946	5.00E-05	0.00250269

PRRX1	0.436354	2.13841	2.29296	5.00E-05	0.00250269
IRAK2	1.56249	7.08976	2.18189	5.00E-05	0.00250269
MMP9	4.60467	20.6123	2.16233	5.00E-05	0.00250269
MYOCD	0.892883	3.98337	2.15745	5.00E-05	0.00250269
BDKRB2	0.486201	2.14099	2.13865	5.00E-05	0.00250269
INHBA	36.6417	156.893	2.09823	5.00E-05	0.00250269
MSC	3.91042	16.5514	2.08156	5.00E-05	0.00250269
RELB	3.50393	14.6241	2.0613	5.00E-05	0.00250269
LRIG1	5.81136	24.0571	2.04951	5.00E-05	0.00250269
TNFAIP6	0.732721	3.00853	2.03772	5.00E-05	0.00250269
DPP4	0.627	2.57208	2.0364	5.00E-05	0.00250269
FBXO32	1.45808	5.93176	2.02439	5.00E-05	0.00250269
ABI3BP	3.11038	12.535	2.0108	5.00E-05	0.00250269
PTPRR	0.394164	1.58099	2.00396	5.00E-05	0.00250269
MT2A	151.802	607.301	2.00022	5.00E-05	0.00250269
BIRC3	0.156239	0.592258	1.92247	5.00E-05	0.00250269
BDKRB1	2.17119	8.02777	1.88651	5.00E-05	0.00250269
NFKBIA	10.5303	38.8842	1.88463	5.00E-05	0.00250269
PKNOX2	0.13017	0.460538	1.82292	5.00E-04	0.0175599
HAS2	8.95644	31.631	1.82034	5.00E-05	0.00250269
NRP2	5.89352	19.3886	1.71801	5.00E-05	0.00250269
SLC39A14	47.0868	153.491	1.70476	5.00E-05	0.00250269
HDAC9	0.52493	1.695	1.69109	5.00E-05	0.00250269
LINC00623	0.951572	3.03236	1.67206	5.00E-05	0.00250269
LAMB3	1.21163	3.84451	1.66585	5.00E-05	0.00250269
GPRC5B	2.99162	9.39292	1.65065	5.00E-05	0.00250269
VCAM1	0.145164	0.455074	1.64842	0.0012	0.034716
PTGS2	0.488669	1.49152	1.60986	5.00E-05	0.00250269
FOXO1	0.417135	1.26316	1.59845	5.00E-05	0.00250269
EPHB1	0.314117	0.930026	1.56597	5.00E-05	0.00250269
STEAP1	1.52754	4.51533	1.56362	5.00E-05	0.00250269
LOC646999	0.234359	0.692558	1.56321	0.0017	0.0451447
IER3	98.0864	283.539	1.53142	5.00E-05	0.00250269
IL11	46.12	128.087	1.47366	5.00E-05	0.00250269
SBSN	3.1021	8.58323	1.46828	5.00E-05	0.00250269
TNFAIP2	0.22234	0.612636	1.46226	0.001	0.0301504
ADORA2A	1.40065	3.77338	1.42976	5.00E-05	0.00250269
MT1X	17.222	45.5982	1.40473	5.00E-05	0.00250269
ABLIM3	2.12952	5.60423	1.39599	5.00E-05	0.00250269
ICOSLG	0.984273	2.58634	1.39378	5.00E-05	0.00250269
NFKB2	10.6549	27.4248	1.36396	5.00E-05	0.00250269

PAPPA	1.38399	3.53846	1.35429	5.00E-05	0.00250269
F2RL1	1.97948	5.05696	1.35315	5.00E-05	0.00250269
GNAO1	0.392418	1.00154	1.35175	5.00E-05	0.00250269
LPXN	3.67693	9.37986	1.35107	5.00E-05	0.00250269
PLAU	12.5046	31.8127	1.34714	5.00E-05	0.00250269
MIR17HG	0.542116	1.36349	1.33063	4.00E-04	0.0146977
LOC100132891	2.15825	5.41422	1.32689	5.00E-05	0.00250269
COL16A1	1.87041	4.67714	1.32227	5.00E-05	0.00250269
GDNF	2.01334	5.01717	1.31729	5.00E-05	0.00250269
VEGFC	14.2933	35.5713	1.31538	5.00E-05	0.00250269
LRRC17	4.97534	12.2316	1.29775	5.00E-05	0.00250269
ISG20	1.43513	3.51083	1.29063	0.00035	0.0131821
ACTG2	4.74928	11.3979	1.26299	5.00E-05	0.00250269
RELL1	5.27515	12.5649	1.25211	5.00E-05	0.00250269
PPIF	95.0893	219.843	1.20912	5.00E-05	0.00250269
ALPL	0.466514	1.06778	1.19462	0.00125	0.0358101
TMEM45A	4.80274	10.923	1.18543	5.00E-05	0.00250269
JAG1	21.1603	47.5051	1.16672	5.00E-05	0.00250269
CD82	47.8512	106.132	1.14924	5.00E-05	0.00250269
KIAA1024	0.419468	0.930357	1.14923	1.00E-04	0.00461519
LUM	2.16485	4.79494	1.14725	5.00E-05	0.00250269
NFE2L3	5.1587	11.3514	1.13779	5.00E-05	0.00250269
MME	14.6231	31.9811	1.12897	5.00E-05	0.00250269
RASGRP1	0.652184	1.41334	1.11576	1.00E-04	0.00461519
TMEM132A	11.1159	23.9946	1.11009	5.00E-05	0.00250269
PTX3	69.0252	148.671	1.10692	5.00E-05	0.00250269
C1S	5.26634	11.2866	1.09973	5.00E-05	0.00250269
COL5A3	18.6684	39.9125	1.09624	5.00E-05	0.00250269
NAB1	3.69245	7.87635	1.09295	5.00E-05	0.00250269
RFTN1	8.13513	17.2859	1.08736	5.00E-05	0.00250269
WT1	0.65488	1.39136	1.0872	7.00E-04	0.0229046
MPP4	1.59095	3.3779	1.08624	5.00E-05	0.00250269
ETV4	3.13717	6.64221	1.0822	5.00E-05	0.00250269
MAN1A1	4.51558	9.47943	1.06989	5.00E-05	0.00250269
NAMPT	25.4171	53.1299	1.06372	5.00E-05	0.00250269
LOC100507460	0.910262	1.89638	1.05889	5.00E-05	0.00250269
NTN1	2.41857	5.02829	1.05591	5.00E-05	0.00250269
TRAF1	0.518841	1.07714	1.05385	0.00045	0.0161622
DACT1	6.03763	12.4435	1.04333	5.00E-05	0.00250269
IFI44	3.12111	6.42963	1.04268	5.00E-05	0.00250269
DUSP6	6.80646	13.9555	1.03586	5.00E-05	0.00250269

PRDM1	0.698151	1.43131	1.03573	5.00E-05	0.00250269
LOC100506735	10.498	21.4486	1.03077	5.00E-05	0.00250269
CD83	2.45062	4.99173	1.02639	5.00E-05	0.00250269
TFPI2	9.61881	19.5073	1.02008	5.00E-05	0.00250269
STC1	8.20723	16.5972	1.01598	5.00E-05	0.00250269
HS3ST3A1	1.88623	3.80484	1.01233	5.00E-05	0.00250269
CALB2	1.42192	2.86265	1.00951	0.00045	0.0161622
TMEM158	19.7252	39.5921	1.00518	5.00E-05	0.00250269

Appendix C:

Upstream regulators identified by Ingenuity Pathway Analysis for MYD88-regulated genes

Upstream Regulator	Molecule Type	Predicted Activation State	Activation z-score	p-value of overlap
TNF	cytokine	Activated	5.685	4.49E-30
IL1B	cytokine	Activated	5.035	6.91E-25
NFkB (complex)	complex	Activated	4.546	5.60E-30
IL1A	cytokine	Activated	4.456	7.11E-26
TLR7	transmembrane receptor	Activated	3.927	1.33E-17
FOXL2	transcription regulator	Activated	3.441	2.04E-14
IL17A	cytokine	Activated	3.295	3.18E-18
JUN	transcription regulator	Activated	3.159	3.18E-14
ERK1/2	group	Activated	3.077	5.84E-08
Cg	complex	Activated	3.064	2.90E-16
EZH2	transcription regulator	Activated	3.022	5.01E-11

Target molecules in datasets:

TNF:

ADORA2A,BCL2A1,C3,CCL11,CCL2,CD83,CFB,COL16A1,CXCL1,CXCL2,CXCL3,CXCL5,CXCL8,DPP4,F2RL1,HDAC9,ICAM1,ICOSLG/LOC102723996,IER3,IGF2,IGFBP2,IL1B,IL32,IL6,INHBA,LAMB3,MMP1,MMP3,MMP9,NFKB2,NFKBIA,PLAU,PRDM1,PTX3,RELB,RFTN1,SERPINB2,SOD2,STAC,TNFAIP3,VEGFC

IL1B:

AMPD3,BCL2A1,C3,CCL11,CCL2,CXCL1,CXCL2,CXCL3,CXCL5,CXCL8,DPP4,ICAM1,IL1B,IL32,IL6,LCP1,MMP1,MMP3,MMP9,MT2A,NFKBIA,NFKBIZ,PTX3,SERPINB2,SOD2,TNFAIP6,VEGFC

NFkB (complex):

BCL2A1,C3,CCL2,CD83,CXCL1,CXCL2,CXCL3,CXCL8,GDF15,HAS2,ICAM1,IER3,IL1B,IL6,JAG1,KIT,MMP1,MMP3,MMP9,NAMPT,NFKB2,NFKBIA,NFKBIZ,PLAU,RELB,RFTN1,SERPINB2,SOD2,TFPI2,TNFAIP3,TWIST1,VEGFC

IL1A:

ADORA2A,CCL2,CXCL1,CXCL2,CXCL3,CXCL5,CXCL8,ICAM1,IL11,IL1B,IL32,IL6,MMP1,MT2A,NFKBIA,NFKBIZ,PLAU,PTX3,SOD2,TNFAIP3,ZC3H12A

TLR7:

CCL2,CD83,CXCL1,CXCL2,CXCL3,CXCL8,ICAM1,IER3,IL1B,IL6,ISG20,MYD88,NFKBIA,PLAU,PTX3,ZC3H12A

FOXL2:

BCL2A1,CXCL2,CXCL3,GPRC5B,ICAM1,IER3,IL11,LIF,SERPINB2,SMAD6,SOD2,TNFAIP3

IL17A:

BCL2A1,CCL11,CCL2,CD83,CXCL1,CXCL2,CXCL3,CXCL5,CXCL8,ICAM1,IL1B,IL6,MMP3,MMP9

JUN:

CCL2,CXCL1,CXCL5,CXCL8,DIO2,ICAM1,IL1B,IL6,MMP1,MMP9,NFKBIA,NFKBIZ,PTX3,SOD2,ZFP36

ERK1/2:

CCL2,CXCL3,CXCL8,ICAM1,ID1,IL11,IL1B,IL6,MMP1,MMP3

Cg:

CCL2,CXCL8,DUSP6,ESM1,F2RL1,HAS2,IGFBP3,IL11,MMP1,PLAU,PTX3,STC1,STEAP1,TFPI2,TMEM158,VEGFC

EZH2:

C15orf48,C3,CD82,CXCL1,CXCL2,CXCL8,GDF15,ICOSLG/LOC102723996,IL11,IL6,NFKBIA,PPP2R2B

Appendix D:

Differential gene expression between *STAT1*-deficient fibroblasts transduced with lentivirus expressing Fluc or TRIM14

Gene	FPKM Fluc	FPKM TRIM14	Fluc vs TRIM14 log2.fold change	p_value	q_value
SNORA25	0	30.6561		6.00E-04	0.0202906
TRIM14	18.1483	2256.63	6.95819	5.00E-05	0.00250269
RPS17L	0.373915	9.81086	4.7136	3.00E-04	0.0116181
INHBE	0.127332	0.845088	2.73051	3.00E-04	0.0116181
SERPINB2	0.911039	5.94999	2.7073	5.00E-05	0.00250269
KRT34	2.79181	15.6216	2.48427	5.00E-05	0.00250269
IL8	2.37879	13.0846	2.45958	5.00E-05	0.00250269
TNFRSF9	0.130581	0.569508	2.12478	5.00E-05	0.00250269
DUSP8	0.511214	1.97607	1.95064	5.00E-05	0.00250269
CYP24A1	2.85431	10.6927	1.90541	5.00E-05	0.00250269
GALNTL2	0.186202	0.674688	1.85735	5.00E-05	0.00250269
LIPG	0.223379	0.799934	1.84039	5.00E-05	0.00250269
IL11	46.12	160.827	1.80205	5.00E-05	0.00250269
CXCL5	0.183147	0.636443	1.79703	0.00175	0.0461302
CREB5	1.37847	4.78097	1.79424	5.00E-05	0.00250269
DNER	0.282179	0.963401	1.77152	2.00E-04	0.0083258
KRTAP2-3	4.92068	16.2635	1.72471	5.00E-05	0.00250269
CXCR7	0.891801	2.80041	1.65084	5.00E-05	0.00250269
GDNF	2.01334	5.89506	1.54992	5.00E-05	0.00250269
ADAMTS1	14.3568	41.9092	1.54553	5.00E-05	0.00250269
C3orf52	5.31124	15.0044	1.49827	5.00E-05	0.00250269
PTPRR	0.394164	1.08373	1.45914	5.00E-05	0.00250269
FBXO32	1.45808	3.99806	1.45523	5.00E-05	0.00250269
ESM1	1.04591	2.79644	1.41883	5.00E-05	0.00250269
GCSAM	0.201597	0.531765	1.39932	0.00155	0.0420942
AMPD3	0.388526	1.00364	1.36917	5.00E-05	0.00250269
HAS2	8.95644	23.1082	1.36741	5.00E-05	0.00250269
LURAP1L	1.66509	4.25241	1.35268	5.00E-05	0.00250269
RCAN1	53.078	135.436	1.35143	5.00E-05	0.00250269
FGF5	3.30399	8.38738	1.34401	5.00E-05	0.00250269
CALB2	1.42192	3.58227	1.33303	5.00E-05	0.00250269
SCG5	0.707392	1.68329	1.2507	0.0012	0.034716
IRAK2	1.56249	3.70877	1.2471	5.00E-05	0.00250269
PAPPA	1.38399	3.27902	1.24443	5.00E-05	0.00250269
DUSP10	8.26069	19.4132	1.23271	5.00E-05	0.00250269

IFI44	3.12111	7.22552	1.21104	5.00E-05	0.00250269
BTBD11	0.23346	0.538123	1.20476	0.00165	0.0441361
CNN1	12.7876	29.175	1.18999	5.00E-05	0.00250269
SEMA7A	29.3798	66.8079	1.18519	5.00E-05	0.00250269
ABI3BP	3.11038	7.01966	1.17431	5.00E-05	0.00250269
TSPAN13	1.94486	4.38368	1.17247	1.00E-04	0.00461519
NFATC2	1.30247	2.93491	1.17207	5.00E-05	0.00250269
EPHB1	0.314117	0.699054	1.1541	6.00E-04	0.0202906
LOC100507460	0.910262	2.00622	1.14013	5.00E-05	0.00250269
PMAIP1	19.953	43.0593	1.10972	5.00E-05	0.00250269
SLC6A15	0.620305	1.3034	1.07123	5.00E-05	0.00250269
IGIP	0.71415	1.49256	1.06349	0.0014	0.0390113
HDAC9	0.52493	1.09591	1.06193	0.00025	0.00999951
LOC100506303	1.22148	2.45214	1.00541	0.00155	0.0420942
TGFBR2	9.99165	20.0093	1.00187	5.00E-05	0.00250269

Appendix E:

Differential gene expression between *STAT1*-deficient fibroblasts transduced with lentivirus expressing Fluc, uninfected or infected with *Lm*

(only 100 most highly upregulated genes are shown)

Gene	FPKM uninf	FPKM inf	Uninfected vs infected log2.fold change	p_value	q_value
CCL20	0	0.381466	Inf	5.00E-05	0.000499108
MT1G	0	16.872	Inf	5.00E-05	0.000499108
MT1F	1.01964	125.855	6.94756	2.00E-04	0.0016883
MT1X	20.1079	1750.97	6.44425	5.00E-05	0.000499108
MT1M	0.802097	52.5608	6.03407	3.00E-04	0.0023822
MT2A	185.022	9062.84	5.61419	5.00E-05	0.000499108
MT1E	10.3266	390.384	5.24045	5.00E-05	0.000499108
CSNK2A3	0.378917	9.65561	4.67141	5.00E-05	0.000499108
SNORA18	72.9972	1636.45	4.48659	5.00E-05	0.000499108
IL8	2.13186	45.9104	4.42864	5.00E-05	0.000499108
AHCTF1P1	0.0994008	1.4242	3.84075	5.00E-05	0.000499108
PTGS2	0.490987	6.95819	3.82496	5.00E-05	0.000499108
SERPINB2	0.887278	12.3988	3.80467	5.00E-05	0.000499108
BCL2A1	0.18761	2.4059	3.68077	5.00E-05	0.000499108
C4orf22	0.0834526	1.06177	3.66937	0.0018	0.0105685
GLUD2	0.118563	1.45179	3.61411	5.00E-05	0.000499108
LOC647859	0.114085	1.2628	3.46845	0.0046	0.0227771

HIST2H3D	0.819131	8.92764	3.44611	2.00E-04	0.0016883
NTNG1	0.0315313	0.304871	3.27334	0.00165	0.0098357 2
MAP1LC3B2	0.443155	4.22715	3.2538	5.00E-05	0.0004991 08
RPSAP58	17.5983	165.781	3.23578	5.00E-05	0.0004991 08
CXCL5	0.191912	1.68377	3.13318	5.00E-05	0.0004991 08
ESM1	0.934554	8.18363	3.13039	5.00E-05	0.0004991 08
ANKRD36BP1	0.83551	7.04126	3.0751	5.00E-05	0.0004991 08
TBC1D3P1-DHX40P1	0.106046	0.891475	3.0715	5.00E-04	0.0036555 4
MMP3	1.0641	8.64	3.0214	5.00E-05	0.0004991 08
FGF5	3.39016	26.4153	2.96195	5.00E-05	0.0004991 08
NBEAP1	0.358472	2.77027	2.95009	0.0075	0.0339539
CDR1	0.0425813	0.325421	2.93402	0.00395	0.0200996
CXCL3	0.58513	4.47058	2.93363	5.00E-05	0.0004991 08
SNORA40	275.496	2040.27	2.88866	5.00E-05	0.0004991 08
VCAM1	0.124961	0.924665	2.88745	5.00E-05	0.0004991 08
CCL2	4.39234	32.0643	2.86791	5.00E-05	0.0004991 08
GREM2	0.0458406	0.328611	2.84168	0.00025	0.0020435 9
HNRNPA1P10	117.928	839.303	2.83128	5.00E-05	0.0004991 08
LOC646938	0.650204	4.56062	2.81026	8.00E-04	0.0054223 4
KRTAP2-3	6.28569	41.0393	2.70686	5.00E-05	0.0004991 08
SPATA17	0.0850881	0.552089	2.69787	0.003	0.0160514
TNFRSF9	0.12664	0.810903	2.67879	5.00E-05	0.0004991 08
ARL14	0.118141	0.751433	2.66913	0.00045	0.0033518 4

CXCL2	0.445686	2.82592	2.66462	5.00E-05	0.000499108
MLLT10P1	0.549023	3.34158	2.60559	4.00E-04	0.0030434 3
C15orf48	0.279223	1.68858	2.59632	9.00E-04	0.0059820 8
C4orf48	8.69965	52.6098	2.5963	5.00E-05	0.000499108
SLC4A4	0.132438	0.791297	2.57891	5.00E-05	0.000499108
TFPI	9.59627	56.7677	2.56452	5.00E-05	0.000499108
MAST4	0.19742	1.16658	2.56294	5.00E-05	0.000499108
DLX5	0.130213	0.757942	2.54121	0.007	0.0320952
LOC154092	0.152318	0.884229	2.53734	5.00E-05	0.000499108
ANXA2P2	2.49391	14.4096	2.53055	5.00E-05	0.000499108
ZNF724P	1.65196	9.54061	2.52991	5.00E-05	0.000499108
TM4SF1	8.77381	49.5984	2.49902	5.00E-05	0.000499108
NMU	0.263942	1.49061	2.49761	0.00085	0.0057051 9
SLC30A1	4.70422	25.2369	2.42351	5.00E-05	0.000499108
RAET1L	0.150871	0.790767	2.38993	0.0059	0.0278494
IL1B	0.206603	1.06647	2.3679	0.00015	0.0013192 7
LINC00467	2.01688	10.1299	2.32842	5.00E-05	0.000499108
CXCL1	0.817943	4.10265	2.32648	5.00E-05	0.000499108
HIST1H1E	0.484744	2.40006	2.30777	0.00075	0.0051343 2
SRGN	2.91281	14.3895	2.30453	5.00E-05	0.000499108
PDIA3P	1.27041	6.23034	2.29402	5.00E-05	0.000499108
HIATL2	1.99388	9.74508	2.2891	5.00E-05	0.000499108
OLR1	0.160238	0.780235	2.28369	5.00E-	0.0004991

				05	08
HDAC9	0.519506	2.48369	2.25727	5.00E-05	0.000499108
HIST3H2A	4.56338	21.8125	2.25698	5.00E-05	0.000499108
TAF13	33.9319	161.611	2.25181	5.00E-05	0.000499108
HIST1H1C	7.37962	34.8336	2.23886	5.00E-05	0.000499108
OGFRL1	5.47586	25.4093	2.2142	5.00E-05	0.000499108
MRPS28	29.5412	135.747	2.20012	5.00E-05	0.000499108
CCL7	0.345737	1.54702	2.16174	0.0019	0.0110478
SGK196	2.88348	12.8471	2.15555	5.00E-05	0.000499108
EFCAB11	7.6998	33.757	2.13229	5.00E-05	0.000499108
TWIST2	37.5161	162.534	2.11516	5.00E-05	0.000499108
MT1A	2.07923	9.00442	2.11459	0.006	0.0282382
C6orf57	2.32051	9.96857	2.10294	5.00E-05	0.000499108
ZNF626	0.316628	1.34294	2.08454	0.0012	0.0075825
VIT	0.24221	1.02213	2.07725	5.00E-05	0.000499108
CMC1	8.72602	36.5256	2.06551	5.00E-05	0.000499108
STX8	22.5672	93.938	2.05748	5.00E-05	0.000499108
HAS2	8.63608	35.7551	2.0497	5.00E-05	0.000499108
MALL	0.811228	3.24473	1.99992	5.00E-05	0.000499108
SSTR1	6.14369	24.4718	1.99394	5.00E-05	0.000499108
XRCC4	6.96637	27.4528	1.97848	5.00E-05	0.000499108
MNAT1	16.1788	62.8148	1.957	5.00E-05	0.000499108
MILR1	0.408739	1.58438	1.95467	0.00715	0.0326576
GRAMD1B	0.151461	0.58431	1.94778	5.00E-05	0.000499108

ITGB8	0.305166	1.17252	1.94195	5.00E-05	0.000499108
ECSCR	1.41726	5.42663	1.93695	5.00E-05	0.000499108
PPP4R2	24.9289	94.6341	1.92454	5.00E-05	0.000499108
ZNF573	0.409288	1.54882	1.91998	5.00E-05	0.000499108
BIRC3	0.143759	0.539432	1.90779	5.00E-05	0.000499108
TNFAIP2	0.202353	0.749169	1.88842	5.00E-05	0.000499108
ID4	0.293213	1.056	1.84858	5.00E-05	0.000499108
TNFAIP3	1.71625	6.14731	1.84069	5.00E-05	0.000499108
KITLG	11.9327	42.5989	1.8359	5.00E-05	0.000499108
NSMCE2	12.3883	44.1748	1.83425	5.00E-05	0.000499108
AGTR1	0.958136	3.4119	1.83227	5.00E-05	0.000499108
NDUFAF2	49.7349	176.78	1.82963	5.00E-05	0.000499108
DGKI	0.224306	0.793426	1.82263	5.00E-05	0.000499108
KRTAP1-5	0.344214	1.19333	1.79362	0.0036	0.0186422

Appendix F:

Upstream regulators identified by Ingenuity Pathway Analysis for genes, regulated by *Lm* infection

Upstream Regulator	Molecule Type	Predicted Activation State	Activation z-score	p-value of overlap
TNF	cytokine	Activated	5.593	4.48E-10
IL1B	cytokine	Activated	3.999	8.75E-05
IL1A	cytokine	Activated	3.569	9.06E-09
CD24	other	Activated	3.464	2.21E-06
ERG	transcription regulator	Activated	3.464	7.42E-03
NFkB (complex)	complex	Activated	3.449	2.24E-05
TLR7	transmembrane receptor	Activated	3.434	8.63E-05
Cg	complex	Activated	3.431	4.52E-13
SMARCA4	transcription regulator	Activated	3.297	4.68E-03
TREM1	transmembrane receptor	Activated	3.258	5.56E-06
PDGF BB	complex	Activated	3.000	3.54E-03

Target molecules in datasets:

TNF:

ALDH1A3,APLN,APOE,ATP2B1,BCL2A1,BIRC2,BTG3,CCL2,CCND1,CDH2,CXCL1,CXCL2,CXCL3,CXCL8,DUSP10,FST,GPR176,H19,HDAC9,ICAM1,IFIT3,INHBA,KRT34,MMP2,MMP3,NEDD9,NFKBIA,PMAIP1,PPP1R15A,PSMB9,PTGS2,PTPN12,PTX3,RBPMS,RFTN1,RGS14,RGS20,RND3,SDC4,SEMA3C,SERPINB2,SERPINB8,SOX9,TM4SF1,TNFAIP3,TNFRSF11B,VEGFC,ZNF267

IL1B:

APOE,BCL2A1,CCL2,CEBPB,CXCL1,CXCL2,CXCL3,CXCL8,FGF2,ICAM1,MMP3,MT2A,NFKBIA,NMI,PTGS2,PTX3,SEMA3A,SERPINB2,SRGN,VEGFC

IL1A:

ALDH1A3,BIRC2,CCL2,CXCL1,CXCL2,CXCL3,CXCL8,FGF2,ICAM1,KITLG,LOX,MT2A,NFKBIA,PTGS2,PTX3,TNFAIP3,TNFRSF11B

CD24:

ASPM,ATP13A3,CXCL8,DEPDC1,DIAPH2,HMMR,ICAM1,JMJD1C,KIF18A,PPP1R15A,RASA1,SLC30A1,SMC4,TFPI,THBS1,TOP2A

ERG:

ARHGAP24,CXCL1,DIAPH2,DIAPH3,EPB41L3,HMMR,MYO10,PHACTR2,PPAP2B,RALGPS2,RASA2,ROCK2

NFkB(complex):

BCL2A1,BIRC2,CCL2,CCND1,CEBPB,CLU,CXCL1,CXCL2,CXCL3,CXCL8,HAS2,ICAM1,MMP2,MMP3,NFKBIA,PSMB9,PTGS2,RFTN1,SDC4,SERPINB2,TFPI2,TNFAIP3,VEGFC

TLR7:

CCL2,CPEB2,CXCL1,CXCL2,CXCL3,CXCL8,FGF2,GNG2,ICAM1,IFIT3,NFKBIA,PTX3

Cg:

CCL2,CDH2,CEP170,CXCL8,ELK3,EMP1,ESM1,FST,HAS2,HMGA2,MMP2,PHLDA1,PMAIP1,PODXL,PPAP2B,PTGS2,PTX3,RGS20,RGS4,STC1,TFPI2,TM4SF1,TMEM158,VEGFC

SMARCA4:

AHR,ALDH1A3,ANTXR2,C6orf203,CCL2,DLX2,FAM167A,GCHFR,HMGA2,ICAM1,INHBA,KHDRBS3,LOX,LPXN,MAP1B,MAPK1,MMP2,PDE4B,PPAP2B,PSMB9,PTX3,S100A2,S100A6,SERPINB2,SERPINB7,SERPINB8,STK33,TCAF2,TSPAN13

TREM1:

CXCL1,CXCL2,CXCL3,CXCL8,ETS2,FNDC3A,GREM1,IFIT2,INHBA,MT1E,MT1F,MT1M,NT5E,PHLDA1,PPAP2B,PTGS2,SERPINB2,TFPI2,THBS1,TMEM158,WBP5

PDGF BB:

ATP2B1,CCL2,CEBPB,CXCL8,PHLDA1,PPP1R15A,RND3,THBS1,TNFAIP3

APPENDIX G:

Characterization of the *CDH1/MET*-deficient HEK293A clone

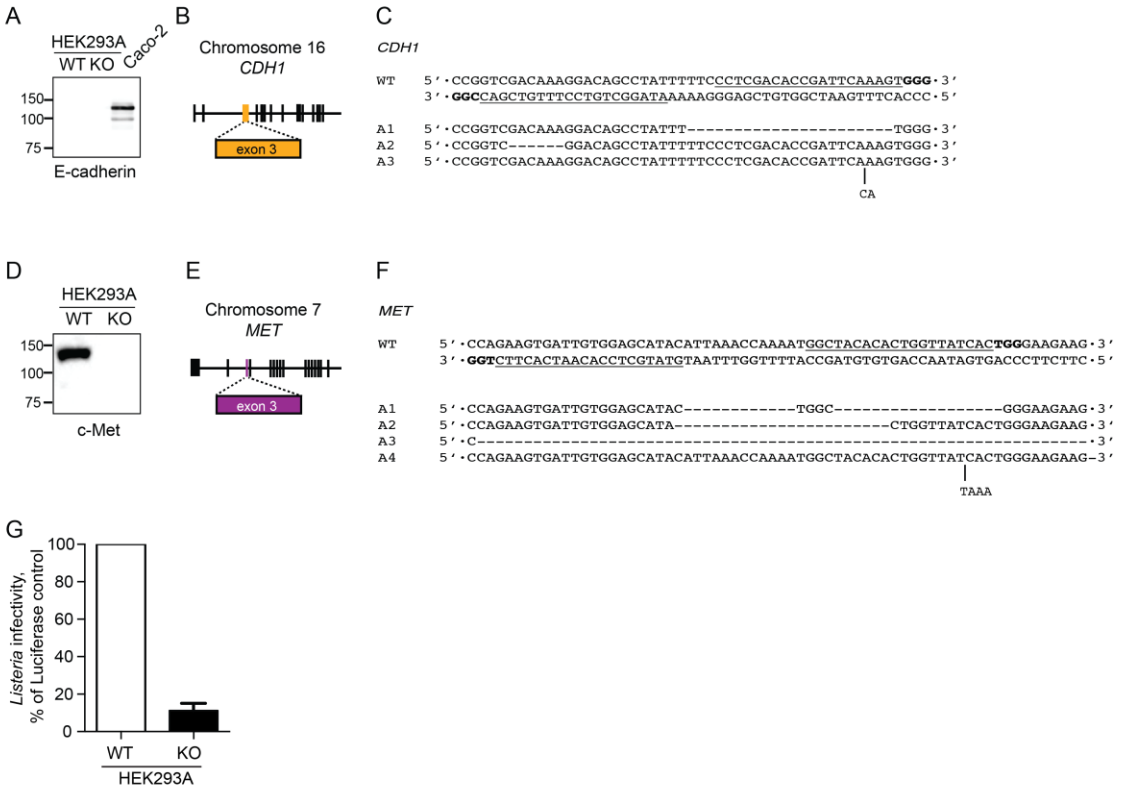

(A) Western blot analysis of wild type HEK2939A, *CDH1/MET*-deficient HEK293A (clone P4E4) and Caco-2 cell lysates stained for E-cadherin. Equal amounts of each lysate (30µg total protein as measured by BCA assay) were loaded per lane. (B) Exon structure of human CDH1 gene, chromosome 7. Exon 3 was targeted for CRISPR/Cas9-mediated gene editing. (C) Sequence confirmation of the single-cell sorted clone used in Fig 9. The wild type reference sequence is shown on top, with the guide sequences underlined and Protospacer Adjacent Motif (PAM) highlighted in bold. Sequencing revealed 3 distinct alleles with frameshift insertions or deletions. (D) Western blot analysis of wild type HEK2939A and *CDH1/MET*-deficient HEK293A (clone P4E4) cell

lysates stained for c-Met. Equal amounts of each lysate (30μg total protein as measured by BCA assay) were loaded per lane. (E) Exon structure of human MET gene, chromosome 16. Exon 3 was targeted for CRISPR/Cas9-mediated gene editing. (F) Sequence confirmation of the single-cell sorted clone used in Fig 9. The wild type reference sequence is shown on top, with the guide sequences underlined and PAM highlighted in bold. Sequencing revealed 4 distinct alleles with frameshift insertions or deletions. (G) Infectivity of wild type *Lm* in wild type (WT) and *CDH1/MET*-deficient (KO) HEK293A cells. Error bars represent s.d., n=3

Appendix H:

Alignment of FcγRIa protein sequences from different species

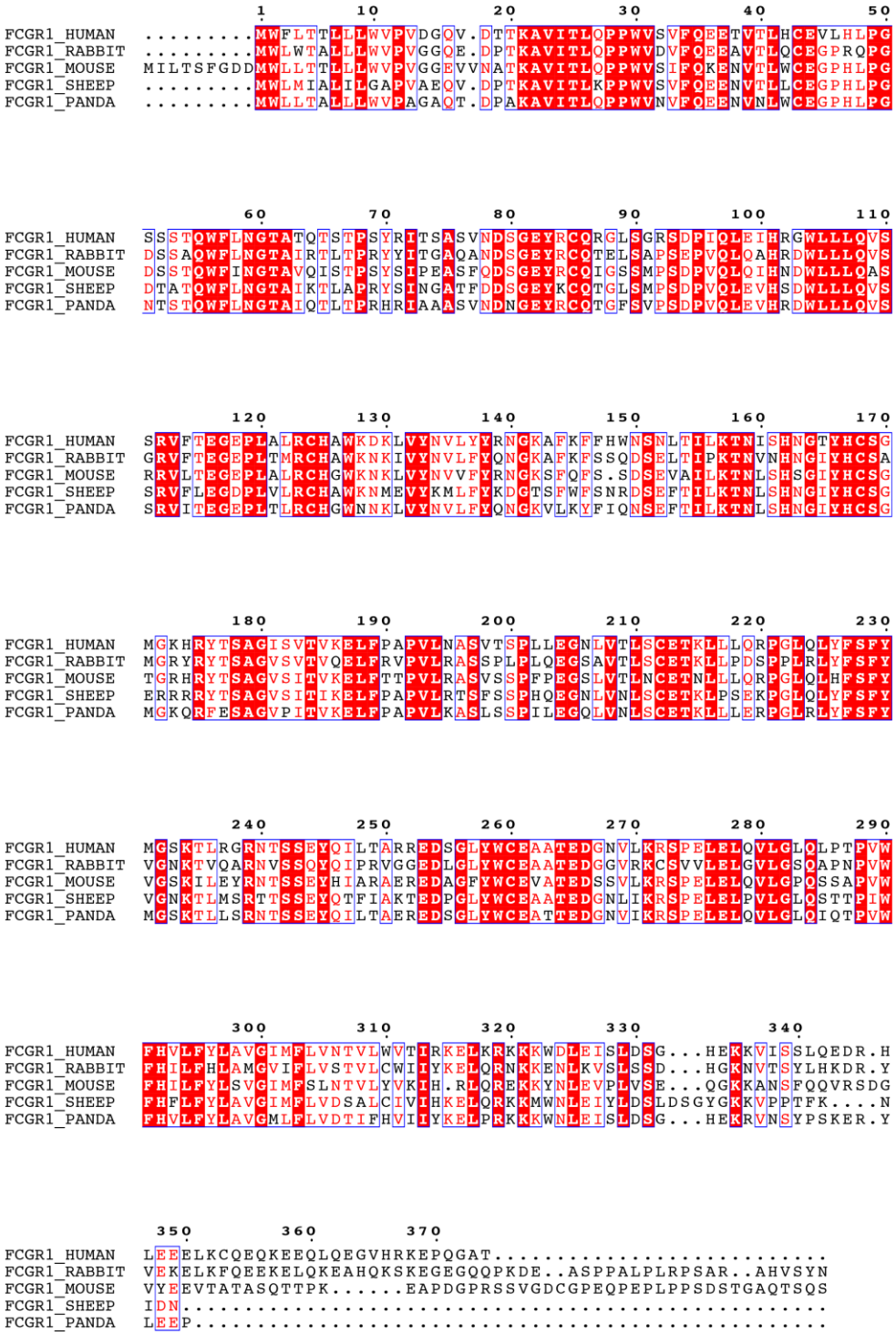

The amino acid alignment was performed using Clustal Omega and visualized using ESPript 3.0 server http://espript.ibcp.fr (206). Highly conserved residues are shown in red text and boxed in blue; positions that are identical between the receptors are highlighted with a red background.

BIBLIOGRAPHY

1. Medzhitov R, Janeway C, Jr. Innate immunity. N Engl J Med. 2000;343(5):338-44.
2. Janeway CA, Jr. Approaching the asymptote? Evolution and revolution in immunology. Cold Spring Harb Symp Quant Biol. 1989;54 Pt 1:1-13.
3. O'Neill LA, Golenbock D, Bowie AG. The history of Toll-like receptors - redefining innate immunity. Nature reviews Immunology. 2013;13(6):453-60.
4. Takeuchi O, Akira S. Pattern recognition receptors and inflammation. Cell. 2010;140(6):805-20.
5. Medzhitov R. Recognition of microorganisms and activation of the immune response. Nature. 2007;449(7164):819-26.
6. Brubaker SW, Bonham KS, Zanoni I, Kagan JC. Innate immune pattern recognition: a cell biological perspective. Annual review of immunology. 2015;33:257-90.
7. Akira S, Uematsu S, Takeuchi O. Pathogen recognition and innate immunity. Cell. 2006;124(4):783-801.
8. O'Neill LA, Bowie AG. The family of five: TIR-domain-containing adaptors in Toll-like receptor signalling. Nature reviews Immunology. 2007;7(5):353-64.
9. Hoving JC, Wilson GJ, Brown GD. Signalling C-type lectin receptors, microbial recognition and immunity. Cellular microbiology. 2014;16(2):185-94.
10. Chen G, Shaw MH, Kim YG, Nunez G. NOD-like receptors: role in innate immunity and inflammatory disease. Annu Rev Pathol. 2009;4:365-98.
11. Motta V, Soares F, Sun T, Philpott DJ. NOD-like receptors: versatile cytosolic sentinels. Physiol Rev. 2015;95(1):149-78.
12. Kim YK, Shin JS, Nahm MH. NOD-Like Receptors in Infection, Immunity, and Diseases. Yonsei Med J. 2016;57(1):5-14.
13. Yoneyama M, Kikuchi M, Matsumoto K, Imaizumi T, Miyagishi M, Taira K, et al. Shared and unique functions of the DExD/H-box helicases RIG-I, MDA5, and LGP2 in antiviral innate immunity. Journal of immunology. 2005;175(5):2851-8.
14. Seth RB, Sun L, Ea CK, Chen ZJ. Identification and characterization of MAVS, a mitochondrial antiviral signaling protein that activates NF-kappaB and IRF 3. Cell. 2005;122(5):669-82.
15. Gack MU. Mechanisms of RIG-I-like receptor activation and manipulation by viral pathogens. J Virol. 2014;88(10):5213-6.
16. Anon - Nobel Lectures - Physiology or Medicine 1901-1921. Lancet. 1967;2(7529):1288-&.
17. Cai X, Chiu YH, Chen ZJ. The cGAS-cGAMP-STING pathway of cytosolic DNA sensing and signaling. Molecular cell. 2014;54(2):289-96.
18. Sun L, Wu J, Du F, Chen X, Chen ZJ. Cyclic GMP-AMP synthase is a cytosolic DNA sensor that activates the type I interferon pathway. Science. 2013;339(6121):786-91.

19. Gao P, Ascano M, Wu Y, Barchet W, Gaffney BL, Zillinger T, et al. Cyclic [G(2',5')pA(3',5')p] is the metazoan second messenger produced by DNA-activated cyclic GMP-AMP synthase. Cell. 2013;153(5):1094-107.
20. Zhang X, Shi H, Wu J, Zhang X, Sun L, Chen C, et al. Cyclic GMP-AMP containing mixed phosphodiester linkages is an endogenous high-affinity ligand for STING. Molecular cell. 2013;51(2):226-35.
21. Burdette DL, Monroe KM, Sotelo-Troha K, Iwig JS, Eckert B, Hyodo M, et al. STING is a direct innate immune sensor of cyclic di-GMP. Nature. 2011;478(7370):515-8.
22. Barker JR, Koestler BJ, Carpenter VK, Burdette DL, Waters CM, Vance RE, et al. STING-dependent recognition of cyclic di-AMP mediates type I interferon responses during Chlamydia trachomatis infection. mBio. 2013;4(3):e00018-13.
23. Saitoh T, Fujita N, Hayashi T, Takahara K, Satoh T, Lee H, et al. Atg9a controls dsDNA-driven dynamic translocation of STING and the innate immune response. Proceedings of the National Academy of Sciences of the United States of America. 2009;106(49):20842-6.
24. Ishikawa H, Ma Z, Barber GN. STING regulates intracellular DNA-mediated, type I interferon-dependent innate immunity. Nature. 2009;461(7265):788-92.
25. Ishikawa H, Barber GN. STING is an endoplasmic reticulum adaptor that facilitates innate immune signalling. Nature. 2008;455(7213):674-8.
26. Stark GR, Kerr IM, Williams BR, Silverman RH, Schreiber RD. How cells respond to interferons. Annu Rev Biochem. 1998;67:227-64.
27. Der SD, Zhou A, Williams BR, Silverman RH. Identification of genes differentially regulated by interferon alpha, beta, or gamma using oligonucleotide arrays. Proceedings of the National Academy of Sciences of the United States of America. 1998;95(26):15623-8.
28. Isaacs A, Lindenmann J. Virus interference. I. The interferon. Proc R Soc Lond B Biol Sci. 1957;147(927):258-67.
29. Berthold W, Tan C, Tan YH. Purification and in vitro labeling of interferon from a human fibroblastoid cell line. The Journal of biological chemistry. 1978;253(14):5206-12.
30. Rubinstein M, Rubinstein S, Familletti PC, Gross MS, Miller RS, Waldman AA, et al. Human leukocyte interferon purified to homogeneity. Science. 1978;202(4374):1289-90.
31. Platanias LC. Mechanisms of type-I- and type-II-interferon-mediated signalling. Nature reviews Immunology. 2005;5(5):375-86.
32. Ivashkiv LB, Donlin LT. Regulation of type I interferon responses. Nature reviews Immunology. 2014;14(1):36-49.
33. Aaronson DS, Horvath CM. A road map for those who don't know JAK-STAT. Science. 2002;296(5573):1653-5.
34. Schoggins JW. Interferon-stimulated genes: roles in viral pathogenesis. Current opinion in virology. 2014;6:40-6.
35. Bogdan C, Mattner J, Schleicher U. The role of type I interferons in non-viral infections. Immunol Rev. 2004;202:33-48.

36. Carrero JA. Confounding roles for type I interferons during bacterial and viral pathogenesis. Int Immunol. 2013;25(12):663-9.
37. Monroe KM, McWhirter SM, Vance RE. Induction of type I interferons by bacteria. Cellular microbiology. 2010;12(7):881-90.
38. Maier BB, Hladik A, Lakovits K, Korosec A, Martins R, Kral JB, et al. Type I interferon promotes alveolar epithelial type II cell survival during pulmonary Streptococcus pneumoniae infection and sterile lung injury in mice. Eur J Immunol. 2016;46(9):2175-86.
39. LeMessurier KS, Hacker H, Chi L, Tuomanen E, Redecke V. Type I interferon protects against pneumococcal invasive disease by inhibiting bacterial transmigration across the lung. PLoS Pathog. 2013;9(11):e1003727.
40. Lippmann J, Muller HC, Naujoks J, Tabeling C, Shin S, Witzenrath M, et al. Dissection of a type I interferon pathway in controlling bacterial intracellular infection in mice. Cellular microbiology. 2011;13(11):1668-82.
41. Naujoks J, Tabeling C, Dill BD, Hoffmann C, Brown AS, Kunze M, et al. IFNs Modify the Proteome of Legionella-Containing Vacuoles and Restrict Infection Via IRG1-Derived Itaconic Acid. PLoS Pathog. 2016;12(2):e1005408.
42. Mancuso G, Midiri A, Biondo C, Beninati C, Zummo S, Galbo R, et al. Type I IFN signaling is crucial for host resistance against different species of pathogenic bacteria. Journal of immunology. 2007;178(5):3126-33.
43. Guler R, Parihar SP, Spohn G, Johansen P, Brombacher F, Bachmann MF. Blocking IL-1alpha but not IL-1beta increases susceptibility to chronic Mycobacterium tuberculosis infection in mice. Vaccine. 2011;29(6):1339-46.
44. Mayer-Barber KD, Andrade BB, Barber DL, Hieny S, Feng CG, Caspar P, et al. Innate and adaptive interferons suppress IL-1alpha and IL-1beta production by distinct pulmonary myeloid subsets during Mycobacterium tuberculosis infection. Immunity. 2011;35(6):1023-34.
45. Moreira-Teixeira L, Sousa J, McNab FW, Torrado E, Cardoso F, Machado H, et al. Type I IFN Inhibits Alternative Macrophage Activation during Mycobacterium tuberculosis Infection and Leads to Enhanced Protection in the Absence of IFN-gamma Signaling. Journal of immunology. 2016;197(12):4714-26.
46. Henry T, Kirimanjeswara GS, Ruby T, Jones JW, Peng K, Perret M, et al. Type I IFN signaling constrains IL-17A/F secretion by gammadelta T cells during bacterial infections. Journal of immunology. 2010;184(7):3755-67.
47. Fujiki T, Tanaka A. Antibacterial activity of recombinant murine beta interferon. Infection and immunity. 1988;56(3):548-51.
48. Kernbauer E, Maier V, Rauch I, Muller M, Decker T. Route of Infection Determines the Impact of Type I Interferons on Innate Immunity to Listeria monocytogenes. Plos One. 2013;8(6).
49. Auerbuch V, Brockstedt DG, Meyer-Morse N, O'Riordan M, Portnoy DA. Mice lacking the type I interferon receptor are resistant to Listeria monocytogenes. The Journal of experimental medicine. 2004;200(4):527-33.

50. Carrero JA, Calderon B, Unanue ER. Type I interferon sensitizes lymphocytes to apoptosis and reduces resistance to Listeria infection. The Journal of experimental medicine. 2004;200(4):535-40.
51. O'Connell RM, Saha SK, Vaidya SA, Bruhn KW, Miranda GA, Zarnegar B, et al. Type I interferon production enhances susceptibility to Listeria monocytogenes infection. The Journal of experimental medicine. 2004;200(4):437-45.
52. Archer KA, Durack J, Portnoy DA. STING-dependent type I IFN production inhibits cell-mediated immunity to Listeria monocytogenes. PLoS Pathog. 2014;10(1):e1003861.
53. Pitts MG, Myers-Morales T, D'Orazio SE. Type I IFN Does Not Promote Susceptibility to Foodborne Listeria monocytogenes. Journal of immunology. 2016;196(7):3109-16.
54. Weis J, Seeliger HP. Incidence of Listeria monocytogenes in nature. Appl Microbiol. 1975;30(1):29-32.
55. Vazquez-Boland JA, Kuhn M, Berche P, Chakraborty T, Dominguez-Bernal G, Goebel W, et al. Listeria pathogenesis and molecular virulence determinants. Clin Microbiol Rev. 2001;14(3):584-640.
56. Orsi RH, Wiedmann M. Characteristics and distribution of Listeria spp., including Listeria species newly described since 2009. Appl Microbiol Biotechnol. 2016;100(12):5273-87.
57. Glaser P, Frangeul L, Buchrieser C, Rusniok C, Amend A, Baquero F, et al. Comparative genomics of Listeria species. Science. 2001;294(5543):849-52.
58. Gouin E, Mengaud J, Cossart P. The virulence gene cluster of Listeria monocytogenes is also present in Listeria ivanovii, an animal pathogen, and Listeria seeligeri, a nonpathogenic species. Infection and immunity. 1994;62(8):3550-3.
59. Murray EGD, Webb RA, Swann MBR. A disease of rabbits characterised by a large mononuclear leucocytosis, caused by a hitherto undescribed bacillus Bacterium monocytogenes (n.sp.). The Journal of Pathology and Bacteriology. 1926;29(4):407-39.
60. Farber JM, Peterkin PI. Listeria monocytogenes, a food-borne pathogen. Microbiol Rev. 1991;55(3):476-511.
61. (CDC) CfDCaP. National Listeria surveillance annual summary, 2013. . Atlanta, Georgia: US Department of Health and Human Services, CDC. 2015.
62. Lorber B. Listeriosis. Clin Infect Dis. 1997;24(1):1-9; quiz 10-1.
63. Buchanan RL, Gorris LGM, Hayman MM, Jackson TC, Whiting RC. A review of Listeria monocytogenes: An update on outbreaks, virulence, dose-response, ecology, and risk assessments. Food Control. 2017;75:1-13.
64. Lemaire V, Cerf O, Audurier A. Thermal resistance of Listeria monocytogenes. Ann Rech Vet. 1989;20(4):493-500.
65. Wilkins PO, Bourgeois R, Murray RG. Psychrotrophic properties of Listeria monocytogenes. Can J Microbiol. 1972;18(5):543-51.
66. George SM, Lund BM, Brocklehurst TF. The effect of pH and temperature on initiation of growth of Listeria monocytogenes. Letters in Applied Microbiology. 1988;6:153-6.

67. McClure PJ, Roberts TA, Oguru PO. Comparison of the effects of sodium chloride, pH and temperature on the growth of Listeria monocytogenes on gradient plates and liquid medium. Letters in Applied Microbiology. 1989;9:95-9.
68. Chakraborty T, Leimeister-Wachter M, Domann E, Hartl M, Goebel W, Nichterlein T, et al. Coordinate regulation of virulence genes in Listeria monocytogenes requires the product of the prfA gene. Journal of bacteriology. 1992;174(2):568-74.
69. Leimeister-Wachter M, Haffner C, Domann E, Goebel W, Chakraborty T. Identification of a gene that positively regulates expression of listeriolysin, the major virulence factor of listeria monocytogenes. Proceedings of the National Academy of Sciences of the United States of America. 1990;87(21):8336-40.
70. Scortti M, Monzo HJ, Lacharme-Lora L, Lewis DA, Vazquez-Boland JA. The PrfA virulence regulon. Microbes Infect. 2007;9(10):1196-207.
71. Milohanic E, Glaser P, Coppee JY, Frangeul L, Vega Y, Vazquez-Boland JA, et al. Transcriptome analysis of Listeria monocytogenes identifies three groups of genes differently regulated by PrfA. Mol Microbiol. 2003;47(6):1613-25.
72. Korner H, Sofia HJ, Zumft WG. Phylogeny of the bacterial superfamily of Crp-Fnr transcription regulators: exploiting the metabolic spectrum by controlling alternative gene programs. FEMS Microbiol Rev. 2003;27(5):559-92.
73. Mengaud J, Vicente MF, Cossart P. Transcriptional mapping and nucleotide sequence of the Listeria monocytogenes hlyA region reveal structural features that may be involved in regulation. Infection and immunity. 1989;57(12):3695-701.
74. Sheehan B, Klarsfeld A, Msadek T, Cossart P. Differential activation of virulence gene expression by PrfA, the Listeria monocytogenes virulence regulator. Journal of bacteriology. 1995;177(22):6469-76.
75. Camilli A, Tilney LG, Portnoy DA. Dual roles of plcA in Listeria monocytogenes pathogenesis. Mol Microbiol. 1993;8(1):143-57.
76. Freitag NE, Rong L, Portnoy DA. Regulation of the prfA transcriptional activator of Listeria monocytogenes: multiple promoter elements contribute to intracellular growth and cell-to-cell spread. Infection and immunity. 1993;61(6):2537-44.
77. Johansson J, Mandin P, Renzoni A, Chiaruttini C, Springer M, Cossart P. An RNA thermosensor controls expression of virulence genes in Listeria monocytogenes. Cell. 2002;110(5):551-61.
78. Schwab U, Bowen B, Nadon C, Wiedmann M, Boor KJ. The Listeria monocytogenes prfAP2 promoter is regulated by sigma B in a growth phase dependent manner. FEMS Microbiol Lett. 2005;245(2):329-36.
79. Freitag NE, Portnoy DA. Dual promoters of the Listeria monocytogenes prfA transcriptional activator appear essential in vitro but are redundant in vivo. Mol Microbiol. 1994;12(5):845-53.
80. Loh E, Dussurget O, Gripenland J, Vaitkevicius K, Tiensuu T, Mandin P, et al. A trans-acting riboswitch controls expression of the virulence regulator PrfA in Listeria monocytogenes. Cell. 2009;139(4):770-9.
81. Reniere ML, Whiteley AT, Hamilton KL, John SM, Lauer P, Brennan RG, et al. Glutathione activates virulence gene expression of an intracellular pathogen. Nature. 2015;517(7533):170-3.

82. Hall M, Grundstrom C, Begum A, Lindberg MJ, Sauer UH, Almqvist F, et al. Structural basis for glutathione-mediated activation of the virulence regulatory protein PrfA in Listeria. Proceedings of the National Academy of Sciences of the United States of America. 2016;113(51):14733-8.
83. Pizarro-Cerda J, Charbit A, Enninga J, Lafont F, Cossart P. Manipulation of host membranes by the bacterial pathogens Listeria, Francisella, Shigella and Yersinia. Semin Cell Dev Biol. 2016.
84. Bierne H, Sabet C, Personnic N, Cossart P. Internalins: a complex family of leucine-rich repeat-containing proteins in Listeria monocytogenes. Microbes Infect. 2007;9(10):1156-66.
85. Mengaud J, Ohayon H, Gounon P, Mege RM, Cossart P. E-cadherin is the receptor for internalin, a surface protein required for entry of L. monocytogenes into epithelial cells. Cell. 1996;84(6):923-32.
86. Bonazzi M, Veiga E, Pizarro-Cerda J, Cossart P. Successive post-translational modifications of E-cadherin are required for InlA-mediated internalization of Listeria monocytogenes. Cellular microbiology. 2008;10(11):2208-22.
87. Bonazzi M, Vasudevan L, Mallet A, Sachse M, Sartori A, Prevost MC, et al. Clathrin phosphorylation is required for actin recruitment at sites of bacterial adhesion and internalization. The Journal of cell biology. 2011;195(3):525-36.
88. Bonazzi M, Kuhbacher A, Toledo-Arana A, Mallet A, Vasudevan L, Pizarro-Cerda J, et al. A common clathrin-mediated machinery co-ordinates cell-cell adhesion and bacterial internalization. Traffic. 2012;13(12):1653-66.
89. Lecuit M, Nelson DM, Smith SD, Khun H, Huerre M, Vacher-Lavenu MC, et al. Targeting and crossing of the human maternofetal barrier by Listeria monocytogenes: role of internalin interaction with trophoblast E-cadherin. Proceedings of the National Academy of Sciences of the United States of America. 2004;101(16):6152-7.
90. Shen Y, Naujokas M, Park M, Ireton K. InIB-dependent internalization of Listeria is mediated by the Met receptor tyrosine kinase. Cell. 2000;103(3):501-10.
91. Veiga E, Cossart P. Listeria hijacks the clathrin-dependent endocytic machinery to invade mammalian cells. Nat Cell Biol. 2005;7(9):894-900.
92. Veiga E, Guttman JA, Bonazzi M, Boucrot E, Toledo-Arana A, Lin AE, et al. Invasive and adherent bacterial pathogens co-Opt host clathrin for infection. Cell Host Microbe. 2007;2(5):340-51.
93. Ireton K, Payrastre B, Chap H, Ogawa W, Sakaue H, Kasuga M, et al. A role for phosphoinositide 3-kinase in bacterial invasion. Science. 1996;274(5288):780-2.
94. Pentecost M, Kumaran J, Ghosh P, Amieva MR. Listeria monocytogenes internalin B activates junctional endocytosis to accelerate intestinal invasion. PLoS Pathog. 2010;6(5):e1000900.
95. Hamon MA, Ribet D, Stavru F, Cossart P. Listeriolysin O: the Swiss army knife of Listeria. Trends Microbiol. 2012;20(8):360-8.
96. Henry R, Shaughnessy L, Loessner MJ, Alberti-Segui C, Higgins DE, Swanson JA. Cytolysin-dependent delay of vacuole maturation in macrophages infected with Listeria monocytogenes. Cellular microbiology. 2006;8(1):107-19.

97. Shaughnessy LM, Hoppe AD, Christensen KA, Swanson JA. Membrane perforations inhibit lysosome fusion by altering pH and calcium in Listeria monocytogenes vacuoles. Cellular microbiology. 2006;8(5):781-92.
98. Beauregard KE, Lee KD, Collier RJ, Swanson JA. pH-dependent perforation of macrophage phagosomes by listeriolysin O from Listeria monocytogenes. The Journal of experimental medicine. 1997;186(7):1159-63.
99. Smith GA, Marquis H, Jones S, Johnston NC, Portnoy DA, Goldfine H. The two distinct phospholipases C of Listeria monocytogenes have overlapping roles in escape from a vacuole and cell-to-cell spread. Infection and immunity. 1995;63(11):4231-7.
100. Portnoy DA, Jacks PS, Hinrichs DJ. Role of hemolysin for the intracellular growth of Listeria monocytogenes. The Journal of experimental medicine. 1988;167(4):1459-71.
101. Marquis H, Bouwer HG, Hinrichs DJ, Portnoy DA. Intracytoplasmic growth and virulence of Listeria monocytogenes auxotrophic mutants. Infection and immunity. 1993;61(9):3756-60.
102. Chico-Calero I, Suarez M, Gonzalez-Zorn B, Scortti M, Slaghuis J, Goebel W, et al. Hpt, a bacterial homolog of the microsomal glucose- 6-phosphate translocase, mediates rapid intracellular proliferation in Listeria. Proceedings of the National Academy of Sciences of the United States of America. 2002;99(1):431-6.
103. Keeney KM, Stuckey JA, O'Riordan MX. LplA1-dependent utilization of host lipoyl peptides enables Listeria cytosolic growth and virulence. Mol Microbiol. 2007;66(3):758-70.
104. Stritzker J, Janda J, Schoen C, Taupp M, Pilgrim S, Gentschev I, et al. Growth, virulence, and immunogenicity of Listeria monocytogenes aro mutants. Infection and immunity. 2004;72(10):5622-9.
105. Kocks C, Gouin E, Tabouret M, Berche P, Ohayon H, Cossart P. L. monocytogenes-induced actin assembly requires the actA gene product, a surface protein. Cell. 1992;68(3):521-31.
106. Boujemaa-Paterski R, Gouin E, Hansen G, Samarin S, Le Clainche C, Didry D, et al. Listeria protein ActA mimics WASp family proteins: it activates filament barbed end branching by Arp2/3 complex. Biochemistry. 2001;40(38):11390-404.
107. Skoble J, Auerbuch V, Goley ED, Welch MD, Portnoy DA. Pivotal role of VASP in Arp2/3 complex-mediated actin nucleation, actin branch-formation, and Listeria monocytogenes motility. The Journal of cell biology. 2001;155(1):89-100.
108. Lambrechts A, Gevaert K, Cossart P, Vandekerckhove J, Van Troys M. Listeria comet tails: the actin-based motility machinery at work. Trends in cell biology. 2008;18(5):220-7.
109. Rajabian T, Gavicherla B, Heisig M, Muller-Altrock S, Goebel W, Gray-Owen SD, et al. The bacterial virulence factor InlC perturbs apical cell junctions and promotes cell-to-cell spread of Listeria. Nat Cell Biol. 2009;11(10):1212-8.
110. Poussin MA, Goldfine H. Evidence for the involvement of ActA in maturation of the Listeria monocytogenes phagosome. Cell Res. 2010;20(1):109-12.

111. Suarez M, Gonzalez-Zorn B, Vega Y, Chico-Calero I, Vazquez-Boland JA. A role for ActA in epithelial cell invasion by Listeria monocytogenes. Cellular microbiology. 2001;3(12):853-64.
112. Yoshikawa Y, Ogawa M, Hain T, Yoshida M, Fukumatsu M, Kim M, et al. Listeria monocytogenes ActA-mediated escape from autophagic recognition. Nat Cell Biol. 2009;11(10):1233-40.
113. Travier L, Guadagnini S, Gouin E, Dufour A, Chenal-Francisque V, Cossart P, et al. ActA promotes Listeria monocytogenes aggregation, intestinal colonization and carriage. PLoS Pathog. 2013;9(1):e1003131.
114. Lecuit M, Dramsi S, Gottardi C, Fedor-Chaiken M, Gumbiner B, Cossart P. A single amino acid in E-cadherin responsible for host specificity towards the human pathogen Listeria monocytogenes. The EMBO journal. 1999;18(14):3956-63.
115. Khelef N, Lecuit M, Bierne H, Cossart P. Species specificity of the Listeria monocytogenes InlB protein. Cellular microbiology. 2006;8(3):457-70.
116. Lecuit M, Vandormael-Pournin S, Lefort J, Huerre M, Gounon P, Dupuy C, et al. A transgenic model for listeriosis: role of internalin in crossing the intestinal barrier. Science. 2001;292(5522):1722-5.
117. Disson O, Grayo S, Huillet E, Nikitas G, Langa-Vives F, Dussurget O, et al. Conjugated action of two species-specific invasion proteins for fetoplacental listeriosis. Nature. 2008;455(7216):1114-8.
118. Wollert T, Pasche B, Rochon M, Deppenmeier S, van den Heuvel J, Gruber AD, et al. Extending the host range of Listeria monocytogenes by rational protein design. Cell. 2007;129(5):891-902.
119. Tsai YH, Disson O, Bierne H, Lecuit M. Murinization of internalin extends its receptor repertoire, altering Listeria monocytogenes cell tropism and host responses. PLoS Pathog. 2013;9(5):e1003381.
120. Stockinger S, Kastner R, Kernbauer E, Pilz A, Westermayer S, Reutterer B, et al. Characterization of the interferon-producing cell in mice infected with Listeria monocytogenes. PLoS Pathog. 2009;5(3):e1000355.
121. O'Riordan M, Yi CH, Gonzales R, Lee KD, Portnoy DA. Innate recognition of bacteria by a macrophage cytosolic surveillance pathway. Proceedings of the National Academy of Sciences of the United States of America. 2002;99(21):13861-6.
122. Abdullah Z, Schlee M, Roth S, Mraheil MA, Barchet W, Bottcher J, et al. RIG-I detects infection with live Listeria by sensing secreted bacterial nucleic acids. The EMBO journal. 2012;31(21):4153-64.
123. Stockinger S, Reutterer B, Schaljo B, Schellack C, Brunner S, Materna T, et al. IFN regulatory factor 3-dependent induction of type I IFNs by intracellular bacteria is mediated by a TLR- and Nod2-independent mechanism. Journal of immunology. 2004;173(12):7416-25.
124. Jin L, Hill KK, Filak H, Mogan J, Knowles H, Zhang B, et al. MPYS is required for IFN response factor 3 activation and type I IFN production in the response of cultured phagocytes to bacterial second messengers cyclic-di-AMP and cyclic-di-GMP. Journal of immunology. 2011;187(5):2595-601.

125. Woodward JJ, Iavarone AT, Portnoy DA. c-di-AMP secreted by intracellular Listeria monocytogenes activates a host type I interferon response. Science. 2010;328(5986):1703-5.
126. Sauer JD, Sotelo-Troha K, von Moltke J, Monroe KM, Rae CS, Brubaker SW, et al. The N-ethyl-N-nitrosourea-induced Goldenticket mouse mutant reveals an essential function of Sting in the in vivo interferon response to Listeria monocytogenes and cyclic dinucleotides. Infection and immunity. 2011;79(2):688-94.
127. Yang P, An H, Liu X, Wen M, Zheng Y, Rui Y, et al. The cytosolic nucleic acid sensor LRRFIP1 mediates the production of type I interferon via a beta-catenin-dependent pathway. Nature immunology. 2010;11(6):487-94.
128. Aubry C, Corr SC, Wienerroither S, Goulard C, Jones R, Jamieson AM, et al. Both TLR2 and TRIF contribute to interferon-beta production during Listeria infection. Plos One. 2012;7(3):e33299.
129. Jin L, Xu LG, Yang IV, Davidson EJ, Schwartz DA, Wurfel MM, et al. Identification and characterization of a loss-of-function human MPYS variant. Genes Immun. 2011;12(4):263-9.
130. Diner EJ, Burdette DL, Wilson SC, Monroe KM, Kellenberger CA, Hyodo M, et al. The innate immune DNA sensor cGAS produces a noncanonical cyclic dinucleotide that activates human STING. Cell Rep. 2013;3(5):1355-61.
131. Collins AC, Cai H, Li T, Franco LH, Li XD, Nair VR, et al. Cyclic GMP-AMP Synthase Is an Innate Immune DNA Sensor for Mycobacterium tuberculosis. Cell Host Microbe. 2015;17(6):820-8.
132. Hansen K, Prabakaran T, Laustsen A, Jorgensen SE, Rahbaek SH, Jensen SB, et al. Listeria monocytogenes induces IFNbeta expression through an IFI16-, cGAS- and STING-dependent pathway. The EMBO journal. 2014;33(15):1654-66.
133. Hagmann CA, Herzner AM, Abdullah Z, Zillinger T, Jakobs C, Schuberth C, et al. RIG-I detects triphosphorylated RNA of Listeria monocytogenes during infection in non-immune cells. Plos One. 2013;8(4):e62872.
134. Schoggins JW, Wilson SJ, Panis M, Murphy MY, Jones CT, Bieniasz P, et al. A diverse range of gene products are effectors of the type I interferon antiviral response. Nature. 2011;472(7344):481-5.
135. Schoggins JW, MacDuff DA, Imanaka N, Gainey MD, Shrestha B, Eitson JL, et al. Pan-viral specificity of IFN-induced genes reveals new roles for cGAS in innate immunity. Nature. 2014;505(7485):691-5.
136. Liu SY, Sanchez DJ, Aliyari R, Lu S, Cheng G. Systematic identification of type I and type II interferon-induced antiviral factors. Proceedings of the National Academy of Sciences of the United States of America. 2012;109(11):4239-44.
137. Kane M, Zang TM, Rihn SJ, Zhang F, Kueck T, Alim M, et al. Identification of Interferon-Stimulated Genes with Antiretroviral Activity. Cell Host Microbe. 2016;20(3):392-405.
138. Tilney LG, Portnoy DA. Actin filaments and the growth, movement, and spread of the intracellular bacterial parasite, Listeria monocytogenes. The Journal of cell biology. 1989;109(4 Pt 1):1597-608.

139. Dussurget O, Bierne H, Cossart P. The bacterial pathogen Listeria monocytogenes and the interferon family: type I, type II and type III interferons. Frontiers in cellular and infection microbiology. 2014;4:50.
140. Dupuis S, Jouanguy E, Al-Hajjar S, Fieschi C, Al-Mohsen IZ, Al-Jumaah S, et al. Impaired response to interferon-alpha/beta and lethal viral disease in human STAT1 deficiency. Nature genetics. 2003;33(3):388-91.
141. Gedde MM, Higgins DE, Tilney LG, Portnoy DA. Role of listeriolysin O in cell-to-cell spread of Listeria monocytogenes. Infection and immunity. 2000;68(2):999-1003.
142. Marquis H, Doshi V, Portnoy DA. The broad-range phospholipase C and a metalloprotease mediate listeriolysin O-independent escape of Listeria monocytogenes from a primary vacuole in human epithelial cells. Infection and immunity. 1995;63(11):4531-4.
143. Sun LJ, Wu JX, Du FH, Chen X, Chen ZJJ. Cyclic GMP-AMP Synthase Is a Cytosolic DNA Sensor That Activates the Type I Interferon Pathway. Science. 2013;339(6121):786-91.
144. Yoneyama M, Kikuchi M, Natsukawa T, Shinobu N, Imaizumi T, Miyagishi M, et al. The RNA helicase RIG-I has an essential function in double-stranded RNA-induced innate antiviral responses. Nature immunology. 2004;5(7):730-7.
145. Ishibashi M, Wakita T, Esumi M. 2',5'-Oligoadenylate synthetase-like gene highly induced by hepatitis C virus infection in human liver is inhibitory to viral replication in vitro. Biochemical and biophysical research communications. 2010;392(3):397-402.
146. Akira S, Takeda K. Toll-like receptor signalling. Nature reviews Immunology. 2004;4(7):499-511.
147. Lee BL, Barton GM. Trafficking of endosomal Toll-like receptors. Trends in cell biology. 2014;24(6):360-9.
148. Nagpal K, Plantinga TS, Sirois CM, Monks BG, Latz E, Netea MG, et al. Natural loss-of-function mutation of myeloid differentiation protein 88 disrupts its ability to form Myddosomes. The Journal of biological chemistry. 2011;286(13):11875-82.
149. George J, Motshwene PG, Wang H, Kubarenko AV, Rautanen A, Mills TC, et al. Two human MYD88 variants, S34Y and R98C, interfere with MyD88-IRAK4-myddosome assembly. The Journal of biological chemistry. 2011;286(2):1341-53.
150. Tsukaguchi H, Shayakul C, Berger UV, Mackenzie B, Devidas S, Guggino WB, et al. Molecular characterization of a broad selectivity neutral solute channel. The Journal of biological chemistry. 1998;273(38):24737-43.
151. Sun SC. Non-canonical NF-kappaB signaling pathway. Cell Res. 2011;21(1):71-85.
152. Hausser A, Storz P, Martens S, Link G, Toker A, Pfizenmaier K. Protein kinase D regulates vesicular transport by phosphorylating and activating phosphatidylinositol-4 kinase IIIbeta at the Golgi complex. Nat Cell Biol. 2005;7(9):880-6.
153. Chen M, Meng Q, Qin Y, Liang P, Tan P, He L, et al. TRIM14 Inhibits cGAS Degradation Mediated by Selective Autophagy Receptor p62 to Promote Innate Immune Responses. Molecular cell. 2016;64(1):105-19.
154. Zhou Z, Jia X, Xue Q, Dou Z, Ma Y, Zhao Z, et al. TRIM14 is a mitochondrial adaptor that facilitates retinoic acid-inducible gene-I-like receptor-mediated innate

immune response. Proceedings of the National Academy of Sciences of the United States of America. 2014;111(2):E245-54.
155. Wang S, Chen Y, Li C, Wu Y, Guo L, Peng C, et al. TRIM14 inhibits hepatitis C virus infection by SPRY domain-dependent targeted degradation of the viral NS5A protein. Sci Rep. 2016;6:32336.
156. Ozato K, Shin DM, Chang TH, Morse HC, 3rd. TRIM family proteins and their emerging roles in innate immunity. Nature reviews Immunology. 2008;8(11):849-60.
157. Rajsbaum R, Garcia-Sastre A, Versteeg GA. TRIMmunity: the roles of the TRIM E3-ubiquitin ligase family in innate antiviral immunity. Journal of molecular biology. 2014;426(6):1265-84.
158. Weinert C, Morger D, Djekic A, Grutter MG, Mittl PR. Crystal structure of TRIM20 C-terminal coiled-coil/B30.2 fragment: implications for the recognition of higher order oligomers. Sci Rep. 2015;5:10819.
159. Goldstone DC, Walker PA, Calder LJ, Coombs PJ, Kirkpatrick J, Ball NJ, et al. Structural studies of postentry restriction factors reveal antiparallel dimers that enable avid binding to the HIV-1 capsid lattice. Proceedings of the National Academy of Sciences of the United States of America. 2014;111(26):9609-14.
160. Pizarro-Cerda J, Kuhbacher A, Cossart P. Entry of Listeria monocytogenes in mammalian epithelial cells: an updated view. Cold Spring Harbor perspectives in medicine. 2012;2(11).
161. Nimmerjahn F, Ravetch JV. Fcgamma receptors as regulators of immune responses. Nature reviews Immunology. 2008;8(1):34-47.
162. Boross P, van de Poel K, Van de Winkel JG, Leusen JH. Fc Receptors. Encyclopedia of Life Sciences (ELS). 2008.
163. Davis W, Harrison PT, Hutchinson MJ, Allen JM. Two distinct regions of FC gamma RI initiate separate signalling pathways involved in endocytosis and phagocytosis. The EMBO journal. 1995;14(3):432-41.
164. Swanson JA, Hoppe AD. The coordination of signaling during Fc receptor-mediated phagocytosis. Journal of leukocyte biology. 2004;76(6):1093-103.
165. Cameron AJ, Harnett MM, Allen JM. Differential recruitment of accessory molecules by FcgammaRI during monocyte differentiation. Eur J Immunol. 2001;31(9):2718-25.
166. Indik ZK, Park JG, Hunter S, Schreiber AD. Structure/function relationships of Fc gamma receptors in phagocytosis. Semin Immunol. 1995;7(1):45-54.
167. Huang ZY, Barreda DR, Worth RG, Indik ZK, Kim MK, Chien P, et al. Differential kinase requirements in human and mouse Fc-gamma receptor phagocytosis and endocytosis. Journal of leukocyte biology. 2006;80(6):1553-62.
168. Kim MK, Pan XQ, Huang ZY, Hunter S, Hwang PH, Indik ZK, et al. Fc gamma receptors differ in their structural requirements for interaction with the tyrosine kinase Syk in the initial steps of signaling for phagocytosis. Clin Immunol. 2001;98(1):125-32.
169. Harrison PT, Bjorkhaug L, Hutchinson MJ, Allen JM. The interaction between human Fc gamma RI and the gamma-chain is mediated solely via the 21 amino acid transmembrane domain of Fc gamma RI. Molecular membrane biology. 1995;12(4):309-12.

170. Harrison PT, Hutchinson MJ, Allen JM. A convenient method for the construction and expression of GPI-anchored proteins. Nucleic Acids Res. 1994;22(18):3813-4.
171. Lu JH, Chu J, Zou ZC, Hamacher NB, Rixon MW, Sun PD. Structure of Fc gamma RI in complex with Fc reveals the importance of glycan recognition for high-affinity IgG binding. Proceedings of the National Academy of Sciences of the United States of America. 2015;112(3):833-8.
172. Sanjana NE, Shalem O, Zhang F. Improved vectors and genome-wide libraries for CRISPR screening. Nat Methods. 2014;11(8):783-4.
173. Smith P, DiLillo DJ, Bournazos S, Li F, Ravetch JV. Mouse model recapitulating human Fcgamma receptor structural and functional diversity. Proceedings of the National Academy of Sciences of the United States of America. 2012;109(16):6181-6.
174. Mittal R, Sukumaran SK, Selvaraj SK, Wooster DG, Babu MM, Schreiber AD, et al. Fcgamma receptor I alpha chain (CD64) expression in macrophages is critical for the onset of meningitis by Escherichia coli K1. PLoS Pathog. 2010;6(11):e1001203.
175. Lingnau A, Domann E, Hudel M, Bock M, Nichterlein T, Wehland J, et al. Expression of the Listeria monocytogenes EGD inlA and inlB genes, whose products mediate bacterial entry into tissue culture cell lines, by PrfA-dependent and -independent mechanisms. Infection and immunity. 1995;63(10):3896-903.
176. Gaillard JL, Berche P, Frehel C, Gouin E, Cossart P. Entry of L. monocytogenes into cells is mediated by internalin, a repeat protein reminiscent of surface antigens from gram-positive cocci. Cell. 1991;65(7):1127-41.
177. Dramsi S, Biswas I, Maguin E, Braun L, Mastroeni P, Cossart P. Entry of Listeria monocytogenes into hepatocytes requires expression of inIB, a surface protein of the internalin multigene family. Mol Microbiol. 1995;16(2):251-61.
178. Poyart C, Abachin E, Razafimanantsoa I, Berche P. The zinc metalloprotease of Listeria monocytogenes is required for maturation of phosphatidylcholine phospholipase C: direct evidence obtained by gene complementation. Infection and immunity. 1993;61(4):1576-80.
179. Gouin E, Dehoux P, Mengaud J, Kocks C, Cossart P. iactA of Listeria ivanovii, although distantly related to Listeria monocytogenes actA, restores actin tail formation in an L. monocytogenes actA mutant. Infection and immunity. 1995;63(7):2729-37.
180. Lauer P, Chow MY, Loessner MJ, Portnoy DA, Calendar R. Construction, characterization, and use of two Listeria monocytogenes site-specific phage integration vectors. Journal of bacteriology. 2002;184(15):4177-86.
181. Pistor S, Chakraborty T, Niebuhr K, Domann E, Wehland J. The ActA protein of Listeria monocytogenes acts as a nucleator inducing reorganization of the actin cytoskeleton. The EMBO journal. 1994;13(4):758-63.
182. Skoble J, Portnoy DA, Welch MD. Three regions within ActA promote Arp2/3 complex-mediated actin nucleation and Listeria monocytogenes motility. The Journal of cell biology. 2000;150(3):527-38.
183. Pistor S, Grobe L, Sechi AS, Domann E, Gerstel B, Machesky LM, et al. Mutations of arginine residues within the 146-KKRRK-150 motif of the ActA protein of Listeria monocytogenes abolish intracellular motility by interfering with the recruitment of the Arp2/3 complex. J Cell Sci. 2000;113 (Pt 18):3277-87.

184. Welch MD, Rosenblatt J, Skoble J, Portnoy DA, Mitchison TJ. Interaction of human Arp2/3 complex and the Listeria monocytogenes ActA protein in actin filament nucleation. Science. 1998;281(5373):105-8.
185. Zalevsky J, Grigorova I, Mullins RD. Activation of the Arp2/3 complex by the Listeria acta protein. Acta binds two actin monomers and three subunits of the Arp2/3 complex. The Journal of biological chemistry. 2001;276(5):3468-75.
186. Loisel TP, Boujemaa R, Pantaloni D, Carlier MF. Reconstitution of actin-based motility of Listeria and Shigella using pure proteins. Nature. 1999;401(6753):613-6.
187. Laurent V, Loisel TP, Harbeck B, Wehman A, Grobe L, Jockusch BM, et al. Role of proteins of the Ena/VASP family in actin-based motility of Listeria monocytogenes. The Journal of cell biology. 1999;144(6):1245-58.
188. Gouin E, Adib-Conquy M, Balestrino D, Nahori MA, Villiers V, Colland F, et al. The Listeria monocytogenes InlC protein interferes with innate immune responses by targeting the I{kappa}B kinase subunit IKK{alpha}. Proceedings of the National Academy of Sciences of the United States of America. 2010;107(40):17333-8.
189. Uhlen M, Fagerberg L, Hallstrom BM, Lindskog C, Oksvold P, Mardinoglu A, et al. Proteomics. Tissue-based map of the human proteome. Science. 2015;347(6220):1260419.
190. Drevets DA, Sawyer RT, Potter TA, Campbell PA. Listeria monocytogenes infects human endothelial cells by two distinct mechanisms. Infection and immunity. 1995;63(11):4268-76.
191. Drevets DA, Campbell PA. Roles of complement and complement receptor type 3 in phagocytosis of Listeria monocytogenes by inflammatory mouse peritoneal macrophages. Infection and immunity. 1991;59(8):2645-52.
192. Alvarez-Dominguez C, Carrasco-Marin E, Leyva-Cobian F. Role of complement component C1q in phagocytosis of Listeria monocytogenes by murine macrophage-like cell lines. Infection and immunity. 1993;61(9):3664-72.
193. Alvarez-Dominguez C, Vazquez-Boland JA, Carrasco-Marin E, Lopez-Mato P, Leyva-Cobian F. Host cell heparan sulfate proteoglycans mediate attachment and entry of Listeria monocytogenes, and the listerial surface protein ActA is involved in heparan sulfate receptor recognition. Infection and immunity. 1997;65(1):78-88.
194. Mitchell G, Ge L, Huang Q, Chen C, Kianian S, Roberts MF, et al. Avoidance of autophagy mediated by PlcA or ActA is required for Listeria monocytogenes growth in macrophages. Infection and immunity. 2015;83(5):2175-84.
195. Travier L, Lecuit M. Listeria monocytogenes ActA: a new function for a 'classic' virulence factor. Curr Opin Microbiol. 2014;17:53-60.
196. Garcia-Garcia E, Rosales C. Signal transduction during Fc receptor-mediated phagocytosis. Journal of leukocyte biology. 2002;72(6):1092-108.
197. Dai X, Jayapal M, Tay HK, Reghunathan R, Lin G, Too CT, et al. Differential signal transduction, membrane trafficking, and immune effector functions mediated by FcgammaRI versus FcgammaRIIa. Blood. 2009;114(2):318-27.
198. Campeau E, Ruhl VE, Rodier F, Smith CL, Rahmberg BL, Fuss JO, et al. A versatile viral system for expression and depletion of proteins in mammalian cells. Plos One. 2009;4(8):e6529.

199. Cong L, Ran FA, Cox D, Lin S, Barretto R, Habib N, et al. Multiplex genome engineering using CRISPR/Cas systems. Science. 2013;339(6121):819-23.
200. Simon R, Priefer U, Pühler A. A Broad Host Range Mobilization System for In Vivo Genetic Engineering: Transposon Mutagenesis in Gram Negative Bacteria. Nature Biotechnology. 1983;1(9):784-91.
201. Trapnell C, Roberts A, Goff L, Pertea G, Kim D, Kelley DR, et al. Differential gene and transcript expression analysis of RNA-seq experiments with TopHat and Cufflinks. Nature protocols. 2012;7(3):562-78.
202. Ran FA, Hsu PD, Wright J, Agarwala V, Scott DA, Zhang F. Genome engineering using the CRISPR-Cas9 system. Nature protocols. 2013;8(11):2281-308.
203. Dodd DA, Worth RG, Rosen MK, Grinstein S, van Oers NS, Hansen EJ. The Haemophilus ducreyi LspA1 protein inhibits phagocytosis by using a new mechanism involving activation of C-terminal Src kinase. mBio. 2014;5(3):e01178-14.
204. Cheng LW, Portnoy DA. Drosophila S2 cells: an alternative infection model for Listeria monocytogenes. Cellular microbiology. 2003;5(12):875-85.
205. Keestra AM, de Zoete MR, Bouwman LI, van Putten JP. Chicken TLR21 is an innate CpG DNA receptor distinct from mammalian TLR9. Journal of immunology. 2010;185(1):460-7.
206. Robert X, Gouet P. Deciphering key features in protein structures with the new ENDscript server. Nucleic Acids Res. 2014;42(Web Server issue):W320-4.